Lateral Post-stall Aerodynamic Modeling using Flight Test Data

by

Zane Zhanhong Luo

A thesis submitted in conformity with the requirements
for the degree of Master of Applied Science
Graduate Department of Aerospace Science and Engineering
University of Toronto

Abstract

Lateral Post-stall Aerodynamic Modeling using Flight Test Data

Zane Zhanhong Luo
Master of Applied Science
Graduate Department of Aerospace Science and Engineering
University of Toronto
2016

Loss-of-control resulting from airplane upset is a leading cause of worldwide commercial aircraft accidents. In response, the Federal Aviation Administration requires all U.S. air carrier pilots to receive upset-recovery training in flight simulators by 2020. However, the aerodynamic models in most flight simulators are not valid at upset conditions and must be updated before they can be used for training. In this thesis, a method is proposed for generating representative lateral stall models to better represent the aircraft dynamics at stall. Using certification flight test data and supplementary data provided by the manufacturer, the aerodynamic database of a turboprop aircraft is extended to cover large-angle-of-attack flight, while leaving the original model untouched at low angles of attack. It is then integrated into a 6-DOF simulator and shows reasonable match to the behavior observed in flight tests.

Acknowledgements

I would like to express my special appreciation and thanks to my supervisor, Professor Dr. Peter Grant, for the patient guidance, encouragement and advice he has provided throughout my time as his student. I would also like to thank my research assessment committee members, Professor Hugh Liu and Professor Christopher Damaren for providing valuable advice and taking the time to review my research.

I gratefully acknowledge the funding received towards this project from the Federal Aviation Administration and the data received from Bombardier Aerospace.

I owe my deepest gratitude to Stacey Liu for her tremendous support in the lab, help on technical knowledge, and for creating a longitudinal model that integrated well with my lateral model.

I would like to thank Bruce Haycock for his support in maintaining the simulator in working condition for testing the developed models. I am also grateful to the students of the Vehicle Simulation Group, Faizan Rehmatullah and Gregory Moszczynski for feedback related to this study.

Special thanks go out to the People of Simulation (POS) group, Tim Teng, Tony Zhang, and Jacek Khan; together we were the 'four' musketeers of this lab, unconditionally offering each other technical advice to complete the thesis, sometimes at the risk of our own.

Last but not least, I would like to thank my family for their constant support during the course of my studies.

Contents

List of Tables

List of Figures

Nomenclature

α	Angle of attack
α_l	Lower bound of blending region
α_u	Upper bound of blending region
β	Angle of sideslip
$\hat{\boldsymbol{\theta}}$	Estimated parameter vector
$\hat{\boldsymbol{R}}$	Covariance matrix of innovation
$\boldsymbol{\nu}$	Innovation vector
$\boldsymbol{\theta}$	Parameter vector
$\boldsymbol{f}$	Nonlinear state equations
$\boldsymbol{h}$	Measurement model equations
$\boldsymbol{u}$	Control input vector
$\boldsymbol{X}$	Regressor matrix
$\boldsymbol{x}$	State vector
$\boldsymbol{y}$	Model output vector
$\boldsymbol{z}$	Measurement vector
ΔC_i	The Δ model for coefficient C_i
δ_a	Aileron input
δ_e	Elevator input

δ_r	Rudder input
$\dot{(\cdot)}$	time derivative
$\hat{(\cdot)}$	non-dimentionalized value
$\hat{p}, \hat{q}, \hat{r}$	Non-dimensionalized roll, pitch, yaw rates
ϕ	Roll angle
ϕ'	Dynamic roll attitude
ψ	Yaw angle
θ	Pitch angle
a_y	measured specific force in y-direction
b	span
C_l, C_m, C_n	Non-dimensionalized moment coefficients in x,y,z-direction
C_m	non-dimensional pitching moment
C_X	non-dimensional force in body axis x-direction
C_X, C_Y, C_Z	Non-dimensionalized force coefficients in x,y,z-direction
C_Y	non-dimensional force in body axis y-direction
C_Z	non-dimensional force in body axis z-direction
$C_{i,extended}$	The output from the extended model for coefficient C_i
$C_{i,j}$	The effect of j on the coefficient C_i, where i = X,Y,Z,l,m,n
$C_{i,qualified}$	The output from the qualified model for coefficient C_i
C_{i_j}	The derivative of C_i as a function of j
$C_{l,0}, C_{n,0}, C_{Y,0}$	Constant term in the model structure for C_l, C_n, C_Y
J	Cost function
p	roll rate
p, q, r	Pitch, roll, yaw rates

q	pitch rate
r	yaw rate
rho	air density
S	wing area
u, v, w	Component of total airspeed along x,y,z body axes
V	total speed
$(\cdot)$	Time derivative of $(\cdot)$
BA	Bombardier Aerospace
DRC	Dynamic Roll Control
LOC-I	Loss-of-Control: Inflight
m	mass
NTSB	National Transportation Safety Board
RNG	Random-Number Generator
SUPRA	Simulation of Upset Recovery in Aviation
TAS	True Airspeed
TsAGI	The Central Aerohydrodynamic Institute
UTIAS	University of Toronto Institute for Aerospace Studies
UTIAS	University of Toronto Institute for Aerospace Studies
V	Total velocity
QTG	Qualification Test Guide

something long now what are you doing to do

Chapter 1

Introduction

1.1 Background

The Boeing Company concluded that loss-of-control: inflight (LOC-I) was the leading cause of worldwide fatal commercial aircraft accidents during the period from 2000 to 2009. Wilborn [39] defined LOC-I as an irregular flight condition that is characterized by behaviors such as the aircraft motion not predictably altered by pilot control inputs, disproportionately large responses to small state variable changes that may lead to instability, high angular rates, and the inability to maintain heading, altitude, or wings-level flight.

Aircraft upset, is commonly described as a situation where the aircraft is unintentionally brought outside of its normal flight envelope. An aircraft in upset can often develop into a LOC condition if proper recovery measures are not applied. A study by the U.S. Federal Aviation Administration (FAA) [26] summarized the causes of airplane upsets, which were aerodynamic stall (36%), flight control malfunction (21%), pilot spatial disorientation (11%) , contaminated airfoils (11%), atmospheric disturbance (8%), and other causes (13%). 74 accidents were included in this study, accounting for 3241 fatalities due to LOC-I.

Several high profile accidents involving LOC-I and inappropriate recovery procedures by the pilots spurred the FAA to take action to prevent similar situations from happening again. One such accident is Air France 447, which due to malfunction of the pitot tubes, lost accurate airspeed information and went into a sustained stall, signaled by the stall warning and strong buffet. Despite these persistent symptoms, the crew never understood that they were stalling and consequently never applied a recovery maneuver

[10]. The airliner struck the surface of the sea in a normal flight attitude, with a high rate of descent, killing all on board. In another accidient, A Colgan Air, Inc. aircraft, operating as Continental connection flight 3407, crashed into a residence in Clarence Center, New York, resulting in the death of everyone on board and one person on the ground. The U.S. National Transportation Safety Board (NTSB) determined that the probable cause of this accident was the pilot in command's inappropriate response to the activation of the stick shaker, which led to an aerodynamic stall.

The Federal Aviation Administration enacted a number of requirements to conduct rulemaking related to the results of the NTSB investigation of the Colgan Air accident. It is proposed that better pilot training in stall recovery would reduce stall related accidents. As a result of the rulemaking process, all pilots that fly for air carriers in the United States will receive training to recover from fully developed stalls by 2020 [15]. Studies have shown that using ground-based simulators is a cost-effective way to train pilots to recover from upset, although care must be taken to ensure transfer of training [6]. However, current flight models in ground-based simulators are inaccurate beyond stall and do not exhibit LOC-I conditions as mentioned earlier, which would significantly hinder training efforts. Therefore, the aerodynamic database of simulators must be extended handle a wider flight envelope that depicts proper aircraft behavior in upset conditions. The most common way of developing accurate flight models is through wind-tunnel testing and a well designed flight test program. It is economically infeasible to conduct such testing for all airliners that are flying today and it is certainly not possible it could be done before 2020, when the FAA rule takes effect. Yet, studies have shown insignificant differences in training benefits between a *representative model* and a high-fidelity model that was developed from wind-tunnel or flight test programs [35]. A representative model is a stall model which captures the important qualitative characteristics of an aircraft in upset conditions, but not necessarily in high precision.

A collaborative project between the University of Toronto Institute for Aerospace Studies (UTIAS), the FAA, and Bombardier Aerospace (BA) has been initiated to develop a method for generating representative models for upset recovery training. Through the work done in this project, the FAA would have a better understanding of the potential difficulties that airlines and simulation companies would encounter as they try to equip their training simulators with new flight models.

1.2 Scope and Organization

The objective of the project is to propose a methodology to develop representative models and generate such a model for a currently in service airliner. As part of this project, this thesis documents the methodology and results of the development of a representative model for a T-tailed turboprop regional airliner by Bombardier Aerospace. To support this work, BA has provided certification flight test data and the MATLAB Simulink Qualification Test Guide (QTG) qualified model. The data used for development of the model is mostly from certification and therefore such data is obtainable for every airliner that is in service today. Certification is the process in which manufacturers prove the airworthiness of a new production aircraft through a series of tests as demanded by the appropriate government agencies. As such, the method described in this document is applicable to aircraft other than the turboprop and should help the effort in upgrading simulators so that they are ready for upset recovery by 2020 and beyond. Although a high-fidelity model is not required, the approach taken by UTIAS is to develop as accurate of a model as possible with the given resources.

This thesis focuses on the work that extends the lateral part of the turboprop's qualified model up to an angle of attack that is 10° past stall. The longitudinal model extension is documented in a separate report. The remainder of this document is organized as follows:

- **Chapter 2:** This chapter is a literature review on model structures used for aerodynamic modeling, parameter estimation methods, and projects that extended an aerodynamic database into the stall regime
- **Chapter 3:** This chapter describes in detail the method used to extend the qualified model into the stall regime using flight test data.
- **Chapter 4:** This chapter presents the results from applying the method outlined in Chapter 3, including time-history matches to flight test data, qualitative discussion of the updated aerodynamic database, and the integration into a full 6-DOF simulator.
- **Chapter 5:** This Chapter summarizes the findings of the study and outlines directions for future research.

Chapter 2

Literature Review

This chapter reviews the current literature on flight modeling in the stall regime. To evaluate the fidelity of a stall model, the behavior of the aircraft at stall must be known first for the model to be compared against. Studies have revealed various behaviors one may expect in upset conditions; some are discussed below. For stall modeling, a model structure must first be postulated and then the model must be identified. Both topics are an active field of research, and the most common methods are discussed. Since this thesis focuses on lateral stall modeling, the focus of the literature review is on lateral aerodynamics.

2.1 Aircraft Behavior at Stall

Other than providing thrust, propellers also impart undesired forces and moments on an aircraft. Phillips et al. [34] derived mathematical formulas for calculating the yawing moment and normal force of running propellers and showed that it matched well with empirical data. When a rotating propeller is at some angle of attack relative to the freestream flow, there is a component of the freestream in the plane of propeller rotation. This changes the angle of flow as seen by the blades. At a positive angle of attack, it increases the relative airspeed for the downward moving blades and decreases for the upward moving blades. Thus both lift and drag are increased on the downward moving side of the propeller. This difference in thrust caused by the two sides creates yawing moment, and the difference in drag forces produces a net normal force. By the same reasoning, a sideslip would cause sideforce. These forces and moments become more significant at upset conditions due to large α and β.

Chambers [7] listed and explained some common lateral behaviors of aircraft at stall,

such as asymmetric rolling moments, and unstable roll damping. As a result of positive rate of roll (rolling to the right), the upgoing left wing sees a decrease in local angle of attack, while the downgoing right wing sees a local increase in angle of attack of the same magnitude. Depending on the local lift-curve slope on each wing, the net effects of the rolling motion can propel rather than damp the motion. For low angles of attack, the decrease of local angle of attack on the left wing loses lift and increase of local angle of attack on the right wing gains lift. This opposes (damps) the roll rate. However, at higher angles of attack just before stall, the local increase in angle of attack on the right wing would result in a loss of lift due to stall that is larger than the loss of lift on the upgoing left wing. A net rolling moment that augments the roll rate is created. In this situation, the aircraft is said to be roll unstable. Asymmetric rolling moments occur at stall because of one-wing stalling before the other. Coupled with the unstable roll damping, the initial roll rate caused by one stalled wing further propels the roll and a severe wing-drop may occur.

Foster et al. [16] found that aerodynamic databases for large commercial transport airplanes are typically not designed to be accurate for upset conditions because simulator certification requirements are very limited for conditions beyond the normal flight envelope, and aerodynamic measurements at upset conditions are normally not acquired from wind tunnel nor flight tests. Hence, they conducted an extensive wind tunnel test of a commercial transport aircraft at upset conditions to bridge that gap. Static lateral-directional stability is indicated by the variation of aerodynamic rolling moment and yawing moment with sideslip angle. The data indicated a linear variation of rolling moment with β at low angles of attack, but significant non-linear variations at higher angles. At α near stall, $C_{l,\beta}$ becomes progressively less stable and even becomes unstable. Stability is regained at the extreme angles of attack. The data also showed aerodynamic asymmetries, where side force or rolling/yawing moment coefficients at zero β are non-zero.The source of asymmetries are not well-understood, but the data clearly shows significant rolling moment $C_{l,0}$ as a function of α. The control effectiveness of the rudder is shown to decay with angle of attack in the stall regime and has a reduction of 66% in effectiveness at $\alpha = 30°$. The roll damping is shown to decrease as α increases towards stall. Near stall, the roll damping reverses sign and becomes unstable, but returns to slightly stable at even higher α. The study also showed that roll damping reduction becomes more severe with the extension of trailing edge flaps. In a related study of another aircraft model, Brandon [5] et al. collected wind tunnel data of a transport aircraft that displayed unstable roll damping before the stall angle of attack, which may be explained

by Chamber's description of the reversal of roll damping.

Gingras et al. [17] collected wind tunnel data for various types of aircraft (similar configuration, such as T-tail, low wing, etc.) and built representative models for each type. Pilots who have substantial experience with stalling certain types of aircraft, called Subject Matter Experts (SME), evaluated the models and data showed that the pilots could tell no difference between the representative and the type-specific high-fidelity models. It is also shown that roll-off and other behaviors associated with roll have the largest effect on the perceived fidelity of the models according to the SMEs.

Abramov et al. developed an aerodynamic model in extended flight envelope for a generic airliner as part of a research project *Simulation of Upset Recovery in Aviation* (SUPRA) [1]. It was developed from data obtained in TsAGI's wind tunnels. Consistent with the wind tunnel data collected by Foster, Abramov's data showed that C_{l_β} reduced significantly as α increased, but slightly recovers at the extreme angles of attack. Yawing stability C_{n_β} reduces steadily as angle of attack increases, even becoming zero and inverts at the extreme α's.

2.2 Aerodynamic Model Structure Determination for Stall

One of the most difficult tasks in this project is the postulation of an appropriate model that relate the aerodynamic force and moment coefficients to the states and control inputs of the aircraft. The model structure should be able to capture the underlying aerodynamics in the prestall and stall regimes of flight and be identifiable from the available flight test data. The most common model structures found in literature are discussed subsequently.

The forces and moments on the airplane during flight depend on the states of the aircraft. However, due to the complicated nature of the dependencies and the need for models that are easy to work with, a polynomial function in the states is commonly used to relate the aerodynamic forces and moments. The use of a polynomial model is an assumption about the underlying physics of aircraft dynamics and is based on the observed dependence between aerodynamic coefficients and independent state variables such as α and β in wind tunnels. Mathematically, the polynomial results from series expansions about

a flight condition and assumes the relationships between forces and moments and the states as well as their derivatives are continuous. This is valid in the subsonic regime and in the absence of shocks [19]. However, there is little guidance on what terms should be included and the determination of a good model is for the most part based on experience.

The most basic type of modeling seeks to identify a set of linear aerodynamic derivatives for the flight condition. It has the advantage of associating the results with classical stability derivatives [20]. An example for the lift coefficient would be:

$$C_L = C_{L_o} + C_{L_V}\frac{\Delta V}{V_o} + C_{L_\alpha}\Delta\alpha + C_{L_{\dot\alpha}}\frac{\dot\alpha\bar c}{2V_o} + C_{L_q}\frac{q\bar c}{2V_o} + C_{L_\delta}\Delta\delta \tag{2.1}$$

The idea of expansions could be further extended to allow high-order polynomials to represent the desired functions. However, the advantage afforded by this representation is usually offset by the difficulty of identifiability due to over-parameterization. In general, most of the higher order dependence is on the angle of attack α and β. Therefore, a general expansion for any specific force or moment coefficient is: [23]

$$C_L = C_0(\alpha,\beta) + \sum_i C_{\alpha^i}\alpha^i + \sum_j C_{\beta^j}\beta^j + \sum_i\sum_j C_{\alpha^i\beta^j}\alpha^i\beta^j \tag{2.2}$$

where C_L on the left hand side could be replaced with any of the other five aerodynamic coefficients. The C's on the right hand side are the constant parameters associated with the powers of α and β. Many authors have models based on this general form for the static effects for post-stall modeling and have obtained satisfactory results. The idea is expanded further to include angular rates and control deflections.

Hall [20] used the following models to explain most of the C_l and C_n variations in his dataset of a fully instrumented F-4 Phantom aircraft.

$$C_l = C_{l_\beta}\beta + C_{l_{\delta_a}}\delta_a + C_{l_p}p \tag{2.3a}$$
$$C_l = C_{l_\beta}\beta + C_{l_{\delta_a}}\delta_a + C_{l_{\alpha^2\beta^2}}\alpha^2\beta^2 \tag{2.3b}$$
$$C_l = C_{l_\beta}\beta + C_{l_{\delta_a}}\delta_a + C_{l_p}p + C_{l_r}r \tag{2.3c}$$
$$C_n = C_{n_{\delta_r}}\delta_r + C_{n_\beta}\beta + C_{n_r}r \tag{2.3d}$$
$$C_n = C_{n_{\delta_r}}\delta_r + C_{n_\beta}\beta + C_{n_r}r + C_{n_p}p \tag{2.3e}$$

Equations 2.3a and 2.3d were used to explain data near $\alpha = 5°$, equations 2.3b and 2.3e for data near $\alpha = 15°$ and 2.3c and 2.3d for $\alpha = 25°$.

The models are linear in the parameters so that standard system identification techniques could be used to find the values based on flight test data. To make the notation more compact, only the regressors (functions of the state variables) will be listed, for example, Equation 2.3c would be rewritten as $C_l = f(bias, \beta, \delta_a, p, r)$

Many other authors such as Batterson [3], Eulrich [13], Hall [19], Gupta [20] and Klein have had success with similar models, but the most recent publication regarding this commonly applied method of modeling is Grauer's Generic Global Aerodynamic (GGA) Model, published in 2014 [18]. It uses the following set of regressors for their respective coefficients and have predicted good results for a number of aircraft in high angle of attack regions, including fighters such as the F-4, F-16C, transport T-2, and high agility testing aircraft X-31.

Global Generic Aerodynamics Model

$$C_D = f(bias, \alpha, \alpha\hat{q}, \alpha\delta_e, \alpha^2, \alpha^2\hat{q}, \alpha^2\delta_e, \alpha^3, \alpha^3\hat{q}, \alpha^4) \tag{2.4a}$$

$$C_Y = f(\beta, \hat{p}, \hat{r}, \delta_a, \delta_r) \tag{2.4b}$$

$$C_L = f(bias, \alpha, \hat{q}, \delta_e, \alpha\hat{q}, \alpha^2, \alpha^3, \alpha^4) \tag{2.4c}$$

$$C_l = f(\beta, \hat{p}, \hat{r}, \delta_a, \delta_r) \tag{2.4d}$$

$$C_m = f(bias, \alpha, \hat{q}, \delta_e, \alpha\hat{q}, \alpha^2\hat{q}, \alpha^2\delta_e, \alpha^3\hat{q}, \alpha^3\delta_e, \alpha^4) \tag{2.4e}$$

$$C_n = f(\beta, \hat{p}, \hat{r}, \delta_a, \delta_r, \beta^2, \beta^3) \tag{2.4f}$$

To aid in the process of selecting regressors, Klein [23] applied a method called stepwise regression to the aerodynamic modeling problem. The procedure begins with no variables in the postulated model equation other than a bias term. Independent variable terms are then inserted into the model one at a time based on the correlation of the term and the remainder of the model value that is being fit after taking into account terms that are already in the model. The one with the highest correlation is added first.

$$F = \frac{\hat{\theta}^2}{s^2(\hat{\theta})} \tag{2.5}$$

At each step of the selection process, the partial F-statistic is used to check for redundancy of previously added terms. The F-statistic is given by Equation 2.5 , where $\hat{\theta}$ is

the estimated value of the parameter returned by the regression analysis after adding it to the model, and $s^2(\hat{\theta})$ is the variance of the parameter. The process is usually manual as it requires some engineering judgment to shortlist a pool of regressors based on their correlation and F-statistic, while giving preference to those that have physical meaning.

Klein [24] also suggested the use of the following trial regressors for modeling the non-linear lateral behavior of aircraft outside of the usual flight envelope: β, p, r, δ_a, δ_r, $\beta\alpha$, $p\alpha$, $r\alpha$, $\delta_a\alpha$, $\delta_r\alpha$, $\beta\alpha^2$, $p\alpha^2$, $r\alpha^2$, $\delta_a\alpha^2$, $\delta_r\alpha^2$, β^2, β^3, β^4, β^5, $\beta^3\alpha^2$, $\beta^3\alpha$, α, α^2, α^3. He also noted that additional regressors can also be formed as polynomial spline terms such as $(\alpha - \alpha_{knot})_+^m$, where α_{knot} is value at which the spline takes effect and the subscript '+' denotes that the term is zero when the value inside the brackets is negative. These can be used in conjunction with stepwise regression to determine whether any regressors can improve the fit to the data. Klein believes that this pool of regressors is capable of capturing the aerodynamics of even large perturbation maneuvers, however caution must be exercised in selecting a small enough set suitable for identification yet be still useful.

Instead of using a complicated model to capture the non-linearities of aerodynamic effects with respect to α, Batterson used a method called data partitioning which segregates the data into different bins according to the angle of attack. Data points that have similar angles of attack are used to estimate the parameters of a model that is valid around the given α. Together all these models span the entire α range and therefore the full model constitutes multiple simpler models, each of which does not have dependence on α [4]. In Batterson's work, a linear model using stability derivatives was adopted.

Morelli [32] introduced the method of Multivariate Orthogonal Functions to automatically generate a suitable model structure. Given a list of independent variables, MOF generates combinations of the variables up to a specified order and treats those as the candidate regressors for search of a model structure. For example, an independent variable list of α, β, δ_a up to 2^{nd} order would return regressors α^2,$\alpha\beta$, $\alpha\delta_a$, β^2, $\beta\delta_a$, δ_a^2. These regressors are then orthogonalized which decouples the normal equations associated with equation error parameter estimation. This also enables the evaluation of each orthogonalized regressor's ability to reduce the least-squares fit of the data. The regressors that reduce the error the most are chosen to be included in the model structure.

2.3 Parameter Estimation

Once a candidate model structure is selected, the parameters must be identified using parameter estimation techniques so that it represents the dynamics of a specific aircraft. This procedure is an optimization problem to minimize the error between the model output and the outputs calculated from the measurements. Mathematically, we are trying to minimize the innovations in some way. The innovation $\nu(i)$ is the difference between the measurements $z(i)$ and the model outputs $y(i)$.

$$\nu(i) = z(i) - y(i) \tag{2.6}$$

Once an aerodynamic model structure is postulated, the parameters would need to be estimated so that it represents the dynamics of one specific aircraft. Several common methods in the literature for estimating the parameters in the aerodynamic model to minimize the innovations are discussed.

2.3.1 Equation Error

Equation error refers to the method of using linear regression to estimate parameters that minimize the difference between the output of an equation and the measurements in the least-squares sense. When applied to aerodynamic modeling, the equation is the aerodynamic force and moment coefficients expressed as functions of response and input variables. For example, a simple rolling moment coefficient expressed as a function of response $\hat{p}$ and input δ_a is given in Equation 2.7.

$$C_l = C_{l_0} + C_{l_p}\hat{p} + C_{l_{\delta_a}}\delta_a + C_{l_{\delta_a \alpha}}\delta_a\alpha \tag{2.7}$$

The rolling moment C_l is assumed to depend on $\hat{p}$, δ_a, and $\delta_a\alpha$ in the manner postulated by the form of the model, where $\hat{p}$, δ_a, and α are the measured values of the non-dimensionalized roll rate, the aileron deflection, and angle of attack from flight test respectively. In Equation 2.7, C_{l_0}, C_{l_p}, $C_{l_{\delta_a}}$, and $C_{l_{\delta_a \alpha}}$ are the parameters that we are trying to identify and $\hat{p}$, δ_a, and $\delta_a\alpha$ are the regressors. In order to use linear regression and the associated matrix algebra to solve the least-squares problem, the equation must be linear in the parameters. However, the regressors are not restricted to linear functions of the state variables. Equation 2.7 is linear in the parameters but contains the nonlinear

regressor $\delta_a\alpha$. The parameter vector $\boldsymbol{\theta}$ and regressor matrix $\boldsymbol{X}$ are formulated as follows:

$$\boldsymbol{\theta} = \begin{bmatrix} C_{l_0} \\ C_{l_p} \\ C_{l_{\delta_a}} \\ C_{l_{\delta_a \alpha}} \end{bmatrix} \tag{2.8}$$

$$\boldsymbol{X} = \begin{bmatrix} 1 & \hat{p}(1) & \delta_a(1) & \delta_a(1)\alpha(1) \\ 1 & \hat{p}(2) & \delta_a(2) & \delta_a(2)\alpha(2) \\ \vdots & \vdots & \vdots & \vdots \\ 1 & \hat{p}(N) & \delta_a(N) & \delta_a(N)\alpha(N) \end{bmatrix} \tag{2.9}$$

where N is the number of data points available. Hence, the model outputs $\boldsymbol{y}$ could be expressed as a matrix product of the regressor matrix $\boldsymbol{X}$ and the parameter vector $\boldsymbol{\theta}$:

$$\boldsymbol{y} = \begin{bmatrix} C_l(1) \\ C_l(2) \\ \vdots \\ C_l(N) \end{bmatrix} = \boldsymbol{X}\boldsymbol{\theta} \tag{2.10}$$

The measured rolling moment $C_{l,meas}$ forms the measurement vector $\boldsymbol{z}$:

$$\boldsymbol{z} = \begin{bmatrix} C_{l,meas}(1) \\ C_{l,meas}(2) \\ \vdots \\ C_{l,meas}(N) \end{bmatrix} \tag{2.11}$$

The objective is to estimate the parameters that best describe the aerodynamic forces and moments measured from flight test. In a least-squares sense, the best estimator of $\boldsymbol{\theta}$ is derived from minimizing the sum of squared differences between the measurements $\boldsymbol{z}$ and the model output $\boldsymbol{y}$, which could be expressed as a cost function

$$J(\boldsymbol{\theta}) = \frac{1}{2}(\boldsymbol{z} - \boldsymbol{X}\boldsymbol{\theta})^T(\boldsymbol{z} - \boldsymbol{X}\boldsymbol{\theta}) \tag{2.12}$$

Equation 2.12 is minimized when its derivative with respect $\boldsymbol{\theta}$ is zero due to its quadratic nature. Setting the derivative to zero and solving for $\boldsymbol{\theta}$, we obtain the best estimate of the parameter vector.

$$\hat{\boldsymbol{\theta}} = (\boldsymbol{X}^T\boldsymbol{X})^{-1}\boldsymbol{X}^T\boldsymbol{z} \tag{2.13}$$

The equation error method assumes the regressors are known without error. Error in the state variables would cause inaccurate parameter estimates; Therefore, it is common practice to smooth the state variables that constitute the regressors before formulating the regressor matrix in Equation 2.9 in an attempt to remove part of the error due to random noise. One of the major advantages of equation error method is that it does not involve equations of motion and hence the time relationship of the data points with respect to each other is not important. This implies equation error could use data that is stitched together from multiple flight maneuvers.

2.3.2 Output Error

Discrete time measurements made on a continuous-time dynamic system such as an aircraft in flight could be formulated mathematically into a framework suitable for parameter estimation. In general, the discrete-time dynamic equations are

$$\dot{\mathbf{x}}(t) = \mathbf{f}[\mathbf{x}(t), \mathbf{u}(t), \boldsymbol{\theta}] + \mathbf{B_w}\mathbf{w}(t) \tag{2.14a}$$

$$\mathbf{y}(t) = \mathbf{h}[\mathbf{x}(t), \mathbf{u}(t), \boldsymbol{\theta}] \tag{2.14b}$$

$$\mathbf{z}(i) = \mathbf{y}(i) + \boldsymbol{\nu}(i) \qquad i = 1, 2, \ldots, N \tag{2.14c}$$

where $\boldsymbol{x}$ is the state vector, $\boldsymbol{f}$ is the nonlinear equations of motion, $\boldsymbol{h}$ is the measurement model, $\boldsymbol{u}$ is a vector of control inputs, $\boldsymbol{\theta}$ is the parameters of the aerodynamic model embedded the equations of motion as forces and moments, $\boldsymbol{z}$ is a vector of measurements, and $\boldsymbol{y}$ is the model output. $\boldsymbol{B_w w}$ is the process noise formulated as a stochastic forcing function and its weighting matrix, and $\boldsymbol{\nu}$ is the measurement error.

The so called output error method is a popular parameter estimation method that utilizes this framework. Unlike equation error in which the outputs are aerodynamic coefficients, the output error method uses the aircraft states as outputs. The process minimizes the difference between the measured output states and the model states that are integrated in time. The aerodynamic model contains the parameters $\boldsymbol{\theta}$, which itself is embedded in the state equation. The output error method assumes that there is no process noise but there is measurement noise, which simplifies Equation 2.14 to [29]:

$$\dot{\mathbf{x}}(t) = \mathbf{f}[\mathbf{x}(t), \mathbf{u}(t), \boldsymbol{\theta}] \tag{2.15a}$$

$$\mathbf{y}(t) = \mathbf{h}[\mathbf{x}(t), \mathbf{u}(t), \boldsymbol{\theta}] \tag{2.15b}$$

$$\mathbf{z}(i) = \mathbf{y}(i) + \boldsymbol{\nu}(i) \qquad i = 1, 2, \ldots, N \tag{2.15c}$$

The time history of model states could be obtained by integrating the equations in time for $\mathbf{x}$. Due to the lack of process noise modeling in the state equations, only flight test data that was collected during a calm day with no turbulence should be used with output error.

The cost function to minimize is the weighted squared error of the innovations $\mathbf{z}(i)-\mathbf{y}(i)$ with their covariance matrix $\hat{\mathbf{R}}$

$$\mathbf{J}(\theta)=\frac{1}{2}\sum_{i=1}^{N}[\mathbf{z}(i)-\mathbf{y}(i)]\hat{\mathbf{R}}^{-1}[\mathbf{z}(i)-\mathbf{y}(i)]^T \tag{2.16}$$

Adding a perturbation to the cost function and performing a second-order Taylor series expansion will result in the following expression.

$$\boldsymbol{J}(\boldsymbol{\theta}_o+\Delta\boldsymbol{\theta})\approx\boldsymbol{J}(\boldsymbol{\theta}_o)+\Delta\boldsymbol{\theta}^T\frac{\partial\boldsymbol{J}}{\partial\boldsymbol{\theta}}\bigg|_{\boldsymbol{\theta}=\boldsymbol{\theta}_o}+\Delta\boldsymbol{\theta}^T\frac{\partial^2\boldsymbol{J}}{\partial\boldsymbol{\theta}\partial\boldsymbol{\theta}^T}\bigg|_{\boldsymbol{\theta}=\boldsymbol{\theta}_o}\Delta\boldsymbol{\theta} \tag{2.17}$$

After setting its derivative to zero, the parameter vector change can be calculated and be used to update the solution

$$\Delta\hat{\boldsymbol{\theta}}=-\left[\frac{\partial^2\boldsymbol{J}}{\partial\boldsymbol{\theta}\partial\boldsymbol{\theta}^T}\bigg|_{\boldsymbol{\theta}=\boldsymbol{\theta}_o}\right]^{-1}\frac{\partial\boldsymbol{J}}{\partial\boldsymbol{\theta}}\bigg|_{\boldsymbol{\theta}=\boldsymbol{\theta}_o} \tag{2.18}$$

$$\hat{\boldsymbol{\theta}}=\boldsymbol{\theta}_o+\Delta\boldsymbol{\theta} \tag{2.19}$$

The elements of the second-order gradient matrix in Equation 2.18 are

$$\frac{\partial J(\boldsymbol{\theta})}{\partial\theta_j\partial\theta_k}=\sum_{i=1}^{N}\frac{\partial\boldsymbol{y}^T(i)}{\partial\theta_j}\hat{\boldsymbol{R}}^{-1}\frac{\partial\boldsymbol{y}(i)}{\partial\theta_k}-\sum_{i=1}^{N}\frac{\partial^2\boldsymbol{y}(i)}{\partial\theta_j\partial\theta_k}\hat{\boldsymbol{R}}^{-1}\boldsymbol{\nu}(i) \tag{2.20}$$

The second order gradient is computational expensive to obtain and is susceptible to numerical error due to higher-order differentiation. An approximation to Equation 2.20 can be made by ignoring the 2^{nd} term in the equation. This would alleviate the computational issues while not significantly sacrificing accuracy because as the optimization nears the solution, the innovation $\boldsymbol{\nu}(i)$ becomes small and the approximation is very good at the solution. The optimization algorithm with this approximation scheme is called the modified Newton-Raphson method. Substituting in the cost function of equation 2.16,

the update for the parameters become

$$\Delta\hat{\boldsymbol{\theta}} = \left[\sum_{i=1}^{N} \frac{\partial \mathbf{y}^T(i)}{\partial \boldsymbol{\theta}} \hat{\mathbf{R}}^{-1} \frac{\partial \mathbf{y}^T(i)}{\partial \boldsymbol{\theta}}\right]^{-1}_{\boldsymbol{\theta}=\boldsymbol{\theta}_o} \left[\sum_{i=1}^{N} \frac{\partial \mathbf{y}^T(i)}{\partial \boldsymbol{\theta}} \hat{\boldsymbol{R}}^{-1} \boldsymbol{\nu}(i)\right]_{\boldsymbol{\theta}=\boldsymbol{\theta}_o} \tag{2.21}$$

$$\hat{\mathbf{R}} = \frac{1}{N} \sum_{i=1}^{N} \boldsymbol{\nu}(i)\boldsymbol{\nu}^T(i) \tag{2.22}$$

where the sensitivities $\frac{\partial \mathbf{y}^T(i)}{\partial \boldsymbol{\theta}}$ are calculated using finite difference approximations to partial derivatives. The modified Newton-Raphson process is repeated until the update parameter vector is sufficiently small or the change in the cost is small per step.

The output error method returns more accurate parameter estimates compared to linear regression because the minimization of error between model and measurement is done on the aircraft states rather than the forces and moments. Since linear regression does not involve integration of equations of motion, it is very susceptible to outliers or extraneous data points as the algorithm will try to minimize the large squared error associated with the outliers. In addition, equation error does not account for measurement noise and treats the model outputs as deterministic. The Output error method do not have these problems; However, output error is computationally expensive and may run into convergence issues. Hence, when still in the stage of determining a suitable model, linear regression can be more useful. It would also help in the convergence of output error if provided with initial parameter values that are close to the solution, such as the parameter estimates by equation error [25].

2.3.3 Filter Error Method and related methods

The filter error method was developed as an aircraft parameter estimation technique that would return accurate results even in the presence of measurement and process noise. When a flight test is being conducted in turbulent air, there are wind effects on the dynamics of the aircraft that are not accounted for by the equations of motion such as Equation (2.15). Equations 2.14 cannot be simply integrated due to the stochastic process noise term. Maine and Iliff published the filter error algorithm that combines the output error method and a Kalman state estimator to account for the noise in the state equations [28]. In their work however, linearized aircraft dynamics are used for the state equations in order to easily calculate the Kalman gain associated with the Kalman state estimator. It is known that for flight maneuvers that exhibit a wide range of α, linear

dynamics do not capture the motion well.

Chowdhary and Jategaonkar further developed this concept by using the nonlinear equations of motion along with an extended Kalman Filter or an unscented Kalman Filter as the state estimators [8]. They called these methods recursive parameter estimation (RPE) methods and have applied it to flight test data of the DLR HFB-320 research aircraft. The parameters estimated with RPE methods are in close agreement to the filter error method, demonstrating the validity of the algorithm. However, the aerodynamic model identified was a linear model based on stability derivatives and the data used was from small-amplitude flight maneuvers ranging from an α of 5° to 7.5°. The general use of filter error and related methods for stall modeling involving nonlinear aerodynamics and large ranges of α is still to be explored.

2.3.4 Frequency Domain Parameter Estimation

The above methods could also be applied to flight test data in the frequency domain. Time history data of the states can be transformed into the frequency domain through Fourier transform. Performing parameter estimation in the frequency domain has its advantages, including direct applicability to control system design, physical insight in terms of frequency content, and less susceptibility to measurement sensor bias [25]. For example, the angle of attack vane must be carefully calibrated for a flight test campaign; however, even with the best calibration a bias error may still manifest in conditions that differ from the calibration values. This error would manifest itself in the inaccurate estimate of the parameters if the identification process is done in the time domain. Yet, in the frequency domain, a Fourier Transform of the measured angle of attack data would remove the bias since it has zero frequency.

2.4 Flight Path Reconstruction

Data compatibility or flight path reconstruction is a process performed on flight test data to remove ill effects due to sensor biases, gains and winds. When performed before a parameter estimation process for aerodynamic modeling, it is called an estimation before modeling (EBM) approach or a 2-step approach [37]. This is especially important for the equation error method because it assumes that there is no error in the state variables. Sri-Jayantha applied this method along with equation error and data partitioning techniques to fully estimate a model of a a Scheweizer 2-32 sailplane up to an angle of attack

of 17° [36].

The usual quantities measured in a flight test are $a_x, a_y, a_z, p, q, r, V, \alpha, \beta, \theta, \phi, \psi$, pressure altitude h, and GPS coordinates X,Y, and Z. The idea is to integrate the accelerations and the rates (a_x, a_y, a_z, p, q, r), considered to be inputs, in time using standard 6-degree-of-freedom kinematic relationships to obtain $V, \alpha, \beta, \theta, \phi, \psi$, and h (outputs) and compare it to the measured values. An error model is assumed for all of these quantities and the parameters are estimated using the techniques mentioned above to make the dataset consistent with itself. For example, a bias in the measurement of forward (x-direction) acceleration will cause a drift in the integrated velocity V. The bias would then be estimated to minimize that drift.

The velocity components in the body frame with respect to the Earth u, v, w are related to V, α, β through the following relationships:

$$V = \sqrt{u^2 + v^2 + w^2} \tag{2.23a}$$

$$\alpha = \tan^{-1}\left(\frac{w}{u}\right) \tag{2.23b}$$

$$\beta = \sin^{-1}\left(\frac{v}{\sqrt{u^2 + v^2 + w^2}}\right) \tag{2.23c}$$

and the error model for the output V is

$$V_E(i) = (1 + \lambda_V)\sqrt{u^2(i) + v^2(i) + w^2(i)} + b_V + v_V(i) \tag{2.24}$$

where V_E is the experimental measured value and $u(i), v(i), w(i)$ would be the integrated values from kinematics using a_x, a_y, a_z, p, q, r, each with their own error model with appropriate bias and scaling parameters added to the measured $a_{x_E}, a_{y_E}, a_{z_E}, p_E, q_E, r_E$. For example, the x-acceleration is the experimental value plus bias and random noise, given by:

$$a_x(i) = a_{x_E}(i) + b_{a_x} + v_{a_x}(i) \tag{2.25}$$

The bias and scaling factors are estimated to make the experimental outputs match the integrated ones from dead-reckoning. First the measured rates and accelerations undergo their respective error model corrections, then it is integrated in time to get the states, in which they go through their own error model corrections as well, and finally this quantity

is compared to the measured states. The following illustrates the process

$$V_E \leftarrow (1+\lambda_V)V + b_V + v_V \leftarrow V = f(a_x, a_y, a_z, p, q, r) \leftarrow a_x = a_{x_E} + b_{a_x} \tag{2.26}$$

A more sophisticated flight path reconstruction algorithm using forcing functions is presented by Bach [2]. It can estimate time histories of the winds during the flight test maneuver as well as the sensor biases.

Chapter 3

Stall Flight Model

3.1 Introduction

This chapter describes the methodology used to extend the lateral aerodynamic database of the Bombardier Aerospace turboprop aircraft to cover upset conditions at high angles of attack. First, a brief outline of the available data and existing model is provided, as they serve as the starting point of the model development. The resources available also strongly influenced the methodology that was adopted; lack of wind-tunnel data for lateral coefficients required modeling methods whose prerequisite is flight test data only.

In this chapter, all terms and graphs (non-dimensional coefficients, accelerometer readings, aircraft states) are expressed in the body axes, whose coordinate system is pictorially shown in Figure 3.1. This is a right-handed coordinate system that is centered at the aircraft's center of gravity, with the x-axis pointed out the nose and parallel to the fuselage, the y-axis pointed towards the right, and z-axis pointed directly downwards. The moments about these axes are defined positive according to the right-hand rule and are depicted by the arrows in the figure. Sensors are often mounted in the body-axis because it is stationary with respect to the aircraft and the measured values could be easily used with aircraft equations of motion without the need of transformation. The symbol δ will be used for control surface deflections where δ_a = aileron, δ_r = rudder, δ_s = spoiler, all expressed in degrees of deflection. A positive control surface deflection will tend to generate negative forces and moments. For example, positive aileron causes a rolling moment to the left; and positive rudder causes yawing to the left. This convention is consistent with Etkin and is common in flight dynamics literature [12].

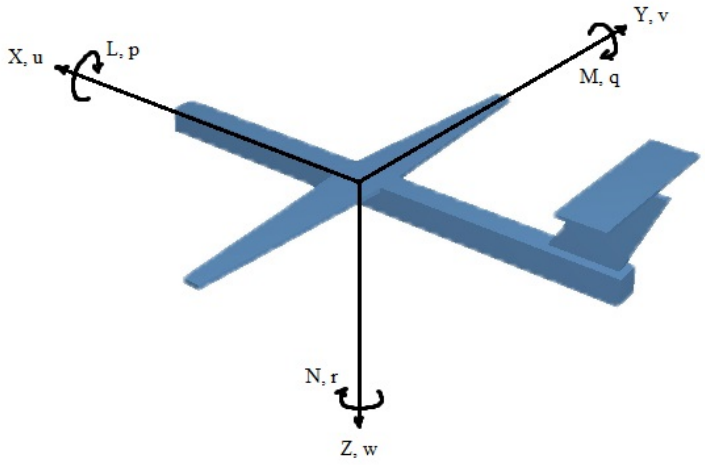

Figure 3.1: Notation for body axes. L = rolling moment, M = pitching moment, N = yawing moment, p = rate of roll, q = rate of pitch, r = rate of yaw, $[X, Y, Z]$ = components of resultant aerodynamic force, $[u, v, w]$ = components of velocity of the c.g. relative to atmosphere

3.1.1 Simulator and Aerodynamic Modeling

Flight modeling mainly consists of two parts, a 6-DOF rigid body dynamics model and an aerodynamic model. The 6-DOF are the location in space (x,y,z) and the attitude (pitch θ, roll ϕ, yaw ψ). The dynamics model contains the equations of motion and the aerodynamic model is a mathematical representation of the physics that would predict the external aerodynamic forces and moments acting on the aircraft. The state of the aircraft is the collective quantities that fully describe the aircraft's situation with respect to the atmosphere and the Earth. The states that are used by the dynamics model are the components of velocity with respect to the atmosphere in the body frame u, v, w, the dynamic rates p, q, r, the attitude ϕ,θ,ψ, the coordinates with respect to Earth x_E, y_E, and altitude h. The aerodynamic and dynamic models form a loop and it can be integrated to simulate the motion of the airplane over time. It is summarized in the Figure 3.2. If the forces and moments acting on the aircraft is known at all times, its trajectory as a function of time can be calculated by integrating the aircraft equations

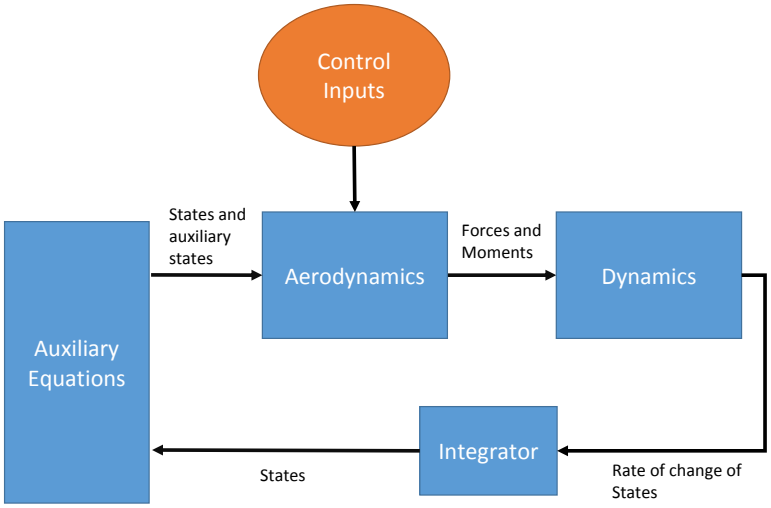

Figure 3.2: Basic Simulator Schematic

of motion [11], which are

$$\dot{u} = rv - qw + \frac{\bar{q}S}{m}C_X - g\sin\theta \tag{3.1a}$$

$$\dot{v} = pw - ru + \frac{\bar{q}S}{m}C_Y + g\cos\theta\sin\theta \tag{3.1b}$$

$$\dot{w} = qu - pv + \frac{\bar{q}S}{m}C_Z + g\cos\theta\cos\phi \tag{3.1c}$$

$$\dot{p} = (c_1 r + c_2 p - c_4 I_p \Omega_p)q + \bar{q}Sb(c_3 C_l l + c_4 C_n) \tag{3.1d}$$

$$\dot{q} = (c_5 p + c_7 I_p \Omega_p)r - c_6(p^2 - r^2) + c_7 \bar{q}S\bar{c}C_m \tag{3.1e}$$

$$\dot{r} = (c_8 p - c_2 r - c_9 I_p \Omega_p)q + \bar{q}Sb(c_9 C_n + c_4 C_l) \tag{3.1f}$$

$$\dot{\phi} = p + \tan\theta(q\sin\phi + r\cos\phi) \tag{3.1g}$$

$$\dot{\theta} = q\cos\phi - r\sin\phi \tag{3.1h}$$

$$\dot{\psi} = \frac{q\sin\phi + r\cos\phi}{\cos\theta} \tag{3.1i}$$

$$\begin{aligned}\dot{x}_E = {} & u\cos\psi\cos\theta + v(\cos\psi\sin\theta\sin\phi - \sin\psi\cos\phi) \\ & + w(\cos\psi\sin\theta\cos\phi + \sin\psi\sin\phi)\end{aligned} \tag{3.1j}$$

$$\begin{aligned}\dot{y}_E = {} & u\sin\psi\cos\theta + v(\sin\psi\sin\theta\sin\phi + \cos\psi\cos\phi) \\ & + w(\sin\psi\sin\theta\cos\phi - \cos\psi\sin\phi)\end{aligned} \tag{3.1k}$$

$$\dot{h} = u\sin\theta - v\cos\theta\sin\phi - w\cos\theta\cos\phi \tag{3.1l}$$

where

$$
\begin{aligned}
c_1 &= [(I_y - I_z)I_z - I_{xz}^2]/\Gamma & \Gamma &= I_x I_z - I_{xz}^2 \\
c_2 &= [(I_x - I_y + I_z)I_x z]/\Gamma & c_3 &= I_z/\Gamma \\
c_4 &= I_{xz}/\Gamma & c_5 &= (I_z - I_x)/\ I_y \\
c_6 &= I_{xz}/I_y & c_7 &= 1/I_y \\
c_8 &= [(I_x - I_y)I_x + I_{xz}^2]/\Gamma & c_9 &= I_x/\Gamma
\end{aligned}
$$

All quantities are expressed in the body axes, u, v, and w are x, y, z components of velocity with respect to the atmosphere; C_X, C_Y, and C_Z are the non-dimensional forces; C_l, C_m, and C_n are the moments about the x, y, and z axes following a right-hand rule convention for pitch, roll and yaw. I_{xx}, I_{yy}, and I_{zz} are principle moments of inertia, I_{xz} is the product of inertia, I_p is the inertia of the spinning propellers; Ω is the angular velocity of the propellers; m is mass; g is the acceleration due to gravity; $\bar{q}$ is dynamic pressure given by $\frac{1}{2}\rho V^2$ where V is total airspeed and ρ the air density; S is the wing area, c is chord, and b is the wingspan. The navigational Equations 3.1j, 3.1j, 3.1j are valid assuming there is no atmospheric wind, however wind effects on aircraft motion relative to an Earth inertial frame can easily be added. In real-time applications such as a flight simulator, the forces and moments experienced at time step t_i is fed into the dynamics block to calculate the rate of change of the states by Equations 3.1. These values are then integrated in time to obtain the states at t_{i+1}. The states at t_{i+1}, along with some auxiliary quantities, such as the air density ρ from h, are fed into the aerodynamic model to predict what the forces and moments are at t_{i+1}. The loop continues as long as the simulation needs to run. Of course, the pilot inputs directly affect the forces and moments, therefore the aerodynamic model has to compute the additional forces and moments due to control surface deflections as well.

Since the dynamics of the aircraft are well understood for rigid body motion, the difficulty in simulating aircraft motion is predicting the aerodynamic forces and moments acting on the aircraft. At low angles of attack, the aerodynamics are relatively linear in the states, and the longitudinal and lateral forces and moments are often decoupled from each other and from the respective lateral and longitudinal states. Hence, stability derivatives are adequate and often used to capture the behavior when the aircraft is perturbed from a trimmed state. At higher angles of attack, flow separation and flow interactions between different parts of the aircraft cause the aerodynamics to be highly non-linear and coupled. This project aims to develop an aerodynamic model that is accurate in predicting the

forces and moments even in upset conditions, and particularly at high angles of attack.

3.2 Resources

3.2.1 Flight Test Data

The two major sources of information that were used to develop the stall model is flight test data and a qualified pre-stall model based on low angle of attack wind-tunnel data. Bombardier Aerospace provided certification flight test data collected in the 1990's for the turboprop aircraft considered in this report. The certification dataset consist of stalls with a stick pusher, a device that automatically applies nose-down control input when conditions nearing a stall are met. There is another set of data that do not have a stick pusher active, which is not from certification. Note that the non-pusher data is not from certification. There are a total of 198 flight maneuvers, categorized into straight stalls, turning stalls, accelerated stalls, and asymmetric thrust stalls. Straight stalls are stalls in which the pilot slows down at $\approx$ 1 knot per second while keeping constant power setting and wings-level. Depending on the power setting, the aircraft may need to climb or descend to achieve the desired deceleration rate. Turning stalls are exactly the same except the aircraft is banked at roughly 30° to either side. Accelerated stalls involve the aircraft slowing down at a progressively faster rate, and achieving a load factor of greater than 1.3 at stall through the use of the elevator. Asymmetric thrust stalls are stalls with significantly different power settings between the left and right engines, while maintaining wings-level and deceleration of $\approx$1 knot per second. Each maneuver is roughly one minute in duration and covers one complete stall starting from quasi-steady (i.e. trim) condition. The data streams are time history recordings of various sensors at the same sampling frequency; measurements that are used in this report include static air temperature, static pressure, total pressure, control surface deflections of rudder, aileron, flaps, spoilers, total pressure from pitot tube, engine torque and rpm, and data from a tri-axial set of accelerometers, a tri-axial of rate-gyros, an α vane, and a β vane. Figure 3.3 shows an example flight test data file containing one straight stall maneuver. a_x, a_y, and a_z are the x, y, z accelerometer readings respectively. Due to proprietary reasons, the presentation of data is without numerical values on the axes.

3.2.2 Qualified Model

The Simulink model of the turboprop aircraft provided by Bombardier Aerospace has passed the Qualification Test Guide (QTG) for flight training simulators as set out by

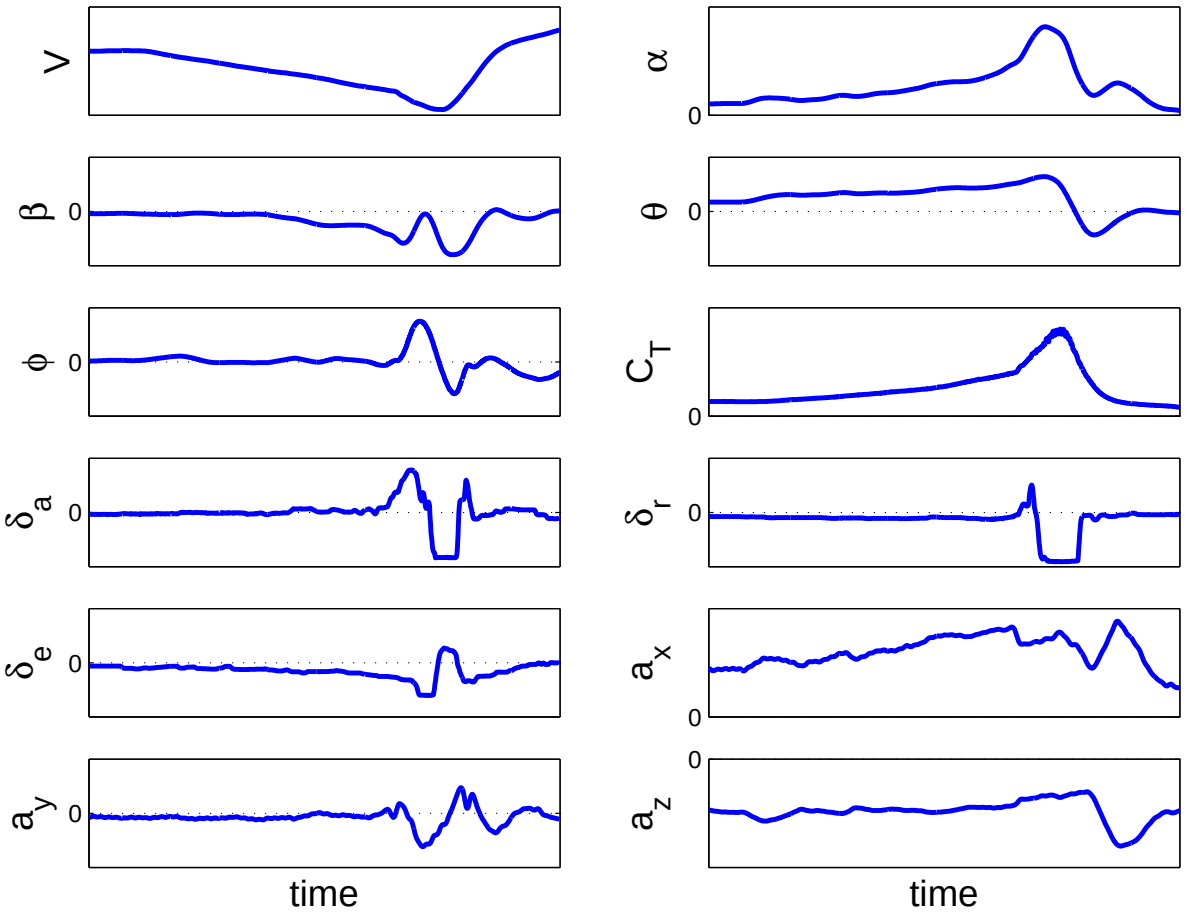

Figure 3.3: Example straight stall flight maneuver

the FAA and Transport Canada. It should be noted that this qualification does not require post-stall modeling [38]. This model is hereinafter referred to as the "qualified model". It employs the full six degrees of freedom nonlinear flight equations governing the motion of a rigid body, as shown in Equation 3.1.

The aerodynamic database of the qualified model was built with wind-tunnel data that Bombardier Aerospace has collected [22]. Most of it is implemented in the form of lookup tables in which aircraft states and are fed into the tables to find the corresponding force and moment coefficients. A small portion of the database is computed from auxiliary equations, such as the tail α computed from kinematic equations. A lookup table is implemented for each independent channel that was tested in the wind-tunnel; for example, $C_{l,\delta_a}(\alpha, \beta, \delta_f, \delta_a)$ is the lookup table for the rolling moment generated due to aileron deflection as a function of angle of attack α, sideslip β, flaps δ_f, and aileron deflection δ_a, and it is one of many lookup tables that constitute the C_l model. Wind-tunnel testing was not done for the lateral force and moment coefficients at high angles of attack, therefore the aerodynamic database does not have data past a certain α. The values used for the simulation outside of the data envelope are either extrapolated or set to be the value of the last data point. Table 3.1 shows the range of states that these lookup tables are valid for, with a different range covered by the basic static wind tunnel tests and the tests for control surfaces. Data does not exist for the forces and moments caused by control surface deflections past $\alpha = 10°$. Based on holding the value at the last data point, all the control surfaces would remain effective as if the aircraft is flying at a relatively low α even though the simulation may be in a stall. It is obvious that this is not true and the qualified model would fail to reproduce representative characteristics of the aircraft at stall. Hence, a stall model must be developed to capture these effects. Although the range of data for β is very large, keep in mind that it was not collected for higher angles of attack.

3.2.3 SIDPAC

System IDentification Programs for AirCraft (SIDPAC) is a MATLAB library written by Eugene A. Morelli that contains useful functions that perform many parameter estimation tasks [31]. The first version was developed at NASA Langley Research Center in 1992, and has been applied to flight data, wind-tunnel data, and simulation data from many different projects. For this particular project, equation error computations, the computation of non-dimensional coefficients, and smoothing of data using a Wiener filter

Table 3.1: QTG Qualified Turboprop Lateral Model Aerodynamic Database Range

State	Min	Max
Static α	-15°	15°
Static β	-40°	40°
Static C_T	-0.1	1.5
Flaps	0	35
Controls α	-4°	10°
Controls β	-35°	35°
Controls C_T	0	1

was carried out with SIDPAC. Version 2.0 of the software package is included with the purchase of the book *Aircraft System Identification: Theory and Practice* by Klein and Morelli [25]. Modifications to the programs have been made to better suit the needs of this particular project.

3.3 Methodology

The turboprop aircraft that is being modeled has 5 different flap conditions, namely 0, 5, 10, 15, and 35. Since flaps significantly change the geometry of the aircraft, it is best to model them separately as the geometry change may affect the aircraft's characteristics at stall. Therefore, the modeling effort is repeated for each flap condition and a total of five models are developed. They are combined later into the extended model.

Before any modeling work can be done, the flight test data has to be processed. All measured states should be transformed to reflect the value as seen from the center of gravity of the aircraft, as the equations of motion in Equation 3.1 are defined at the CG of the aircraft. Although accelerometers are usually mounted with the orientation the same as the body-axis, they rarely can be placed exactly at the center of gravity of the aircraft. Reasons include that the c.g. is not at an accessible location, such as inside a structural element, and that the c.g. is not stationary while the aircraft is burning fuel or when carrying different payloads. Therefore, most flight test measurements will need to be transformed to c.g. values before the modeling process could continue. α and β vanes are mounted externally in a location far away from the fuselage and c.g.; depending on the exact location of the sensor location, rolling, pitching, and yawing of the aircraft will induce local flow changes around the aircraft that may be picked up by the sensor. However, that effect must be removed since it does not represent the values seen from

the aircraft's center of gravity.

Once the sensor data is transformed to c.g., the accelerometer and rate gyro measurements are converted to non-dimensional force and moment coefficients for ease of modeling, since non-dimensional quantities can be related to the states directly through a postulated model and is independent of dynamic pressure and airspeed. The measurements are converted using the following equations; only the lateral coefficients are listed below.

$$C_{l,meas} = \frac{I_{xx}\dot{p} - I_{xz}(\dot{r} + pq) + (I_{zz} - I_{yy})qr}{\frac{1}{2}\rho V^2 Sb} \tag{3.2}$$

$$C_{n,meas} = \frac{I_{zz}\dot{r} - I_{xz}(\dot{p} - qr) + (I_{yy} - I_{xx})pq + I_p\Omega_p q}{\frac{1}{2}\rho V^2 Sb} \tag{3.3}$$

$$C_{Y,meas} = \frac{ma_y}{\frac{1}{2}\rho V^2 S} \tag{3.4}$$

I_p and Ω_p are the propeller's moment of inertia and angular frequency. A pitch rate q of the aircraft would induce a yawing moment due to the gyroscopic effects of the spinning propellers of the turboprop. This effect is accounted for in the dynamics of the training simulator and should not be included in the aerodynamic modeling process. Hence, its effect is removed from the total C_n experienced by the aircraft through Equation 3.3, leaving only the C_n caused by the aerodynamics. For the set of 198 stall maneuvers, the pitch rate was never large enough to make the term $\frac{I_p\Omega_p q}{0.5\rho V^2 Sb}$ significant. The highest pitch rates were near the maximum angle of attack, when the stick-pusher activated and applied a large nose-down moment on the aircraft, or when the aircraft naturally stalled and had a tendency to nose-down. The pilots always applied substantial rudder inputs in those events, resulting in rather large C_n; the effect due to the gyroscopic effects of the spinning blades of the propeller is $< 0.5\%$ of the total C_n.

3.3.1 Data Partitioning

It was found that most of the nonlinearity in the aerodynamics is with respect to angle of attack α. However, in order for a single polynomial model to capture the nonlinear dependence on a wide range of α, nonlinear regressors such as α^2, α^3, $\alpha\beta$, $\alpha\delta_a$ would need to be added. α^2 and α^3 are terms which would model the nonlinear contribution of α directly on the aerodynamic coefficient, whereas $\alpha\beta$ and $\alpha\delta_a$ are terms that model the interdependency of β and δ_a with α on the aerodynamic coefficient. For example, if the change in C_l due to aileron input depends on the angle of attack, cross-terms such as

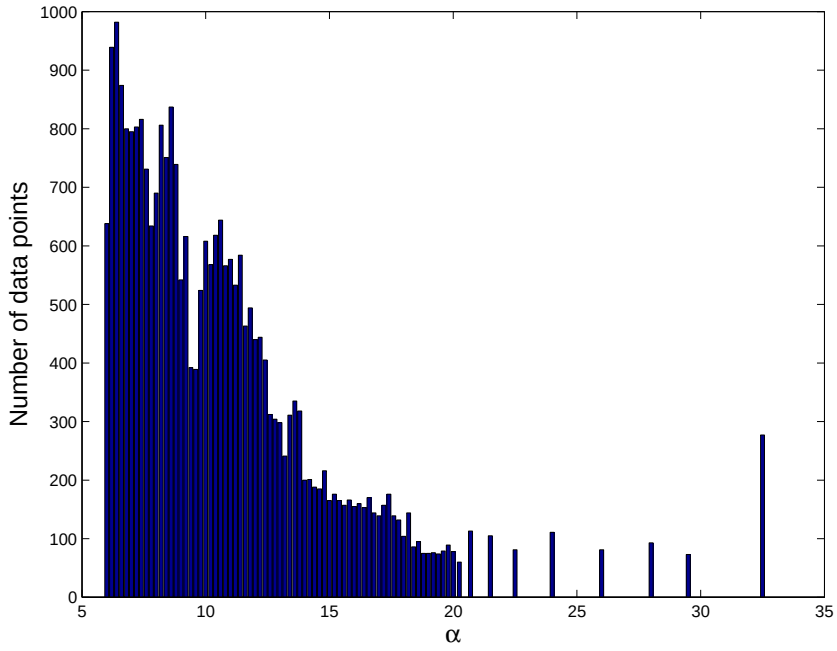

Figure 3.4: Data partitioning into α bins

$\delta_a\alpha$ would be needed. As such, the need to capture other effects' dependency on angle of attack would further increase the number of terms needed in the model. In addition, the coefficients associated with these terms are difficult to estimate well with the data available due to the low excitation of states and data collinearity that are discussed in detail in Section 3.3.3. These are some of the major difficulties associated with the use of a complicated aerodynamic model structure to cover a large range of α.

The method of data partitioning based on an α range as proposed by Batterson solves this problem [4]. Although the total number of parameters that needs to be identified is still very high (number of bins $\times$ number of parameters in the postulated model), lower information content is required in the data to successfully estimate parameters, simply because the problem is subdivided into many smaller estimation problems, each with a fewer number of parameters.

Figure 3.4 shows the data from flight tests with flaps 10 partitioned according to angle of attack. From 6° to 20°, the bins are 0.2° wide. However, the bins at higher angles of attack are coarser and cover a wider range of α due to a lack of data points. Even with wide ranges that span 2.5° of α, the bins barely manage to have over 100 points in the higher angle of attack regions. Since an equation error process has to be set up in each bin, the number of data points should be kept at a reasonable number that is

significantly higher than the number of parameters to be estimated. This ensures a well-posed regression problem. That said, having finer bins whenever possible can offer a good metric on whether a parameter is well-identified; well-identified parameters should have similar values amongst adjacent bins. For example, a stability derivative C_{l_β} should not vary wildly from $\alpha = 15°$ to $\alpha = 15.2°$ and $\alpha = 14.8°$; if it does, there is a high chance that it is due to modeling or estimation error. In addition, if the aerodynamics have a strong dependency on alpha, then a large bin will still have significant alpha dependency left within the bin.

3.3.2 Delta (Δ) Model

Although the qualified model's aerodynamic database does not extend up to high α and is generally not meant for modeling stall, time history comparisons of the qualified model's output to flight test data showed that it was able to capture some of the trends at high α but is not accurate in magnitude. For example, often the qualified model over-predicts the magnitude of yawing moment at stall, but its prediction had the same time history profile as the measured yawing moment.

It is known that a model structure with non-linear terms or with a large number of terms are hard to estimate accurately as previously discussed. Yet, non-linear terms are needed to model the complicated aerodynamics near stall. Furthermore, this conflicting problem is exacerbated by the lack of information content in the available flight test data, so it is virtually impossible to properly identify a highly nonlinear model structure.

As noted previously, the qualified model predicts the trends in the flight test well in most cases, but is not accurate in predicting the magnitude of the forces and moments. To take advantage of this, it is proposed that a relatively linear correction (Δ) model added to the qualified model may be able to correct for the shortcomings of the qualified model. Some of the nonlinearities of the aerodynamics are already captured by the qualified model, as shown by the match with flight data. The Δ model would only need to bridge the gap between the qualified model and the flight test data, which is more linear as opposed to modeling the moments and forces entirely from scratch. In this framework, the quantity that the Δ model would try to match is the error of the qualified model, and not the aerodynamic coefficients themselves.

The error of the qualified model is given by:

$$C_{i,error} = C_{i,meas} - C_{i,qualified} \qquad i = l, m, Y \tag{3.5}$$

A linear regression problem is set up to minimize the difference between the Δ model and the $C_{i,error}$ in Equation 3.5. The outcome of the regression would be a Δ model that is used to cover the shortcomings of the qualified model at stall. The procedure for obtaining the Δ model is analogous to the standard Equation Error discussed in Chapter 2. The process is illustrated in an example below for ΔC_n. First, start with a postulated Δ model:

$$\Delta C_n = \Delta C_{n_0} + \Delta C_{n_\beta}\beta + \Delta C_{n_p}\hat{p} + \Delta C_{n_r}\hat{r} + \Delta C_{n_{\delta_r}}\delta_r + \Delta C_{n_{C_T}}C_T \tag{3.6}$$

For each α partition, formulate the regressor matrix according to the postulated model structure,

$$\boldsymbol{X} = \begin{bmatrix} 1 & \beta(1) & \hat{p}(1) & \hat{r}(1) & \delta_r(1) & C_T(1) \\ 1 & \beta(2) & \hat{p}(2) & \hat{r}(2) & \delta_r(1) & C_T(2) \\ 1 & \beta(3) & \hat{p}(3) & \hat{r}(3) & \delta_r(1) & C_T(3) \\ \vdots & \vdots & \vdots & \vdots & \vdots & \vdots \\ 1 & \beta(N) & \hat{p}(N) & \hat{r}(N) & \delta_r(N) & C_T(N) \end{bmatrix} \tag{3.7}$$

where N is the total number of data points available in an α partition. Note that to estimate a constant offset for the model, the regressor matrix has a column of 1's. Although it appears in the regressor matrix, 1 is not a regressor in the strict sense. It is there so that the constant parameter of the model can be estimated. Next, formulate the vector of values that the Δ model is to match, which is the qualified model error, or in other words, the effects that were not captured by the qualified model,

$$\boldsymbol{z} = \begin{bmatrix} C_{n,error}(1) \\ C_{n,error}(2) \\ C_{n,error}(3) \\ \vdots \\ C_{n,error}(N) \end{bmatrix} \tag{3.8}$$

As mentioned in the literature review section, the goal is to minimize the difference in the least-squares sense between the postulated model output $\boldsymbol{X\theta}$ and the values $\boldsymbol{z}$ through

optimization of the parameter vector:

$$\boldsymbol{\theta} = \begin{bmatrix} \Delta C_{n_0} \\ \Delta C_{n_\beta} \\ \Delta C_{n_p} \\ \Delta C_{n_r} \\ \Delta C_{n_{\delta_r}} \\ \Delta C_{n_{C_T}} \end{bmatrix} \tag{3.9}$$

The best estimate for $\boldsymbol{\theta}$ is one that optimizes the least-squares cost function shown in Equation (2.12). The equation error method of parameter estimation therefore gives:

$$\hat{\boldsymbol{\theta}} = (\boldsymbol{X}^T\boldsymbol{X})^{-1}\boldsymbol{X}^T\boldsymbol{z} \tag{3.10}$$

Suppose the angle of attack bins from the data partitioning are centered at 12°, 12.2°, 12.4°, ..., 20°, the above parameter estimation procedure would be performed for each bin separately. The estimated parameters from each bin $\hat{\boldsymbol{\theta}}_{\alpha=12^\circ}$, $\hat{\boldsymbol{\theta}}_{\alpha=12.2^\circ}$, $\hat{\boldsymbol{\theta}}_{\alpha=12.4^\circ}$, ..., $\hat{\boldsymbol{\theta}}_{\alpha=20^\circ}$ would constitute the Δ model. Finally, the Δ stall model is added to the qualified model to become the extended model shown mathematically in equation (3.11), where $C_{i,qualified}$ is the qualified model.

$$C_{i,extended} = C_{i,qualified} + \Delta C_i \qquad i = l, n, Y \tag{3.11}$$

3.3.3 Difficulties

Data Collinearity

In general, regressor time series must be dissimilar in form for good parameter estimation, because if any regressor can be scaled to approximately match another, there is an indeterminacy in how variations in the dependent variable can be modeled, and data collinearity exists. The data used for this project does not include maneuvers that had control inputs specifically meant for exciting the states for model identification. Morelli has shown that a doublet input or a 3-2-1-1 input can significantly add information content to a flight test maneuver and subsequently help in parameter estimation [33]. Instead, the data available were certification flight tests in which the airplane approaches stall in a quasi-steady manner while the pilot is only using the controls to maintain trim. As expected, a lot of data channels were correlated with each other and it made

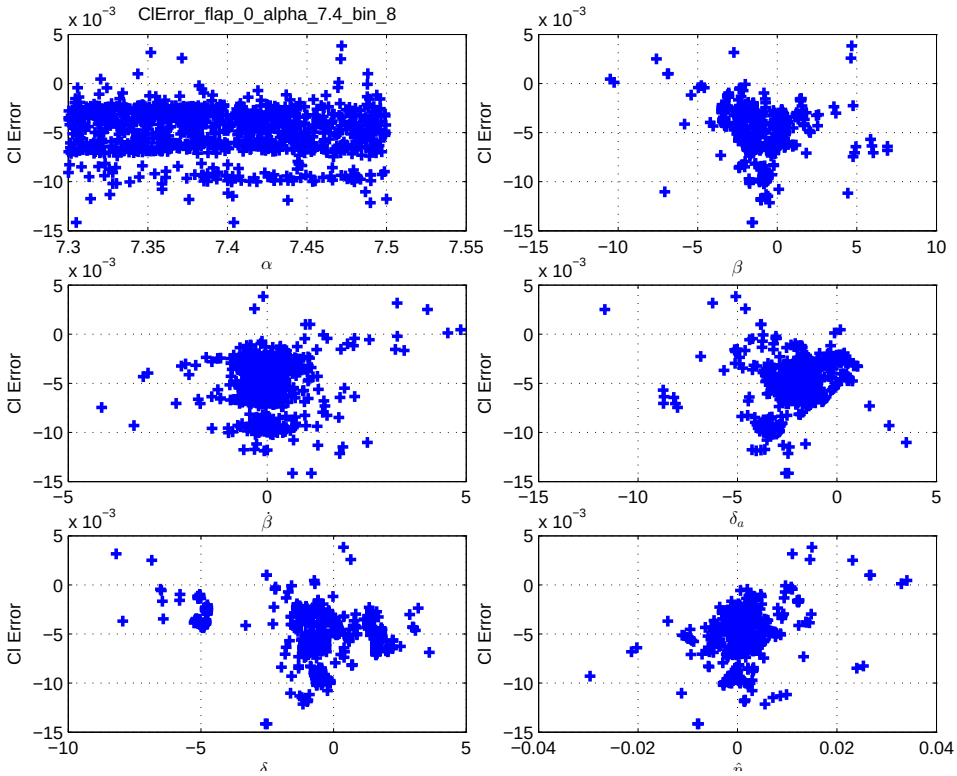

Figure 3.5: Error vs. Regressor Plot with low excitation of states

parameter estimation of anything but a simple model extremely difficult and prone to error. Figure 3.3 shows how α varies with C_T co-linearly, which would make separating their contribution to aerodynamic coefficients very difficult. Any successful identification basically relies on the minute differences between the two channels of data. If they were identical, then the problem becomes ill-posed and a singularity will appear in the math in the form of a non-invertible matrix. This problem was a significant setback in the efforts to make a longitudinal stall model as C_T and α both contribute to C_L but are collinear. Similar difficulties are encountered in the lateral model development since wind-tunnel data from the qualified model showed C_T as a contributor to all coefficients.

Low excitation of important states

Low excitation of states is another problem that effected the lateral model development significantly. As the pilot flies the aircraft into a stall, as seen in Figure 3.3, most of the lateral states stay relatively constant and do not traverse a wide range of values. $delta_a$, δ_r, p, and ϕ have just tiny fluctuations around the zero axis in the pre-stall region. It is not until stall that large changes in the reading occur. If there was no air turbulence and the pilot controlled the aircraft perfectly, ϕ, δ_r, C_l, C_Y, C_n would all be very close

to zero except for perhaps some trim required from the ailerons and rudder to balance various asymmetries in the aircraft or its thrust. Figure 3.5 shows a C_l error vs regressor plot for relatively low α bin, which illustrates this problem. Note that the ailerons have very few data points outside of the -5° to 0° cluster, which meant the pilots did not use the ailerons much in this angle of attack range. Trying to estimate parameters with data that have extremely low signal to noise ratio such as this case will return erroneous results. The C_l and δ_a values are almost 0 throughout this angle of attack range, with slight variations probably due to noise and turbulence only. The erroneously estimated parameter to the aileron effectiveness $\Delta C_{l_{\delta_a}}$ is positive in this particular bin, which from a visual inspection shows that it is inconclusive at best. If the qualified model is very good in its predictive capabilities at low angles of attack, the C_l error should remain zero most of the time; and if there was more excitation in the range and the number of data points in which the ailerons deflected, then a $\Delta C_{l_{\delta_a}}$ would have been identified very close to zero. This would be consistent with the hypothetical assumption that the C_l qualified model is good in that α region. It is believed that the Δ stall models identified are not accurate below a certain angle of attack due to this reason. The coefficient of determination value R^2 could still be satisfactory, but some of the parameters may be erroneously identified. Most of the flight data have more excitation as the α becomes progressively near stall, which would aid in the proper identification of parameters. Another potential problem is caused by the pilots actively trying to maintain all forces and moments in trim. That is beneficial in terms of performing the flight maneuver perhaps; however, the suppressed dynamics do not show up in the measured coefficients and is detrimental in a system identification point of view. For example, consider the roll asymmetry C_{l_0} due to an increase in α be perfectly counteracted by the aileron inputs. In this case, the measured C_l from the rate-gyros would effectively be zero, and from the parameter estimation process we would draw the erroneous conclusion that the aircraft does not exhibit asymmetry and that the ailerons are ineffective in generating rolling moment. In other words, low excitation in the measured C_l, C_n, and C_Y would make parameter estimation virtually impossible. Fortunately, the dynamics are being excited near stall as there are substantial aileron and rudder inputs while the force and moment coefficients are not in trim (i.e. zero).

3.3.4 Model Structure Determination

Morelli's Multivariate Orthogonal Functions (MOF) method was used to generate a model structure for stall modeling. As mentioned in the literature review, MOF is implemented

in MATLAB by Morelli and could be obtained through purchase of his book [25]. It was applied to the datasets of this project, however the results were not satisfactory. The model terms returned often had little physical sense associated with them and were difficult to interpret to the modeler. One example would be $\delta_e\delta_a C_T$; although one could see that the effect exists, it is hard to interpret how the three control inputs would have a coupled effect on the forces and moments on the aircraft. The lack of prior knowledge of how $\delta_e\delta_a C_T$ should behave will limit the amount of engineering insight towards the parameter estimation process. It may be reasonable to include a few such terms if the inclusion of them improves the model fit significantly, but too many would make the model difficult to interpret physically. MOF often generated a model that contains many of these complicated terms. Perhaps for the dataset that was available for this project, the MOF process deemed the model terms as more efficient in explaining the measured forces and moments than terms of a lower degree and simpler nature.

The model structure returned by MOF changes depending on the order in which the independent variables are supplied. For example, if the input vector was $[\alpha, \beta, \delta_a]$, α would have a higher chance of appearing in the final model structure than δ_a. In addition, the model structures returned by MOF also did not have good predictive capabilities since time-history comparisons to flight test did not show good fits for the moment and force coefficients, especially on data that were not used in the identification.

MOF was initially used for the regressor selection of this project, but due to the above reasons it was later used only to generate candidate regressors, which are to be selected through a different process. Note this is in no way suggesting that Multivariate Orthogonal Functions do not work in general. It is suspected that the method did not work well due to the nature of the flight test maneuvers. MOF requires the data to have a clear excitation of states so that it can efficiently capture the dependencies in as few terms as possible using mathematical metrics discussed in Chapter 2. These metrics most likely do not work as well when the data is highly correlated and when there is low excitation [30].

The adopted method for determining the model structure is somewhat of a manual one. First, a list of candidate regressors are generated. These can be from MOF, the public literature, the qualified flight model, or from engineering judgement based on physical insight. For example, $\delta_s\dot{\alpha}$ was included in the candidate regressor pool since $\dot{\alpha}$ affects the flow re-attachment and the spoilers' effectiveness depend on the flow condition on the

wing. This term was later found to be well-identified and improved the model fidelity compared to flight data.

The next step is to plot the model error against all the candidate regressors for each α bin, and observe direct correlations between the regressand and the regressor. An example plot is shown in Figure 3.6 for the model rolling moment error at an angle of attack near stall. There is a clear relationship between aileron δ_a and the C_l model error near stall, which is expected for an aerodynamic database that only covers up to α of $10°$. If a line were to fit through the C_l model error vs δ_a plot, the slope would be positive, meaning positive aileron generates positive rolling moment. When the Δ correction model is added to the qualified model, this translates to a lowered aileron effectiveness at that angle of attack. The figure is for data points that span a small range of α, and the C_l error vs. α graph shows that within that small range of α, C_l can be treated as not dependent on α. The band of data points in the graph span the α range of the bin, but the C_l error is more or less random. All regressors with a visually identifiable trend to model error should be included in the model structure. For the particular figure in discussion, other regressors that have a obvious relationship are the spoilers δ_s, β, and $\hat{r}$.

Once candidate regressors are formed, the selection process an iterative one. A preliminary model structure for the Delta (Δ) model is identified with partitioned data as discussed in Section 3.3.2. As mentioned before, the parameter estimation process is independent for each bin. Therefore, if a parameter is well identified, its estimated value should be similar for bins that are close in α with each other. Large fluctuations in value among adjacent bins suggest that the parameter estimation process struggled to find a strong correlation between the regressor and the measured aerodyanmic coefficients. It is caused by the condition shown in Figure 3.5 where if a line were to be fitted to the C_l error of the qualified model vs β plot, the confidence in the fit would be low. The fluctuations come from a poor fit of a linear line to data that do not suggest any relationship, and the slope of the fitted line is highly sensitive to noise could therefore fluctuate wildly amongst adjacent bins which have a similar condition but with slightly different measurements due to noise. Therefore, this qualitative metric of parameter variance among adjacent bins is used to select or reject candidate regressors in the preliminary model structure. Only the parameters that were well-identified were kept in the structure. After that, the identified Δ-model is combined with the qualified model which forms the extended model. The extended model's output of aerodynamic coefficients is compared to measured flight data in a time-history plot. The plots are deemed satisfactory if the extended model captures

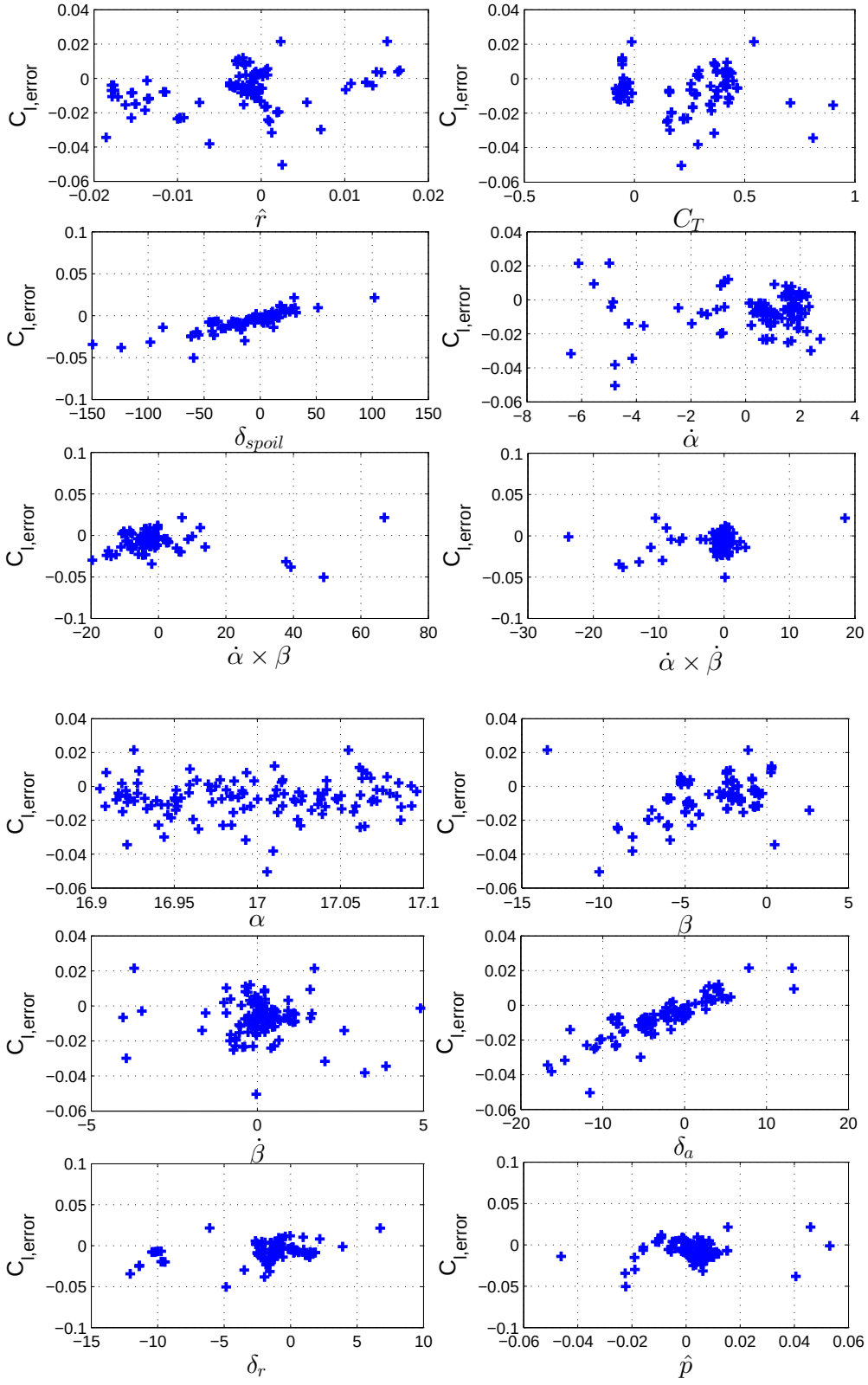

Figure 3.6: Error vs. Regressor Plot

the general trend of the changes of the force and moment coefficients during the flight. If not, then the search for a regressor with better predictive capabilities continues. A more detailed discussion of the comparisons are in Chapter 4.

3.3.5 Blending

At low angles of attack, the qualified aerodynamic model would be used in the training simulator and that would ensure that it is still QTG qualified. At higher angles of attack, the aerodynamic model would be the extended model, which is what the above process generates.

Although it is expected that the stall model corrections to be small at low angles of attack, large corrections could still be erroneously identified due to low excitation of states. Nevertheless the correction is non-zero. To ensure a smooth transition from the qualified model to the extended model, a blending region defined by angle of attack is implemented. This is done to avoid discontinuities in forces and moments triggered by the switching between the extended model and qualified model. A linear blending procedure triggered by angle of attack similar to Liu's work on extending the aerodynamic model of a Boeing 747 is used [27], so the model output transitions from the qualified model to the extended model according to Equation (3.12). $C_{i,extended}$ is the final extended model, $C_{i,qualified}$ is the original qualified model, and ΔC_i is the Δ-model.

$$C_{i,extended} = \begin{cases} C_{i,qualified} & \text{if } \alpha \leq \alpha_l \\ C_{i,qualified} + \frac{\alpha-\alpha_l}{\alpha_u-\alpha_l}\Delta C_i & \text{if } \alpha_l < \alpha \leq \alpha_u \\ C_{i,qualified} + \Delta C_i & \text{if } \alpha > \alpha_u \end{cases} \tag{3.12}$$

3.4 C_l Model

Following the methodology described above, the steps that were used to arrive at the model is

1. Group the flight data based on flap setting, the following steps are to be done for each flap setting.

2. Select bin ranges for alpha partitioning such that each bin will have roughly 10 times the data points as there are parameters to identify in the model.

3. Within the group of data with the same flap condition, partition all the data into their respective α bins.

4. Postulate a model structure based on the error vs. regressor list, adding splines if a non-linearity is observed in the error vs regressor plots.

5. For each bin, estimate the parameters in the model using equation error, and store the parameter values in a vector. Figure 3.4 show the identified parameters in blue for different α bins.

6. Observe the variance of the identified values of parameters compared to that of adjacent α bins. Since each parameter estimation step for the bins are independent, similar values of parameters identified for similar angle of attack conditions strongly suggest that the parameters were well-identified. The values of parameters should change smoothly as a function of angle of attack and not fluctuate wildly, as it is unlikely the aerodynamic forces and moments fluctuate wildly as a function of α. If some of the parameter values seem to vary wildly as α changes, then repeat step 4 to pick parameters that better capture the underlying physical dependency. Judging by this qualitative metric, ΔC_{l_0} in Figure 3.4 is better identified at the α as compared to the middle range of the plotted α axis.

7. Once all the bins have been well-identified, a smoothing spline is fit to the parameters vs. α so that they have a smooth transition as the angle of attack changes. For example, the contribution to rolling moment due to aileron C_{l,δ_a} is $C_{l_{\delta_a}}\delta_a$, but it would be discontinuous at the boundaries of the α bins since $C_{l_{\delta_a}}$ at 12° α is different from $C_{l_{\delta_a}}$ at 12.2° α. By fitting a smoothing spline to each of the parameters, the spline function could then be used to interpolate any α and will ensure a smooth transition of the forces and moments; $C_{l_{\delta_a}}\delta_a$ becomes $C_{l_{\delta_a}}(\alpha)\delta_a$, where $C_{l_{\delta_a}}(\alpha)$ is the spline function. The splines are computed using MATLAB's csaps.m function, which aims to minimize the following cost function shown in Equation (3.13)[9],

$$J = p\sum_{j=1}^{n} |y_j - f(\alpha_j)|^2 + (1-p)\int |\frac{d^2 f}{dt^2}|^2 dt \tag{3.13}$$

where y_j is the parameter value at the j^{th} alpha, p is a parameter that specifies how much smoothing is applied, and f is the smoothing spline. When $p = 1$, the selected spline would go through every y_j exactly, as that would give the lowest cost since the 2^{nd} term is zero. However, when $0 < p < 1$, the integral of the 2^{nd} derivative of the spline function is non-zero and punishes high curvatures. This achieves the

smoothing effect, since an optimization process would return a spline f that would follow y_j values but not as aggressively. The smoothing factor p is chosen to be 0.4 for most of the parameters based on visual inspection of the effects and removing local fluctuations in value. Figure 3.4 shows the smoothing splines in red through the parameters for each regressor.

8. Inspect time history match of the coefficient to flight test data. Example time-history fits are shown in Chapter 4. In addition, inspect the extended aerodynamic database for common effects that occur during stall, such as reduced roll damping and whether such effects are reasonable. More discussion on this topic is in Chapter 4. If either of the two have behavior that is not reasonable based on the literature stall behavior, then consider starting from from step 4 again.

The model structure selected for the C_l model is shown in equation (3.14).

$$\begin{aligned} \Delta C_l \quad = \quad & \Delta C_{l_0} + \Delta C_{l_\beta}\beta + \Delta C_{l_p}\hat{p} + \Delta C_{l_r}\hat{r} \\ & + \Delta C_{l_{\delta_a}}[(\delta_a - 2^\circ)_+ + (\delta_a + 2)_-] + \Delta C_{l_{\delta_r}}\delta_r + \Delta C_{l_{C_T}}C_T \\ & + \Delta C_{l_{C_{T,diff}}}C_{T,diff} + \Delta C_{l_{\delta_s}}\delta_s + \Delta C_{l_{\dot{\beta}}}\dot{\beta} + \Delta C_{l_{\dot{\alpha}\delta_s}}\dot{\alpha}\delta_s \end{aligned} \tag{3.14}$$

$$(\delta_a - 2^\circ)_+ = \begin{cases} \delta_a - 2^\circ, & \text{if } \delta_a - 2^\circ > 0 \\ 0, & \text{otherwise} \end{cases} \tag{3.15}$$

$$(\delta_a + 2^\circ)_- = \begin{cases} \delta_a + 2^\circ, & \text{if } \delta_a + 2^\circ < 0 \\ 0, & \text{otherwise} \end{cases} \tag{3.16}$$

By examining qualified model error vs regressor plots, the terms that had good predictive capability were added to the model. The extended model has relatively few terms yet it is able to closely match the measured C_l from flight data. The only cross-term used is $\dot{\alpha}\delta_s$, which is found to have a clear relationship to the C_l error through error vs regressor plots.

The difference in thrust coefficient $C_{T,diff}$ between the left and the right engines are defined such that a positive value would tend to produce a positive yawing moment C_n. Expressed mathematically,

$$C_{T,diff} = C_{T,left} - C_{T,right} \tag{3.17}$$

$$\delta_s = \delta_{s,right} + \delta_{s,left} \tag{3.18}$$

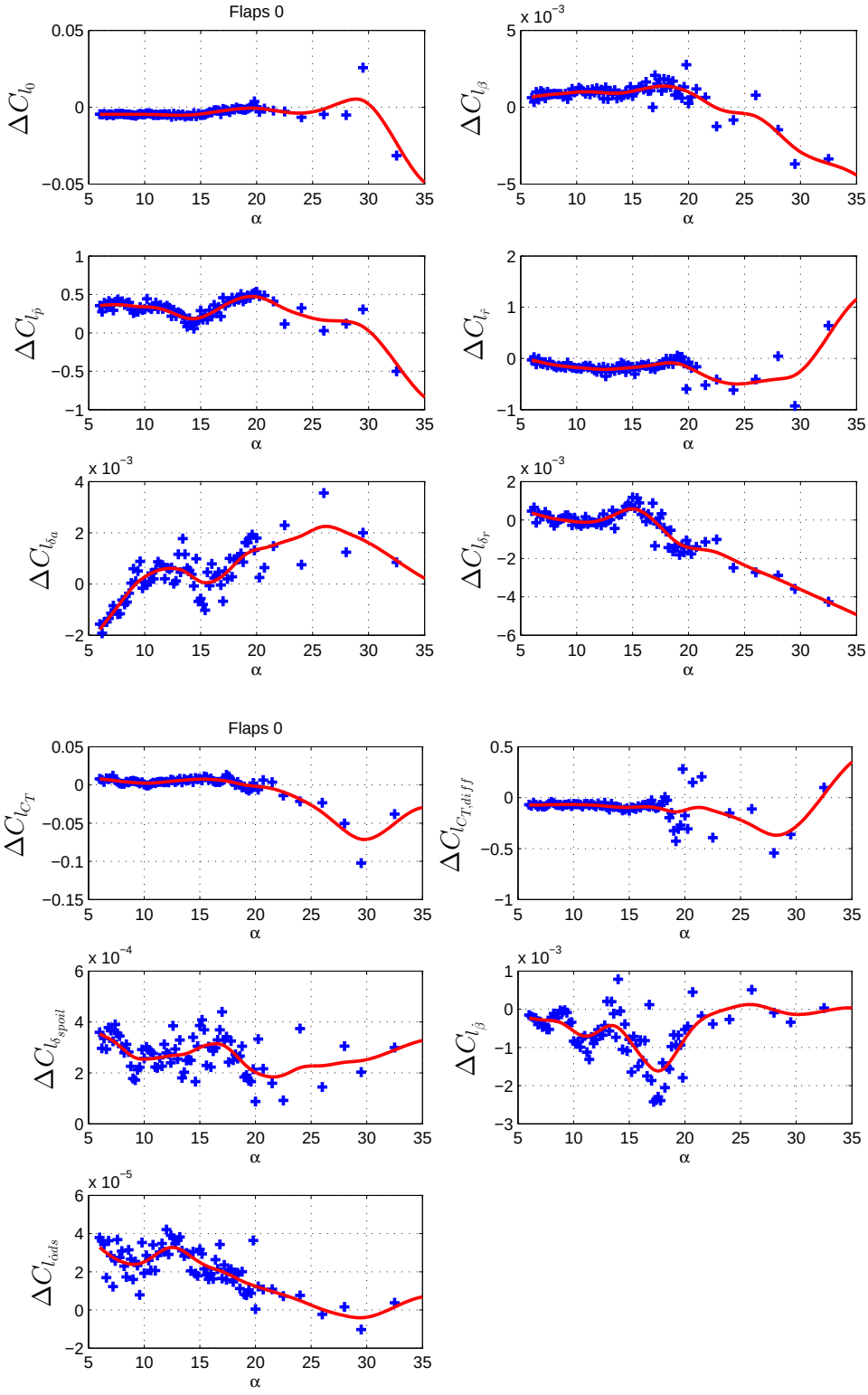

Figure 3.7: Estimated ΔC_l parameters for flaps 0

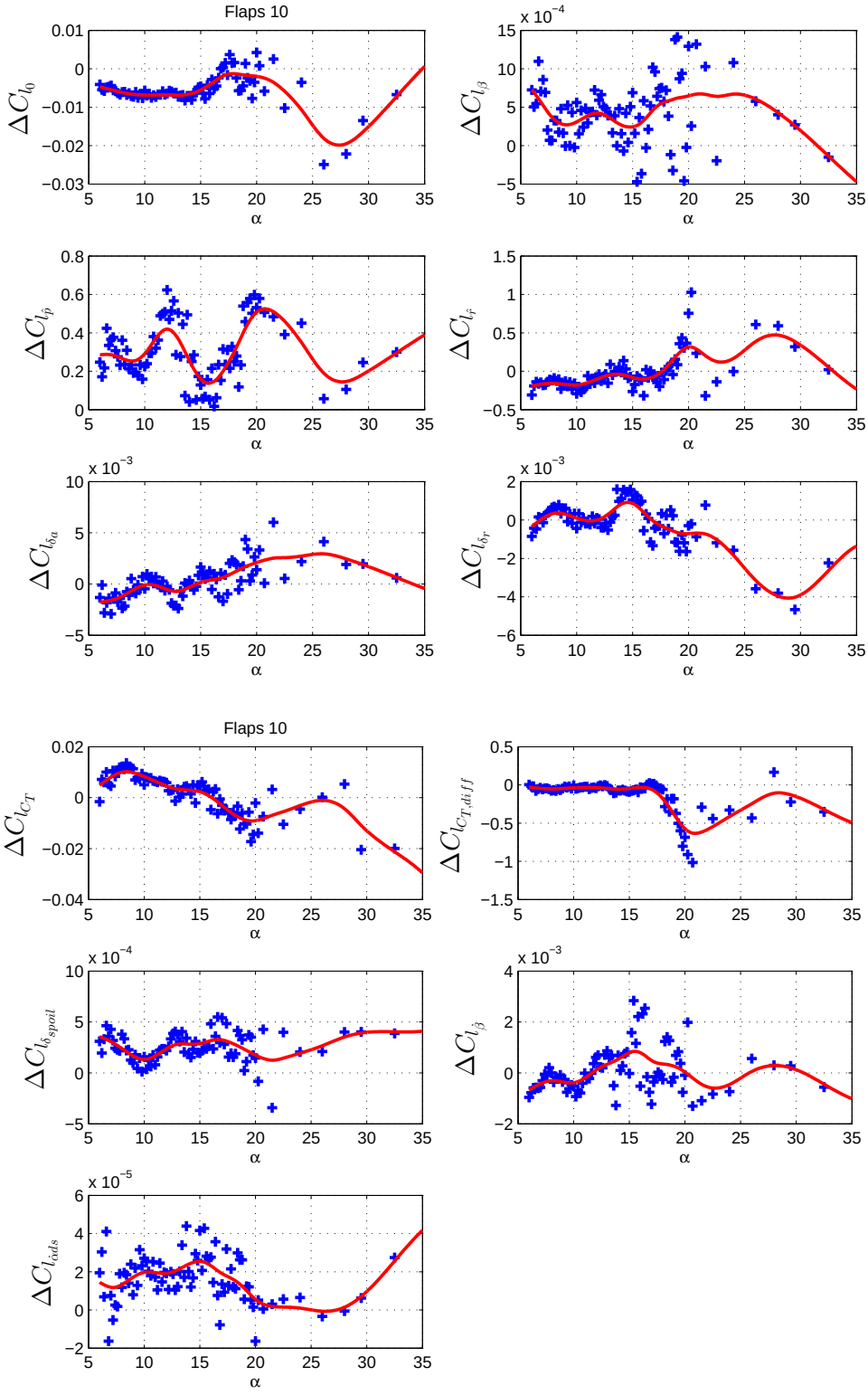

Figure 3.8: Estimated ΔC_l parameters for flaps 10

The parameters in Equation (3.14) are estimated separately in each α partition and each bin would have different values for the parameters. By fitting a spline through the parameters as discussed previously, Equation (3.19) becomes the final ΔC_l stall model. The parameters are cubic splines as a function of α. The parameter values are computed by the splines at the given the angle of attack; they are then multiplied by their respective regressors and summed. That value is then added to the qualified model to become the extended model.

$$\begin{aligned}\Delta C_l \quad = \quad & \Delta C_{l_0}(\alpha) + \Delta C_{l_\beta}(\alpha)\beta + \Delta C_{l_p}(\alpha)\hat{p} + \Delta C_{l_r}(\alpha)\hat{r} \\ & + \Delta C_{l_{\delta_a}}(\alpha)[(\delta_a - 2^\circ)_+ + (\delta_a + 2^\circ)_-] + \Delta C_{l_{\delta_r}}(\alpha)\delta_r + \Delta C_{l_{C_T}}(\alpha)C_T \\ & + \Delta C_{l_{C_{T,diff}}}(\alpha)C_{T,diff} + \Delta C_{l_{\delta_s}}(\alpha)\delta_s + \Delta C_{l_{\dot{\beta}}}(\alpha)\dot{\beta} + \Delta C_{l_{\dot{\alpha}\delta_s}}(\alpha)\alpha\delta_s\end{aligned} \tag{3.19}$$

The final implementation of the stall model is in the form of MATLAB Simulink lookup tables for easy visualization and integration. Several models could be easily tested and swapped by loading a different data file that contains the values for the lookup table. This is useful for running experiments in the future where pilots are asked to fly multiple versions of the model. The extended model being developed is for an angle of attack of up to 10° past stall, as discussed in Chapter 1. Although few, there are data points up to 14° past stall. However, the amount of bins in the extreme α region is small and is therefore hard to judge whether the parameters are reasonably identified by observing adjacent bins. Since the confidence in parameters at high α is not particularly high and the requirement of the project does not call for the modeling of that region, the extended model's lookup tables are clipped at 10° α past stall. If any time during flight simulation the α is beyond what the lookup tables have data for, it will refer to the values at 10° α past stall.

3.4.1 Spoiler Effect

The flight test data files have four separate channels for spoilers; they are: left inboard, left outboard, right inboard, and right outboard spoilers. However, the inboard and outboard spoiler deflections on the same side were always identical. For the turboprop aircraft, the spoilers are deployed based on a schedule that is linked with the pilot's aileron input. They are deployed even if the ailerons are only deflected by a small amount. In addition, only one side of the spoilers would be deployed at any given time. This is expected as it is documented in the reports that Bombardier Aerospace have provided with the qualified model. Based on the above, only a single term is used in the model to capture the effects produced by the spoilers. This would also reduce model complexity

for a better posed parameter estimation problem.

Adding spoilers as a regressor to the stall model improved the time history fits to the flight test data significantly. Note that the spoiler effect is one sided spoilers used to aid roll control (so-called spoilerons) and not flight spoilers that are deployed equally on both wings. As mentioned previously, the qualified model's aerodynamic database covered up to approximately 12° α for the lateral coefficients. It is reasonable to see large changes to the effectiveness of the spoilers as the aircraft approaches stall where separation of flow occurs from the trailing edge of the wing. The spoilers that span a large portion near the trailing edge of the wing would be rendered less effective since flow is disrupted there and subsequent deployment of the spoilers to disrupt it further would see little effect.

3.4.2 δ_a Splines

It was found that a simple δ_a regressor in the model structure returned parameters that were very scattered among the adjacent bins, suggesting that the aileron effect was not well identified. In addition, the identified parameter values suggest aileron effectiveness is lost at the very low angles of attack, which suggest estimation errors. It was strongly believed that this was an erroneous result since the qualified model disagreed with the finding and it was in a region where the qualified model had valid wind tunnel data for. The solution was to not estimate the aileron effectiveness term when it is near 0° deflection. Gusts of wind during flight testing will cause the aircraft to roll slightly to either side, causing fluctuations in C_l. The pilots would try to maintain wings-level and apply an aileron input. If the pilots are extremely efficient and quick in maintaining C_l to be trimmed (zero) at all times, then it would appear that the ailerons are not very effective in generating C_l. This is the problem of low excitation of states that was discussed previously, shown in Figure 3.5, where the estimation of a parameter associated with δ_a is difficult due to the data points being clustered around 0 where no excitation occurs. The data shown in Figure 3.5 is typical of α bins of lower angles of attack, where the aircraft is approaching stall in a very controlled manner. The signal to noise ratio for determining the relationship between C_l and δ_a is low in these low α ranges. The noise, which are the small changes in C_l caused by winds, are more or less constant over a duration of time. Therefore the data points in which aileron deflections are relatively larger, the signal to noise ratio would increase. Instead of using δ_a directly as a regressor, splines of δ_a are used to avoid using aileron data smaller than 2° as a regressor. This is done mathematically shown in Equation (3.15). This is equivalent to ignoring data

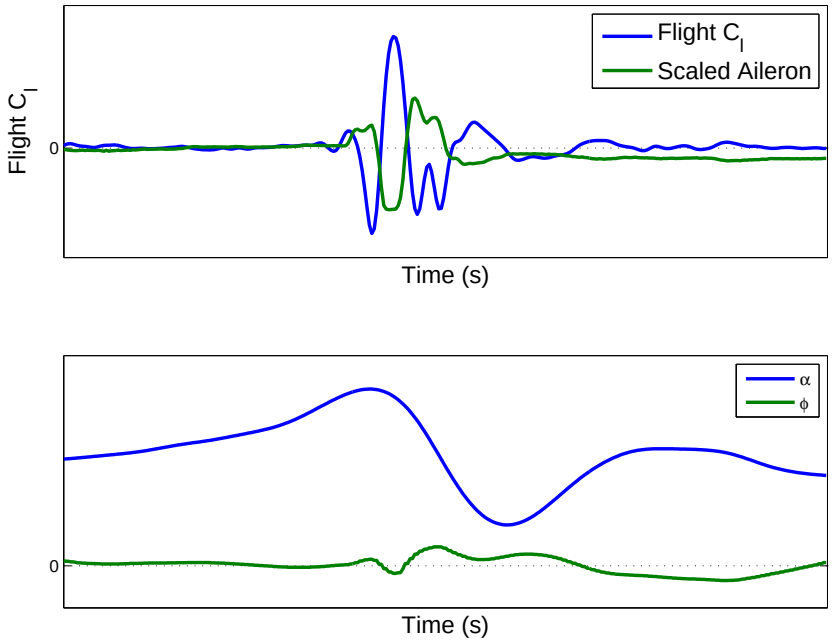

Figure 3.9: C_l and δ_a vs. t graph for observing un-commanded roll-off example 1

points of δ_a within the band of $[-2°, 2°]$ in Figure 3.5.

3.4.3 Stochastic Roll-off

Since the stall maneuvers are done in a quasi-steady manner leading up to stall, none of the recorded lateral aircraft states are changing rapidly in that region. In many flights, there is a sudden C_l spike that is not correlated with any of the states that are still relatively unchanged. It is shortly after this sudden change that aileron inputs were used to generate a roll moment that is opposite to this initial spike. Based to the large inputs the pilots had to put in shortly after the initial spike, it is believed that the spike is a random roll-off that was not predicted by the pilot. Further investigation showed that this initial roll-off happened consistently at the same range of angle of attack. Figure 3.9 shows the measured C_l and aileron input plotted against time for a given flight. The aileron channel is scaled down to match the magnitudes of the rolling moment coefficient. Shortly before the maximum achieved angle of attack, there is a large negative C_l excursion from zero. A sharp negative aileron input followed, which tends to create positive moment to oppose the roll-off. Another interesting observation is that the initial roll-off seems to subside quickly, sometimes even before the pilot took action. It can be seen in Figure 3.9 that the C_l line, shown in blue, is returning to zero before the aileron input by the pilot. However, the stick pusher was activated for this flight and prevented the

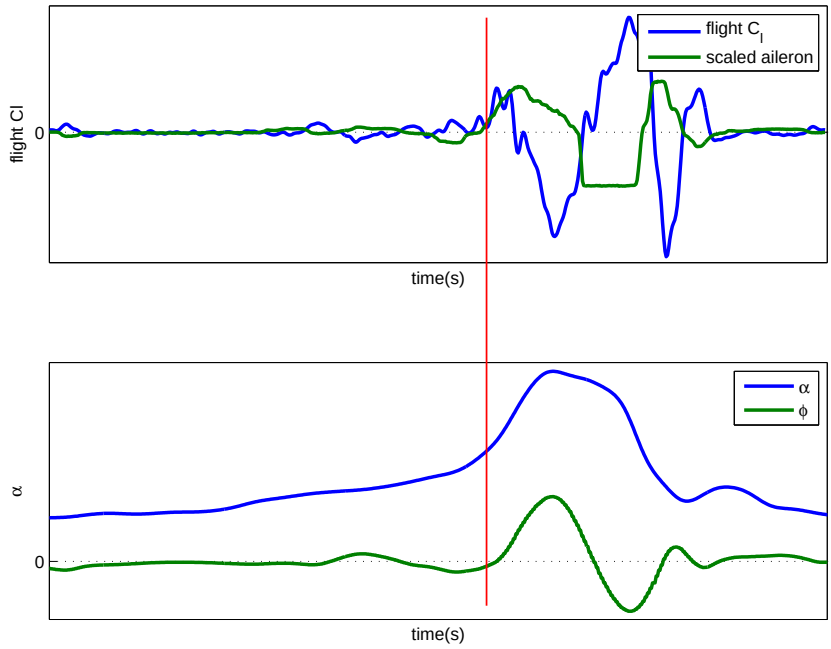

Figure 3.10: C_l and δ_a vs. t graph for observing un-commanded roll-off example 2

aircraft from achieving a higher α. The activation α was only slightly higher than the roll-off α in this flight, so it is not clear if the roll-off subsided due to other dynamics of the aircraft during pusher activation.

Figure 3.10 is a flight from a non-pusher case so that the pitch down motion at stalls does not happen until much later. The spike of the roll-off is marked by the red line in the figure. The initial counter-acting aileron input by the pilots failed to change the C_l in a significant way even when the ailerons are almost at its maximum deflection. It is believed that the roll-off subsided shortly, which caused the C_l to return to zero and subsequently to negative values in response to positive aileron inputs.

Figure 3.11 is another non-pusher flight that illustrates the roll-off occurs consistently at roughly the same α, which is significantly lower than the α achieved in a non-pusher stall maneuver. A positive aileron input creates negative rolling moment, therefore the aileron input after the roll off (depicted by the red line) is in response to the unexpected rolling moment. However, it seems the roll-off magnitude peaked and was returning to zero just when the pilot started to react.

Based on the above observations, there seems to be identifiable roll-off which starts consistently at roughly the same α. Although it is not conclusive for how long of a

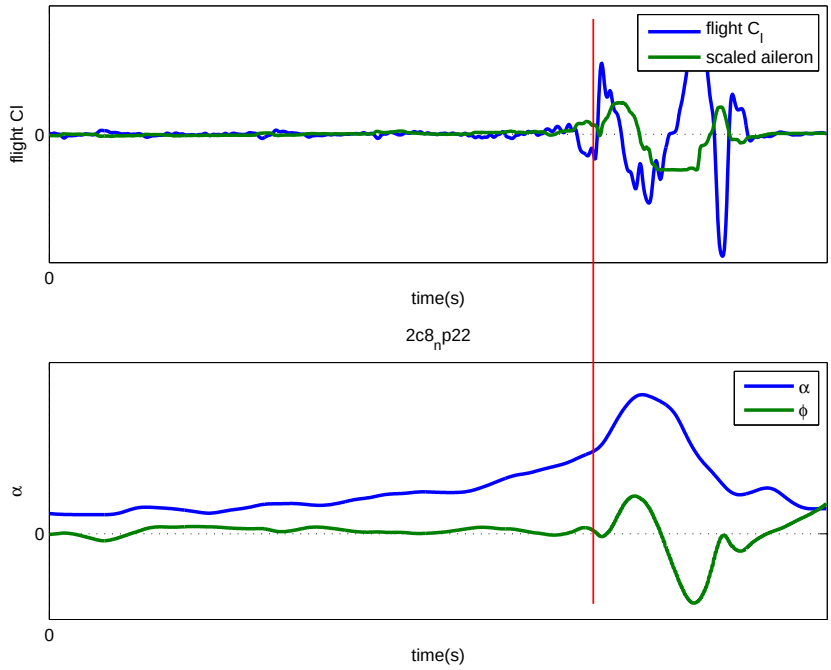

Figure 3.11: C_l and δ_a vs. t graph for observing un-commanded roll-off example 3

duration the roll-off is sustained, flight test data seems to suggest it is relatively short. Nevertheless, useful information regarding the magnitude, direction, and onset α could still be gathered. The following procedure was followed in sifting through the flight data to obtain some statistics to characterize the random roll-off:

1. Look for a sudden uncommanded spike in rolling moment C_l when the aileron input was relatively constant up to that time
2. Verify that the spike in C_l was not caused by any other sudden change in the states
3. Record the angle of attack at which it happens
4. Record the peak magnitude and direction of the uncommanded spike in C_l

Table 3.2 shows the results of the procedure, which was done for straight stalls only because the roll-off characteristics may change due to the other type of stalls maneuvers. Yet, the other types of stall did not have enough flights to perform the same analysis on each flap condition. It was found that the α at which roll-off occurs (identified using the method above) is often before the max α achieved in the flights and are consistent in value; however, the initial roll-off is roughly always at the same α. Note that this method only identifies the initial roll-off as the aircraft approaches stall in a quasi-steady manner. There seems to be additional roll-off experienced by the aircraft at even higher angles of

Table 3.2: Roll-off statistics for straight stalls

Flaps	Mean α	C_l Magnitude	Direction
0	17.09°	0.01030	8 Right 6 Left
5	17.81°	0.01587	9 Right 6 Left
10	17.75°	0.01760	10 Right 7 Left
15	18.04°	0.02315	11 Right 10 Left
35	17.60°	0.02566	10 Right 6 Left

attack and certainly during recovery when flow re-attaches to the left and right wings at different times as angle of attack decreases. However, the roll-off in those conditions is hard to identify since the states and control surfaces are changing rapidly, and it is close to impossible to separate deterministic and stochastic effects on C_l.

Considering that the roll-off happens sharply and ends quickly in most of the flight maneuvers that are available, it should not significantly bias the parameters estimation results. Equation error in principle is a least-squares approach; With the roll-off affecting a small portion of the data-points and being stochastic in nature, it is akin to being measurement noise, which equation error can handle with ease. This is especially true when many flight maneuvers are used for estimation, each having different roll-off magnitude and direction. Generally speaking, the roll-off would be very similar to noise, however it is larger in magnitude and does not fluctuate wildly.

Methods for observing rolloff other than examining time-history plots have been suggested in the public literature. The Boeing Company and the NASA Langley Research Center have jointly developed a set of metrics for defining loss of control. These metrics, called Quantitative Loss-of-Control Criteria (QLC), offer insight to accident investigators as to why loss of control occurred in a graphical and quantitative sense [39]. The Dynamic Roll Control (DRC) metric maps roll axis control against dynamic roll attitude ϕ', which represents the sum of the current roll angle with its expected change after one second:

$$\phi' = \phi + \dot{\phi} \tag{3.20}$$

Therefore, an aircraft that is at a large roll angle but rolling back towards wings level would get a lowered value of ϕ' for recovering properly, whereas another aircraft that is banked less aggressively but rolling quickly that further increases bank would have a rather large ϕ'.

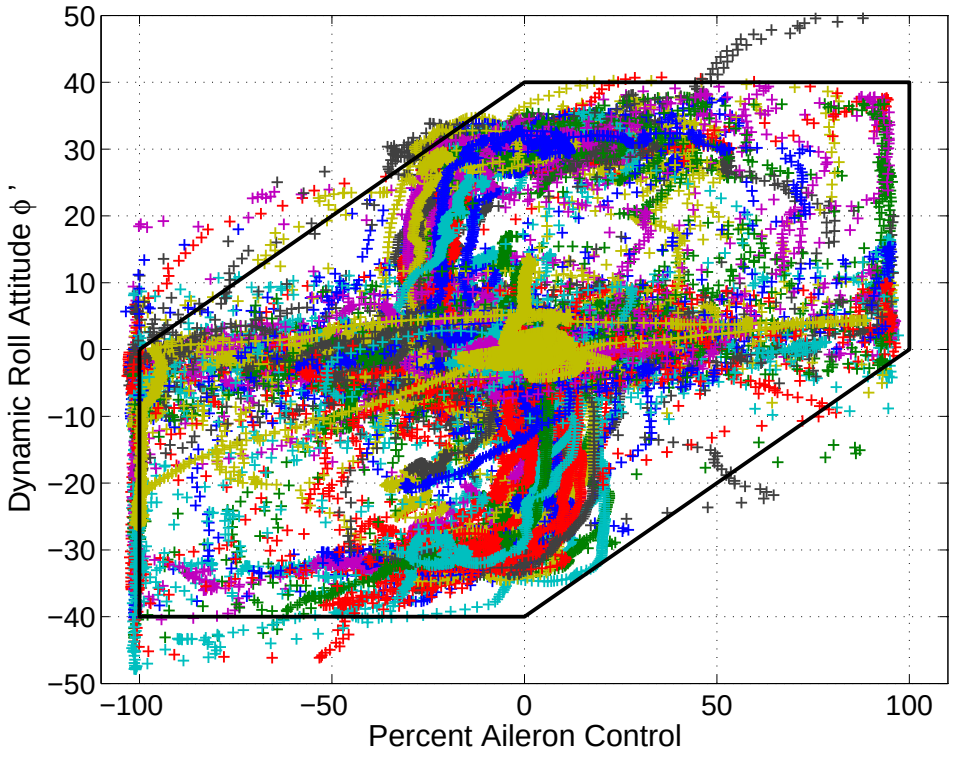

Figure 3.12: Dynamic Roll Control Envelope $\phi\prime$

Figure 3.12 plots the aileron input against dynamic roll ϕ' for all 198 flights that are in the dataset. The DRC envelope, depicted as a the black boundary in the figure, reflects whether the trend in roll attitude is consistent with the roll control inputs or whether the inputs are opposing the roll motion. The aircraft is considered to be in a loss-of-control situation if it exceeds the boundary. Figure 3.12 confirms that there is a clear roll-off at the beginning of flights when the pilot was not expecting a roll-off to occur, therefore allowing the dynamic roll attitude to reach high values without aileron input. The sudden spike in ϕ' occurs in both directions, suggesting randomness associated with roll-off. For a typical stall maneuver, $\phi' \approx 0$ and $\%\delta_a \approx 0$ at the beginning; then a sudden spike in ϕ' occurs, showing the roll-off. It is not until the ϕ' almost exceeds the DRC envelope before the pilots applied aileron to correct for the roll. Since positive aileron input generates negative rolling moment, quadrants I and III in the figure represents proper recovery actions. Lateral pilot-induced-oscillations (PIO) would appear in quadrants II and IV, where inappropriate control input augments the roll excursion. Note that the pilots hit the maximum physical limit of the ailerons very often, suggesting that they did not have enough roll control authority. The figure also shows the pilots

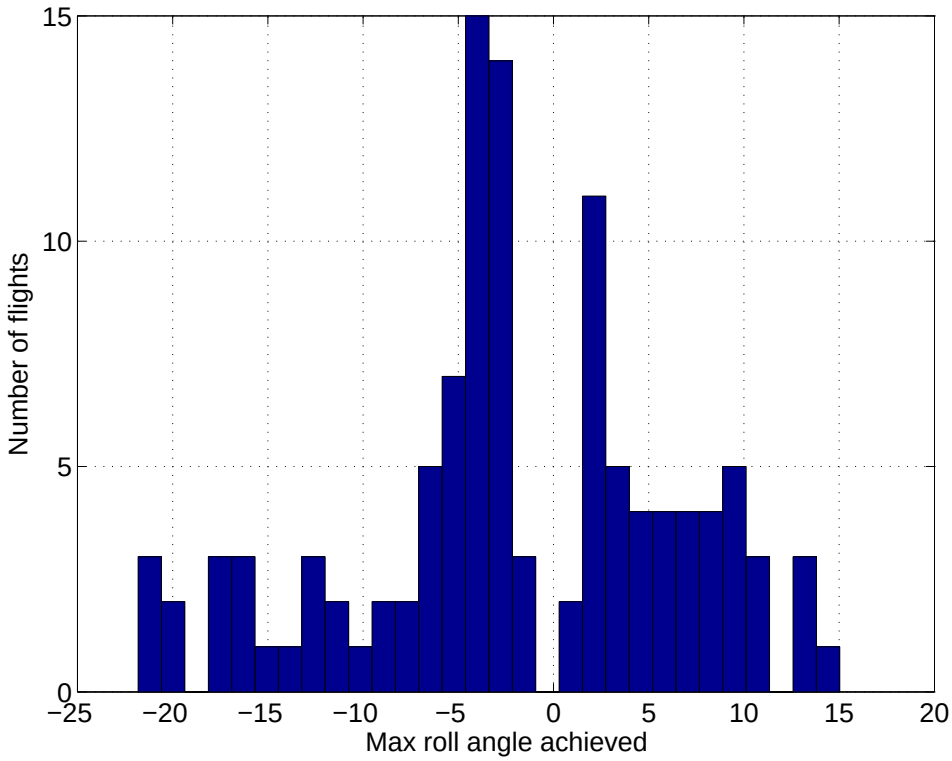

Figure 3.13: Maximum roll angle achieved during straight stalls

applied correct aileron inputs to oppose the roll-off in the flight tests. However, this observation is only accurate if the aileron control effectiveness is not reversed, which is the assumption of the DRC metric.

Figure 3.13 show the maximum roll angle achieved in all the Straight Stalls, which started with wings level flight. According to the FAA Federal Aviation Regulations Part 25, aircraft must demonstrate the following stall characteristics for airworthiness: "For level wing stalls, the roll occurring between the stall and the completion of the recovery may not exceed approximately 20 degrees" [14]. Most of the flights managed to keep roll angle during stall below 20°. The flights that exceeded 20° were all non-pusher flights in which the aircraft reached significantly higher α than the pusher flights, where often the pilot applied max aileron input for a sustained period of time. This demonstrates that either he/she did not have enough control authority to arrest the roll, or that the application of ailerons worsened the situation. It is difficult to conclude from the flight test data.

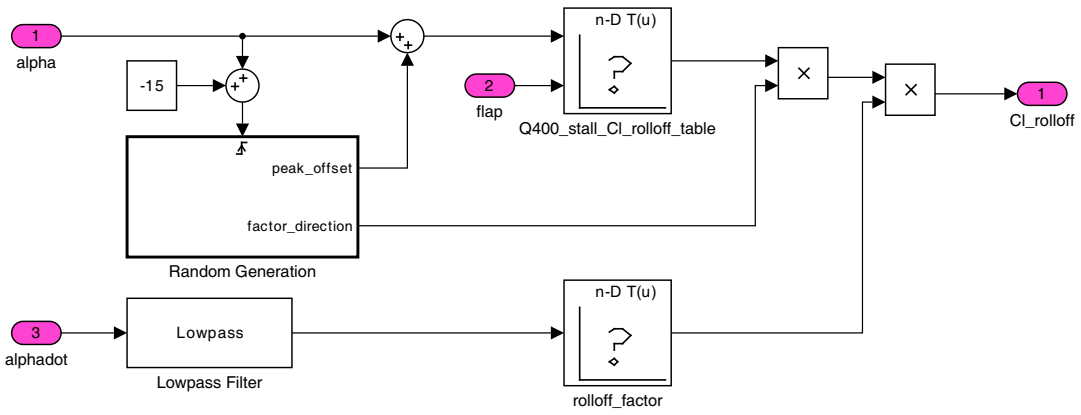

Figure 3.14: Stochastic roll-off implementation in Simulink

Implementation

A Simulink block with the above statistics is implemented for generating the roll-off experienced at stall. Through observation of flight tests, although there is variability in terms of the angle of attack in which roll-off starts, once started the roll-off seems to end within 1° angle of attack. The pilots often has already taken measures to correct for the spike in rolling moment by the time that happens, but the abrupt end of the roll-off causes the pilots to over compensate slightly. A Gaussian function centered at the respective mean α of each flap condition serve as the general shape of the roll-off. The magnitude of the Gaussian functions are set to the mean roll-off magnitude observed in each flap condition. The Gaussian's standard deviation is set to 0.5, to roughly account for roll-off that happens within a 1 degree window while having a smooth ramp up.

Figure 3.14 shows the implementation of the Gaussian functions in the lookup table block. Some of the observed statistics associated with the randomness is listed below:

- α standard deviation: 1.31 °
- Magnitude variance: 22.5% of mean magnitudes for each flap condition
- Direction statistics: 58% Right, 42% Left

For variability in the magnitude of the rolloff, a random number generator (RNG) with the observed statistics is used to generate a factor that scales the output of the lookup table. A RNG that outputs -1 42% of the time and +1 58% of the time is used for the creating the randomness in direction as it flips the signs of the output roll-off coefficient. For variability of the α when roll-off occurs, a zero-mean random number is added to the true α which is then used to sample the lookup table, effectively changing where the

Gaussian shape functions are centered at. A random factor and direction, as well as a α offset is generated every time the simulation passes through $15°\alpha$ from below.

3.5 C_n Model

Following the same procedure and methodology used to develop the C_l model, the finalized C_n model structure is:

$$\begin{aligned}\Delta C_n &= \Delta C_{n_0} + \Delta C_{n_\beta}\beta + \Delta C_{n_p}\hat{p} + \Delta C_{n_r}\hat{r} \\ &\quad + \Delta C_{n_{\delta_a}}[(\delta_a - 2°)_+ + (\delta_a + 2)_-] + \Delta C_{n_{\delta_r}}\delta_r + \Delta C_{n_{C_T}}C_T \\ &\quad + \Delta C_{n_{C_{T,diff}}}C_{T,diff} + \Delta C_{n_{\delta_s}}\delta_s\end{aligned} \tag{3.21}$$

During the initial stages of model development, only the straight stalls were used in the identification process. The parameters for the correction yawing moment due to differential thrust $C_{T,diff}$ was poorly identified since it was more or less zero at all times. The parameters were very scattered when compared to the values of adjacent bins. Once data for the asymmetric power stalls were added to the data pool, the parameter estimates improved and clearly showed a trend as a function of angle of attack. This is shown in Figures 3.15 and 3.16, with the flaps 10 parameters showing that the qualified model requires a bigger C_n modification due to thrust effects. This is the general trend observed as the flaps continue to extend. Other parameters that exhibit a well-identified trend include ΔC_{n_0}, ΔC_{n_β}, ΔC_{n_p}, ΔC_{n_r}, and $\Delta C_{n_{\delta_s}}$. It is difficult to interpret the results of the Δ model without knowing the qualified model. Effects of the extended model are shown in Chapter 4, which adds the Δ models to the qualified model so that physical interpretations could be made.

3.6 C_Y Model

$$\begin{aligned}\Delta C_Y &= \Delta C_{Y_0} + \Delta C_{Y_\beta}\beta + \Delta C_{Y_p}\hat{p} + \Delta C_{Y_r}\hat{r} \\ &\quad + \Delta C_{Y_{\delta_a}}[(\delta_a - 2°)_+ + (\delta_a + 2)_-] + \Delta C_{Y_{\delta_r}}\delta_r + \Delta C_{Y_{C_T}}C_T \\ &\quad + \Delta C_{Y_{\delta_s}}\delta_s + \Delta C_{Y_{\dot{\alpha}\beta}}\dot{\alpha}\beta + \Delta C_{Y_{\dot{\beta}}}\dot{\beta} + \Delta C_{Y_{\dot{\alpha}\dot{\beta}}}\dot{\alpha}\dot{\beta} + \Delta C_{Y_{\dot{\beta}\delta_s}}\beta\delta_s\end{aligned} \tag{3.22}$$

The estimated ΔC_Y parameters for flaps 0 and flaps 10 are shown in Figure 3.17 and 3.18 respectively. There is a slight negative offset at low angles of attack for both flap conditions. The state that C_Y depend on the most is β; its parameter show that as α increases, the sideforce generated by β should be adjusted to be slightly lower in

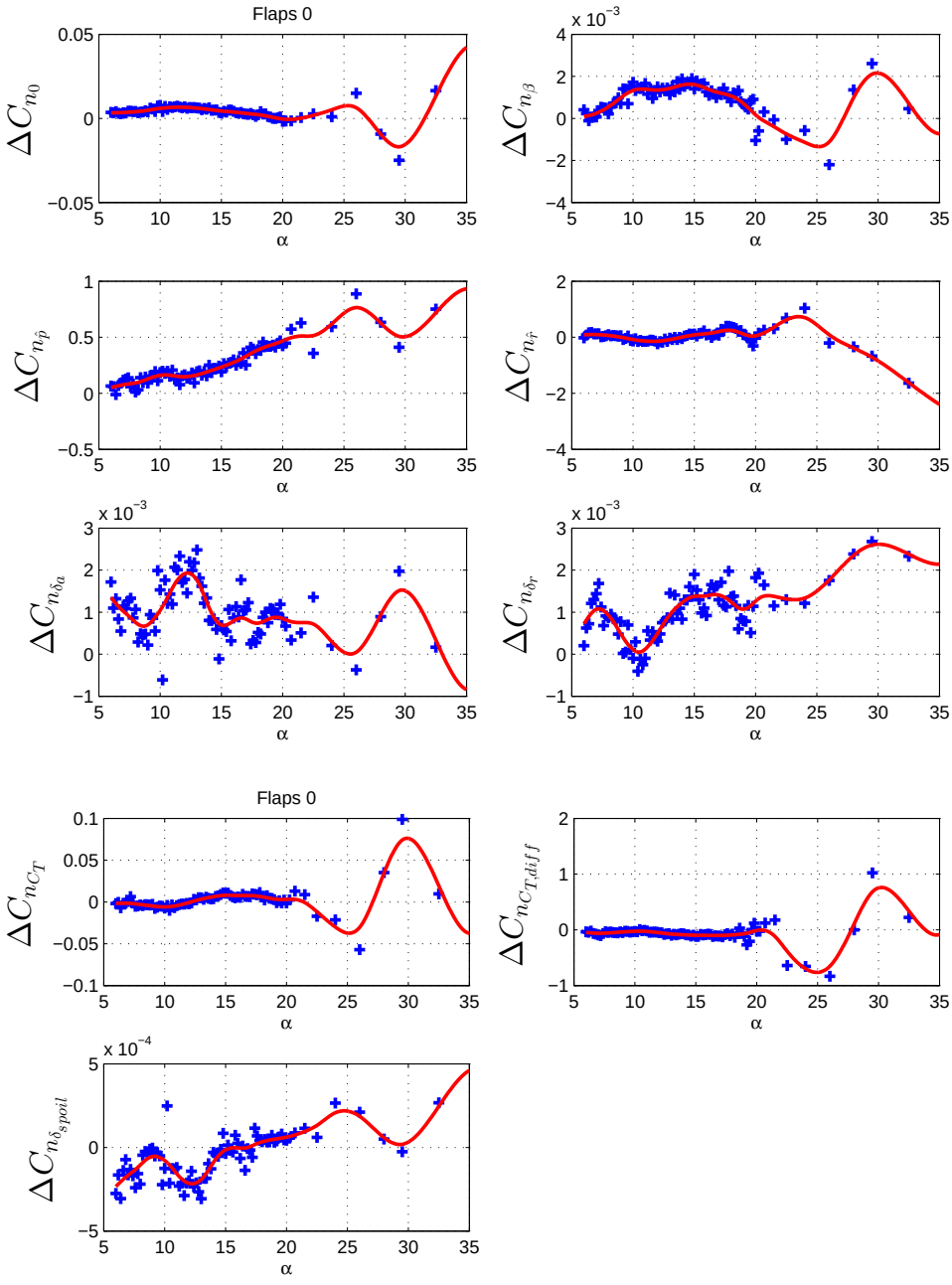

Figure 3.15: Estimated ΔC_n parameters for flaps 0

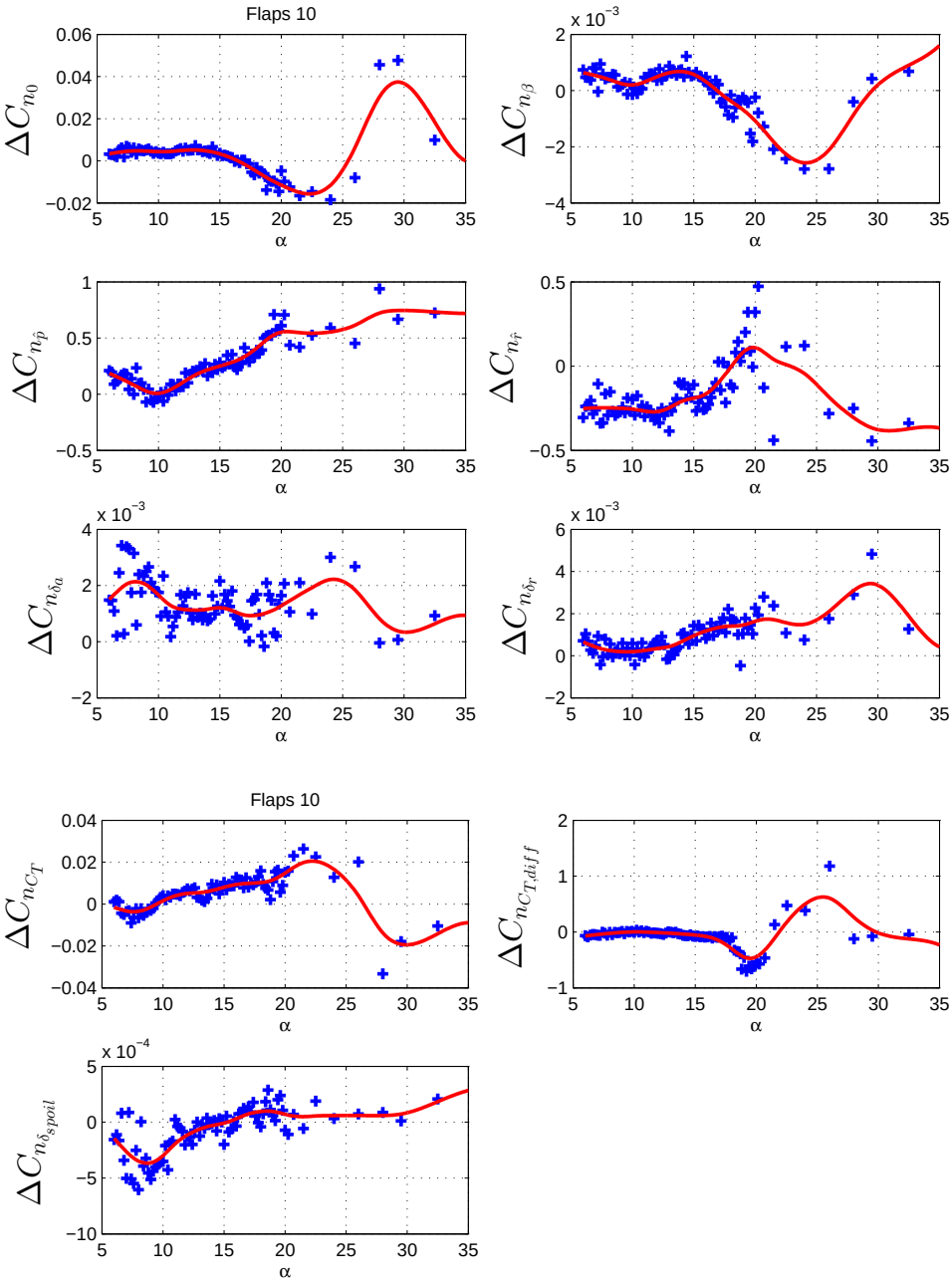

Figure 3.16: Estimated ΔC_n parameters for flaps 10

the qualified model. Both flap conditions show well-identified C_T parameters with low variance among adjacent bins. The propeller slipstream interactions with the fuselage and vertical tail may have contributed to the relationship between thrust and sideforce. The rudder parameters are mostly positive even up to stall, which means the qualified model is over-estimating the sideforce caused by rudder and the Δ model would reduce it.

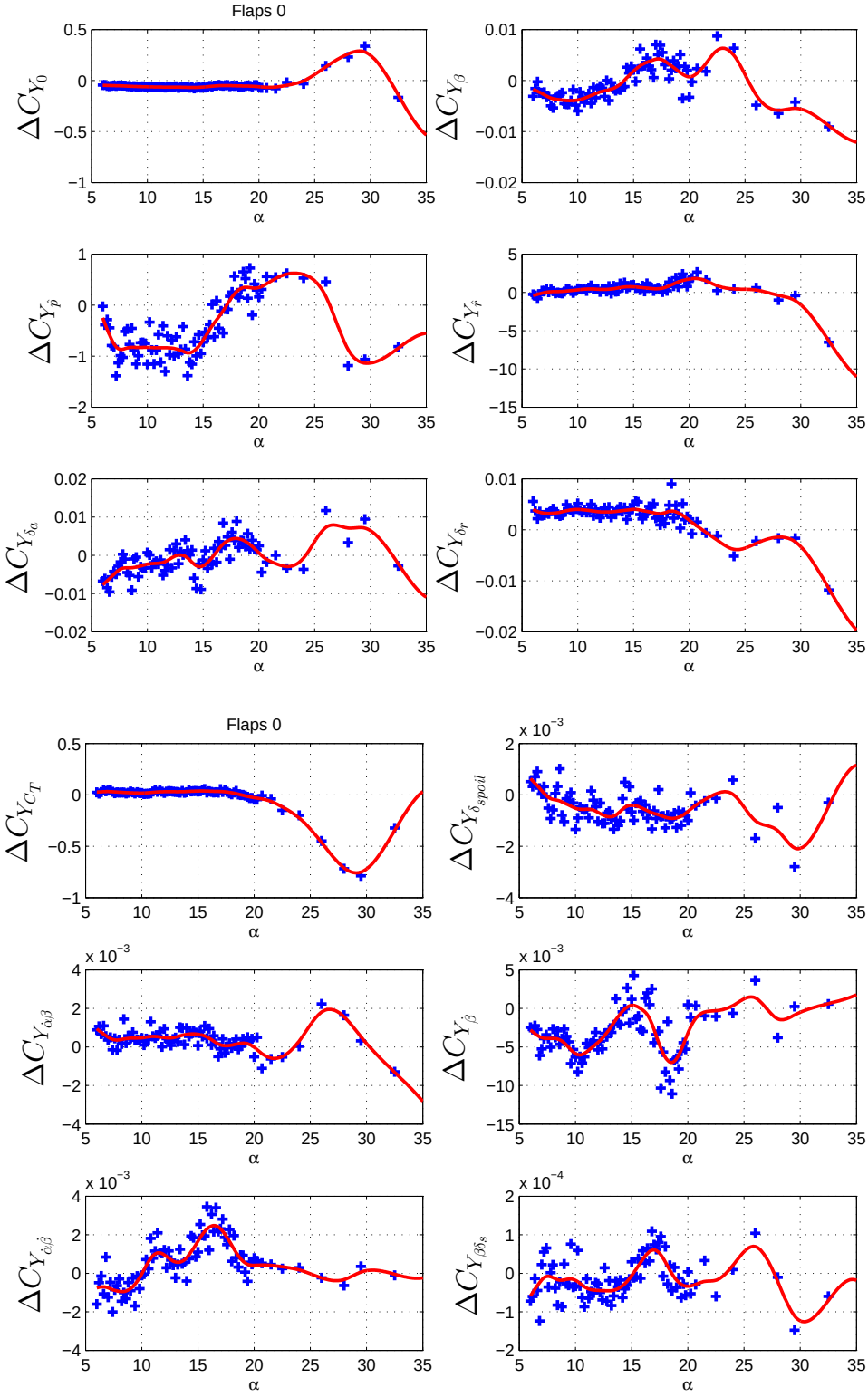

Figure 3.17: Estimated ΔC_Y parameters for flaps 0

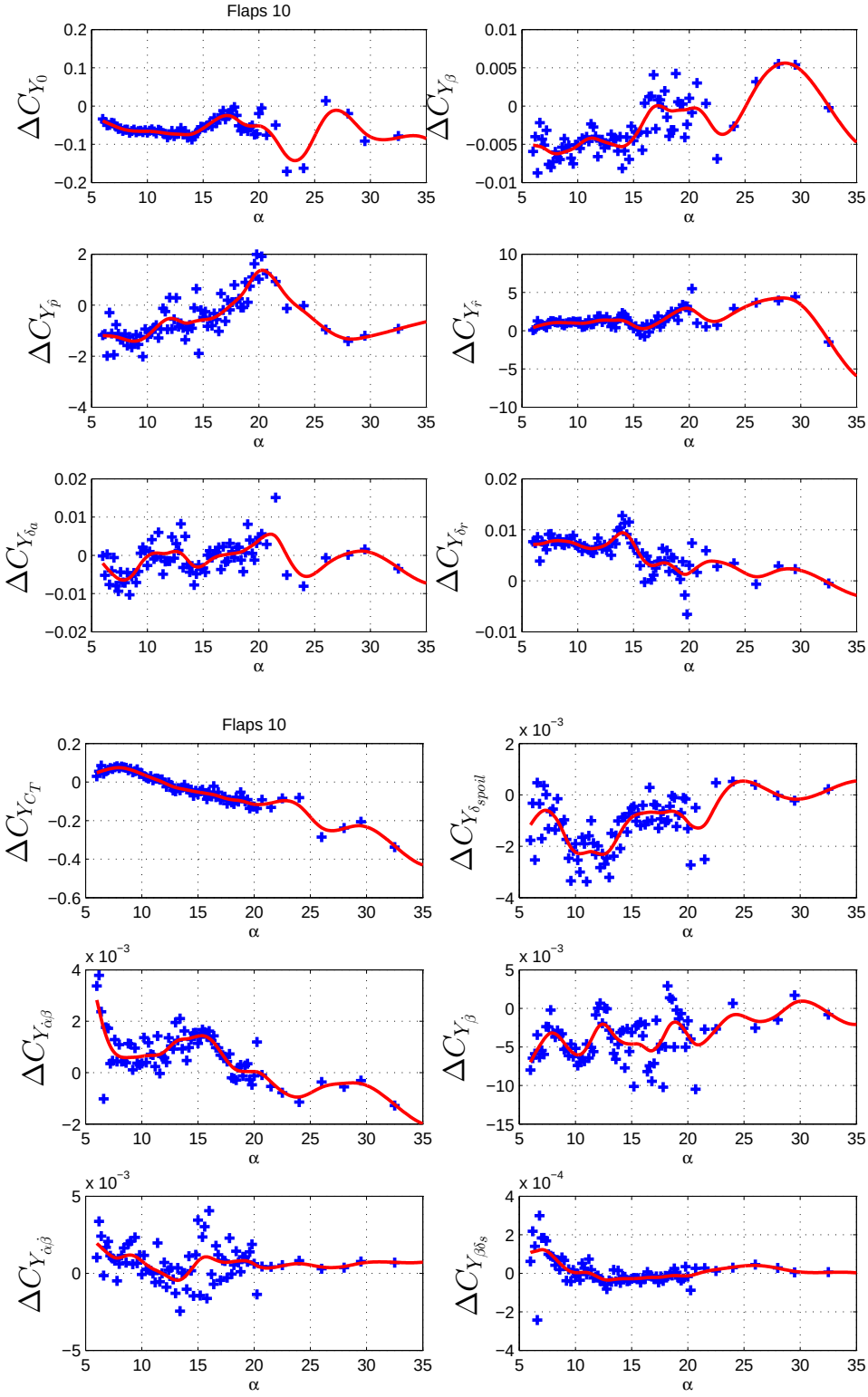

Figure 3.18: Estimated ΔC_Y parameters for flaps 10

Chapter 4

Results and Validation

Although the identified parameters with low variability among adjacent bins suggest that they were well identified and that data had good information content, it is difficult to apply engineering judgement and intuition to the correction terms as they only form part of the total model. Without knowing how the qualified model behaves, it is difficult to make sense of the delta (Δ) model. For example, if the original model is already very good in its predictive capabilities near stall, then the delta (Δ) model will have small corrections. However, if the original model is poor in the stall regime, then relatively large corrections would be added by the Δ stall model, even though the final extended model of these two hypothetical cases may be exactly the same. Therefore, the behavior of the extended model must be examined to apply engineering judgment based on knowledge in the field of aircraft dynamics to identify erroneous effects in the model or to support the findings from parameter estimation. Several validation methods have been chosen for this project. The first method is a time history match of the force and moment coefficients to measured data from flight test stall maneuvers. The second method is to examine some effects that are significant in determining the lateral handling characteristics of an aircraft, such as the the effect of p, r, β, δ_a, δ_r on the forces and moments as a function of α. This would allow the comparison of the extended model's behavior to the expected behavior of an aircraft near stall, such as having reduced roll stability and loss of effectiveness in the controls. As a final validation of the model, the lateral model is integrated with the longitudinal stall model into a 6-DOF simulation. Elevator input time histories from flight tests are fed into the simulation to observe whether it behaves qualitatively the same as the flight tests. In addition, it is also a check for non-sensible behavior that may be hard to spot while purely examining forces and moments, such as one that would cause the simulator to integrate a state until it blows up. It should be noted that due to the chaotic behavior at stall, such a comparison may not offer insight

on the accuracy of the model, but it should tell whether the Δ model's parameters are of the proper magnitude and not generating completely senseless values.

4.1 Time History Matches to Flight Test Data

The states of the aircraft are fed into the extended lateral aerodynamic model, which outputs the force and moment coefficients. The coefficients are plotted against time and are compared to the qualified model and flight test measured values. Based on how well the matches are, the model may be rejected and further developments must be made. Since this project is interested in the development of a representative stall model, it is more important that the model behaves qualitatively correct rather than it predicting the magnitudes of the forces and moment coefficients accurately. Needless to say, it is desirable to satisfy both conditions. Generally, we consider the model to be satisfactory if the direction of forces and moments match the measured data and the magnitudes of the peak values are not significantly off. However, it is hard to establish a metric which would characterize this. A coefficient of determination R^2 value for example would not capture this and would also weigh constant offsets in the pre-stall region too high. For most lateral coefficients, if the model outputs are offset slightly from the actual measured data, then all it amounts to is a different trim value on some of the control surfaces in the simulation. It would not take away fidelity of the core functionality of simulator, which is to train pilots in the post-stall regime and allow them to feel the response of the aircraft to changes in input.

4.1.1 C_l time history matches

Figure 4.1 shows a time history match that is relatively poor for the C_l coefficient. Although the extended model did not completely match the flight test data, especially in the recovery region during stall, it was still a major improvement over the qualified model, in which it erroneously predicted large rolling moment oscillations. Upon closer inspection it was found that these spikes in the qualified model are from pilot aileron inputs. The pilots must have used a lot of wheel input in the actual flight since they felt that the controls were not very responsive and larger inputs have to be applied. However, the qualified model does not capture such effects very well and therefore translated that large aileron input into large rolling moments. Note that there is also a relatively

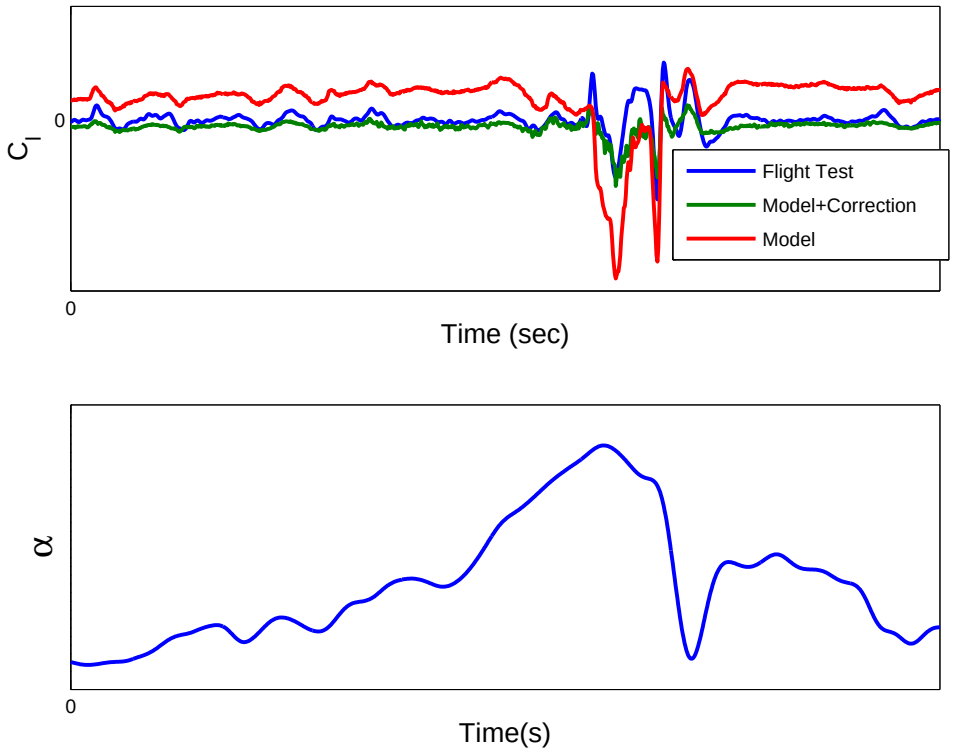

Figure 4.1: C_l time history match: relatively poor fit (pusher active)

significant offset in C_l in the quasi-steady conditions as the aircraft approaches stall. The initial spike in C_l of the flight test is due to roll-off, shown in blue. Both the qualified model and the extended models fail to capture that since all the independent variables up leading up to that point is quasi-steady. The stochastic rolling moment term is not enabled in the extended model for time history comparisons because these comparisons are for checking fits of the deterministic part of the model. It is also a good visual confirmation that there is roll-off by not including the stochastic model.

Figure 4.2 is an example of a good fit to the data. This particular flight test was not used for the identification of the model and it demonstrates the predictive capability of the model. Roll-off was not observed in this flight as there are no sudden spikes. The extended model's fit to the flight data is excellent. It is a huge improvement over the qualified model. The major contributions in the Δ model were associated with the ailerons and the roll rate. Several times during recovery the pilot hit the maximum limit for ailerons, which demonstrates how hard he had to fight the roll instability of the aircraft at stall and the loss of control authority in upset conditions.

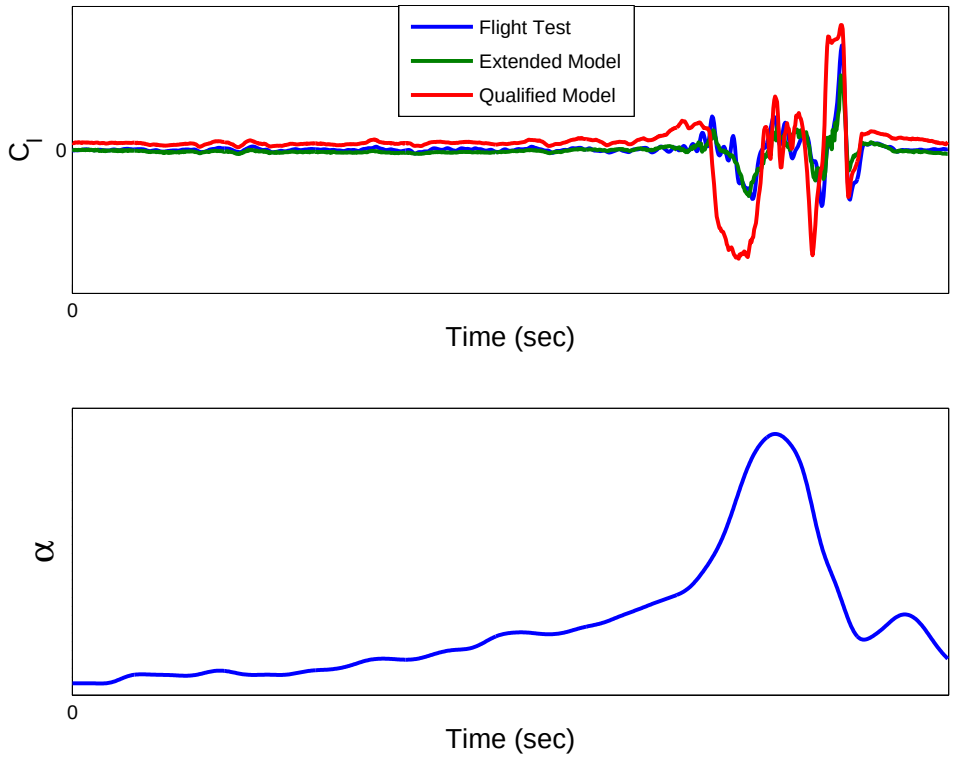

Figure 4.2: C_l time history match: relatively good fit

Figure 4.3 shows a typical pusher flight, which is matched quite well but not as satisfactory as the non-pusher flights such as Figure 4.2. In general, the really good fits are from stall maneuvers that did not have the stick pusher active. This is most likely due to the larger pitch down motion that follows from a high α stall, which can only be achieved without the pusher. The large pitch rate reduces the angle of attack much faster in the recovery portion of the flight, which as mentioned previously is where most of the modeling errors occur. There is less sustained time in the recovery region where flow re-attachment occurs to the main wings could be the reason why non-pusher flight data is better predicted by the extended model.

4.1.2 C_n time history matches

In general, the yawing moment extended model had the best results among the three lateral coefficients in terms of matching flight test data. Corrections that were needed to obtain a good fit are mainly associated with β and δ_r, $\hat{r}$ and C_T effects. Figure 4.4 shows a relatively poor time history match of the extended model. The parts in which discrepancies occur are always in the recovery region when the aircraft is pitching down quickly as it loses lift, so large negative $\dot{\alpha}$ and pitch rates occur. There is probably

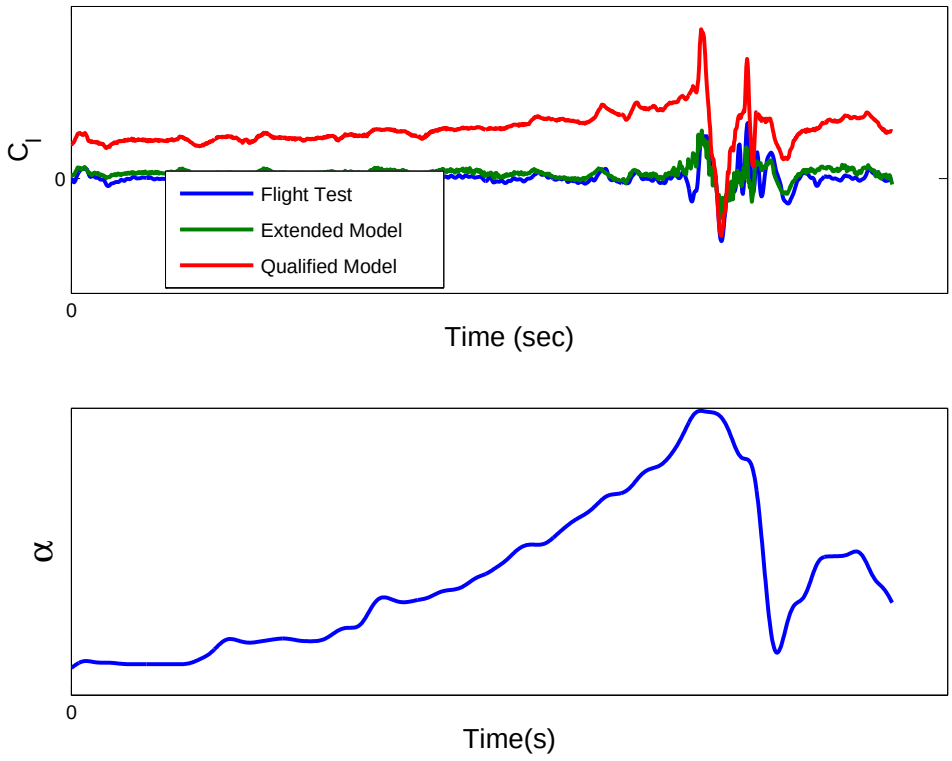

Figure 4.3: C_l time history match: typical fit (pusher active)

some complicated coupling between the longitudinal and lateral aerodynamics that are not captured well by the extended model. Although there are regressors or splines that could be included in the model structure in theory to capture such effects, identifying them is a different issue in which significant difficulties would be encountered due to data limitations mentioned in Chapter 3.

Figure 4.5 shows a relatively good fit of the extended model to the measured C_n. It can be observed that the qualified model produced significantly larger C_n values than was actually measured. This is due to the rather aggressive rudder inputs during the stall in an attempt to keep the aircraft laterally pointed forward. The aircraft loses directional stability at stall due to tail blanking and tends to yaw. However the correction input through the rudder is not effective due to blanking and hence leads to large rudder inputs by the pilots. The qualified model does not capture this tail blanking effect and over estimates the yawing moment generated by the rudder at high angles of attack, causing the large discrepancy. The extended model was able to correct for it and predicted the yawing moment with excellent accuracy.

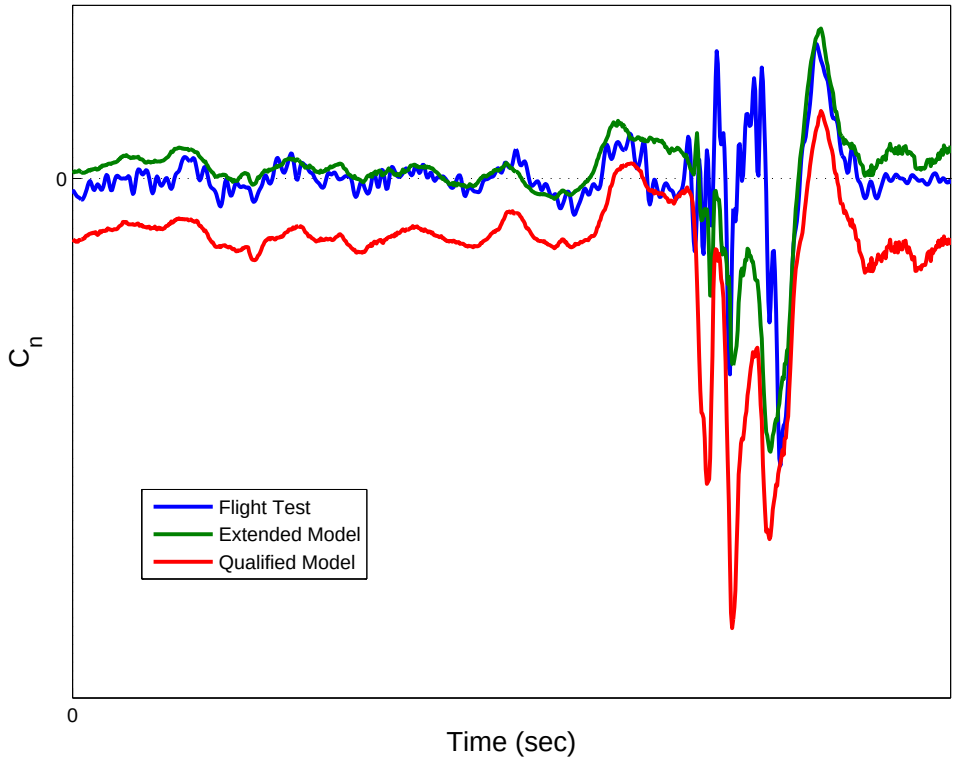

Figure 4.4: C_n time history match: relatively poor fit (pusher active)

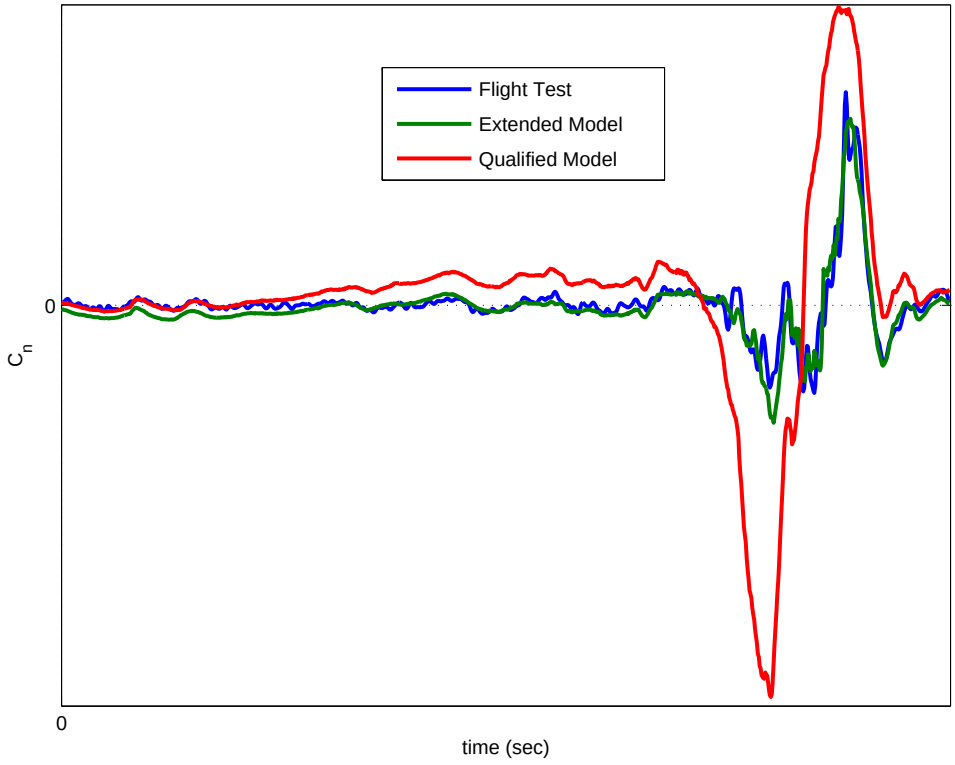

Figure 4.5: C_n time history match: relatively good fit

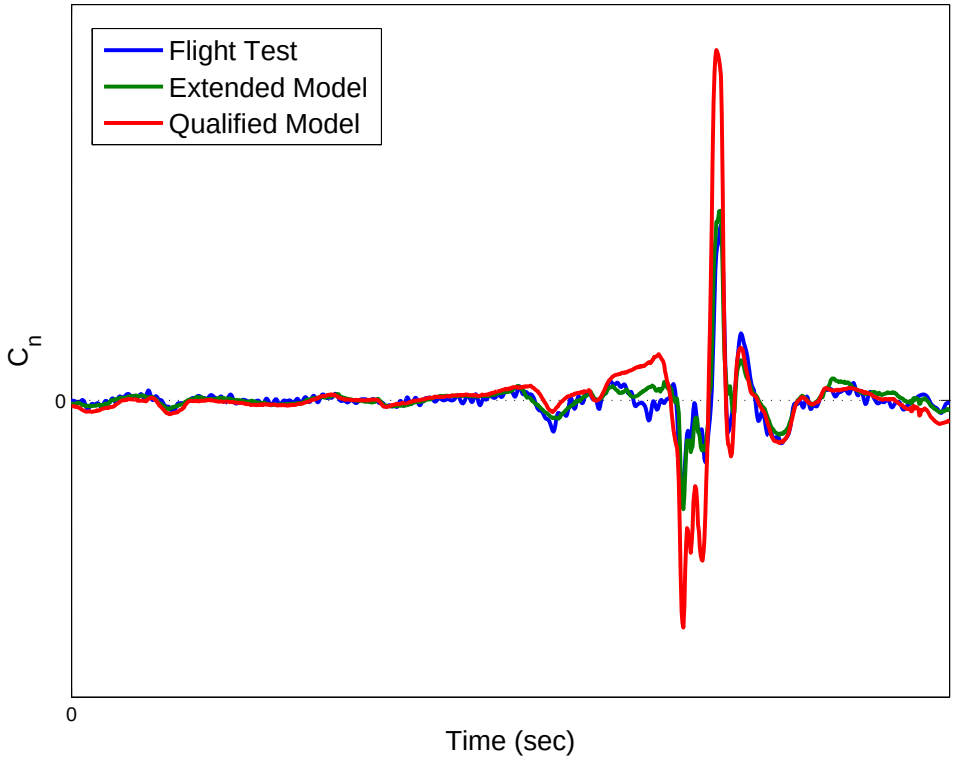

Figure 4.6: C_n time history match: typical fit (pusher active)

Figure 4.6 shows a typical fit from flights that have pusher active. Unlike C_l time history predictions, how well the C_n extended model fits the data does not depend on whether stick pusher was activated.

4.1.3 C_Y time history matches

Shown in Figure 4.7 is a relatively bad fit of the C_Y. The axes values are not shown due to data proprietary reasons, but the scale is small for this flight case. It is small enough such that the noise from the accelerometer reading shows up as fluctuations in the flight test measured C_Y. The absolute value of the error is therefore not big but visually large in the figure. Once again, the major correction in the C_Y model is a constant offset. Even without the stall model, the qualified model itself was able to capture the trend of the forces.

The model structure for C_Y is the hardest one out of the three coefficients to explain physically, with complicated nonlinear cross terms. However, those terms improved the time history fits to the data significantly. Shown in Figure 4.8 is a flight maneuver in which the extended model was able to predict well. Note that the qualified model's fit is somewhat satisfactory except for a visible offset; some of the nonlinearities of the aero-

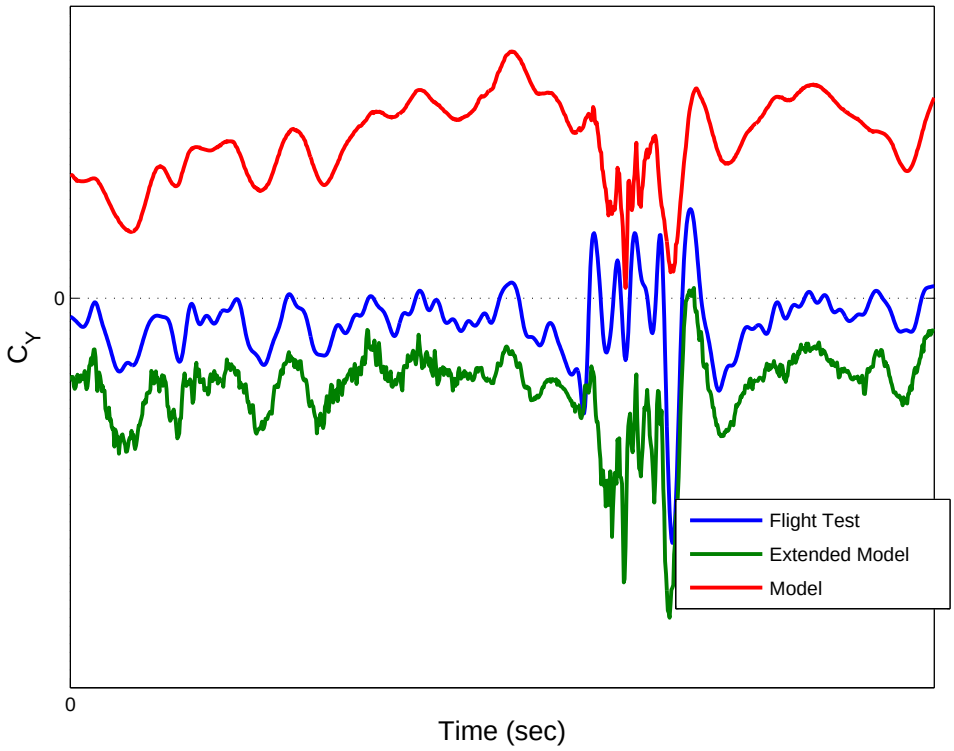

Figure 4.7: C_Y time history match: relative bad fit

dynamics have already been captured by the qualified model. This makes a point for the advantage of the Δ model approach to develop stall models; it allows for a simple model structure to predict the only slightly nonlinear corrections needed.

4.2 Effects of the Updated Aerodynamic Database

After extending the qualified model with the stall delta model, it is of interest to examine the final aerodynamic database and qualitatively evaluate some of the most important effects in aircraft handling. This would serve as support that the delta model was identified correctly and was able to capture some of the lateral effects that are common near stall conditions. The following section discusses the roll stability C_{l_β}, aileron effectiveness $C_{l_{\delta_a}}$, roll damping C_{l_p}, yaw stability C_{n_β}, rudder effectiveness $C_{n_{\delta_a}}$, and the sideforce due to sideslip C_{Y_β}.

4.2.1 C_{l_β} Lateral Stability

In Figure 4.9, it is shown that lateral stability is significantly reduced as angle of attack increases. In general, wing effective dihedral, wing sweep, and the vertical tail are the

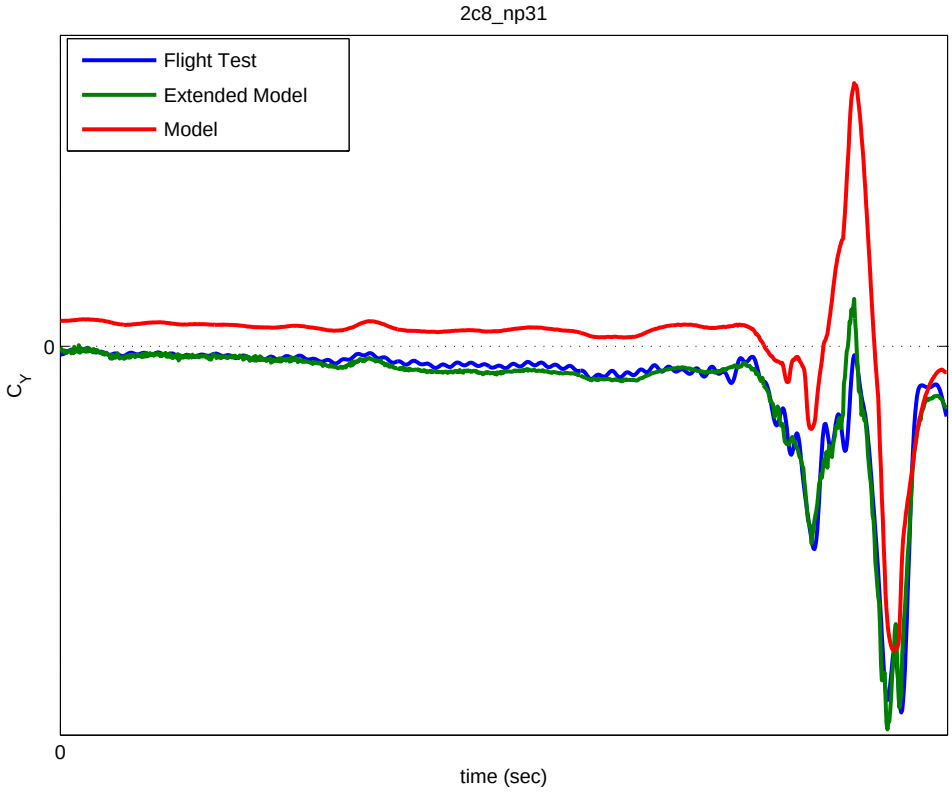

Figure 4.8: C_Y time history match: relatively good fit

main contributors to lateral static stability C_{l_β}. The T-tailed turboprop aircraft that is being modeled does not have sweep but has dihedral on a portion of the wing and it is a high wing so it has an effective dihedral. When an aircraft is in sideslip and a positive α, the wing heading into the wind with dihedral will experience a higher angle of attack from the increase in vertical velocity component v [12]. For example, if Γ is the dihedral angle, then the velocity normal to the wing is $V_{normal} = w\cos\Gamma + v\sin\Gamma$. This increases the lift of the wing heading into the wind and cause a restoring rolling moment.

A stable C_{l_β} is also provided by the flow interactions around the fuselage and the wing for a high-wing aircraft such as the one being modeled. As the airflow goes around the fuselage during a sideslip, the angle of attack of the high wing on the sideslip side is increased slightly and decreased slightly on the other side. This generates a restoring rolling moment.

Even in the absence of dihedral and sweep, a lifting wing has a C_{l_β} proportional to C_L. The vortex wake of a lifting wing is generated at the wingtips due to the pressure difference between the upper and lower surfaces of the wing. If the aircraft is sideslipping to the right with a positive β for example, the induced downwash caused by the vortex is stronger at the left wing then the right simply due to geometry that the left wing is now downstream relative to the right wing and is more susceptible to the wake. The local angle of attack of the left wing is lower than the right, and a negative C_{l_β} results. This effect depends linearly on the vortex wake, which is proportional to the lift [12]. Therefore, when the aircraft stalls, the stable C_{l_β} provided by this effect would diminish at high angles of attack.

Figure 4.9 shows the rolling moment experienced by the aircraft at various sideslip angles for two flap conditions: flaps 0 and flaps 10. The graphs on the left hand column are from the aerodynamic database of the qualified model, and the right hand side graphs are from the extended model. The qualified model shows a trend of decreasing C_{l_β} as α increases in the pre-stall region. Although it contradicts with some of the expected behavior discussed, it is believed that C_{l_β} for this airccraft is mainly provided by the vertical tail; when it is positioned into the wake of the wing as angle of attack increases, its ability to provide lateral stability also diminishes. The condition improves when α is high enough that the vertical tail is free from the wake again. This is the trend observed for the extended model. For the flaps 0 configuration, it decreases until it is almost zero. Both flap configurations show that lateral stability is restored at the extreme angles of

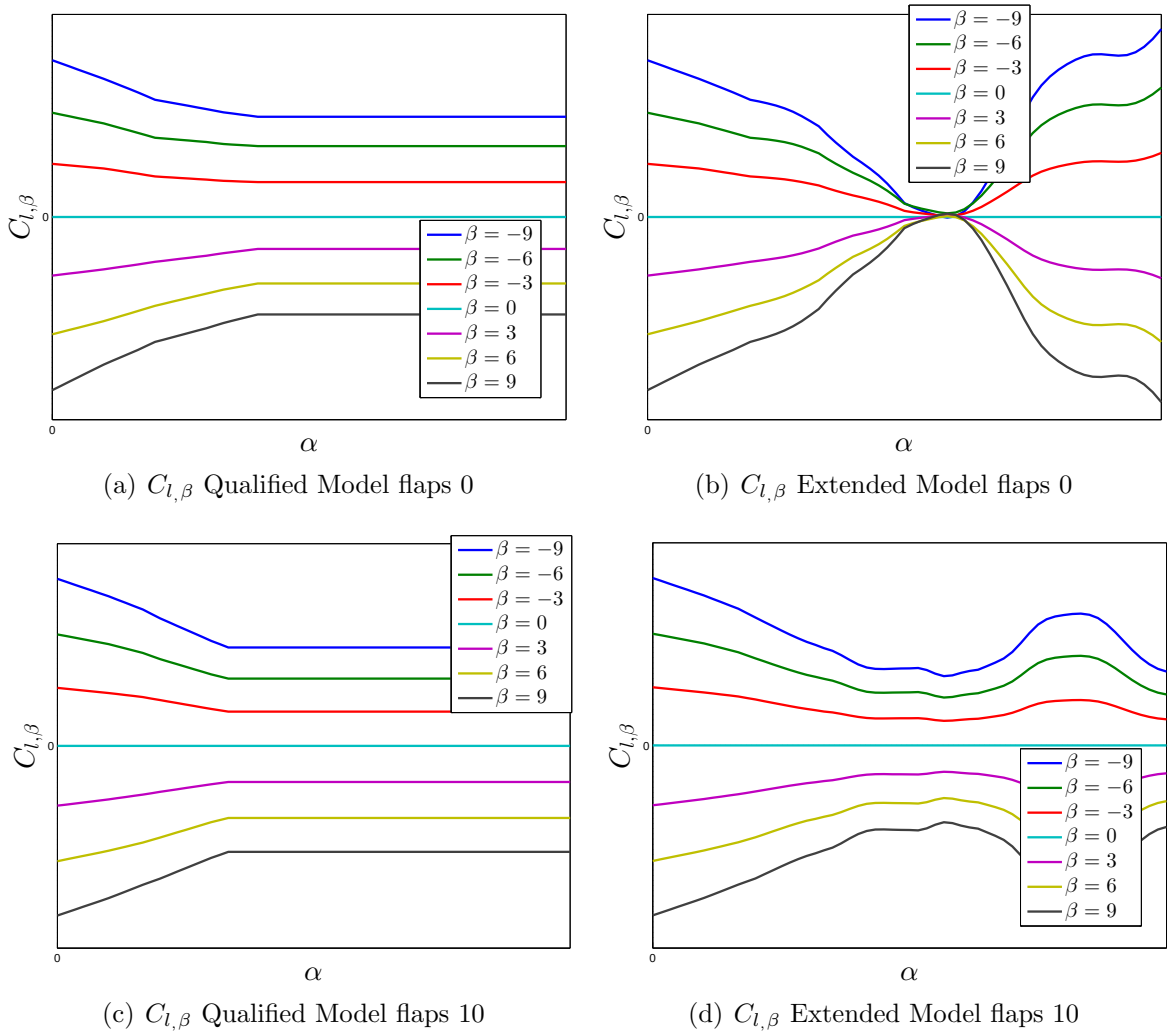

(a) $C_{l,\beta}$ Qualified Model flaps 0

(b) $C_{l,\beta}$ Extended Model flaps 0

(c) $C_{l,\beta}$ Qualified Model flaps 10

(d) $C_{l,\beta}$ Extended Model flaps 10

Figure 4.9: $C_{l,\beta}$ Roll Stability before and after stall extension

attack.

4.2.2 $C_{l_{\delta_a}}$ Aileron effectiveness

Figure 4.10 shows that the qualified model's aerodynamic database has minimal loss in aileron effectiveness up to the maximum range of α it had data for. Extrapolation into the higher angles of attack maintained the aileron's effectiveness. As seen in the figure, both flaps 0 and flaps 10 conditions have the aileron effectiveness decrease significantly near stall. Flaps 10's aileron even exhibit relatively severe control reversal at extreme α. For the aileron deflections of 5° and −5°, they are sufficiently close to the spline points of 2° and −2° as per the ΔC_l model structure that the corrections are not as big compared to the larger aileron deflections.

The ailerons are positioned at the trailing edge of the wing near the tip. The aileron's ability to create extra lift or dump lift is lost when there is flow separation in that area, thus losing the aiblity to roll the aircraft. When the aircraft is stalled it could also cause roll control reversal: as one side of the ailerons deflect downwards in attempt to generate more lift, the local angle of attack increases and wing stalls further, causing a loss of lift instead. The aileron on the other side of the airplane should be deflecting up in attempt to dump lift, but due to the wing already being stalled around that area it is not very effective. If the loss in lift from the side that was stalled further is greater, then control is reversed. The plane rolls in the opposite direction the pilot commanded it to. This is shown in Figure 4.10.

At high angles of attack, the qualified model has almost full roll control, therefore not punishing pilots for not following the correct stall recovery procedures. The proper procedure is to lower the angle of attack first, and then correct for roll. The unstable and unexpected behaviors associated with high-angle-of-attack flight makes lowering α the foremost action in stall recovery. With the extended model showing decreasing aileron effectiveness near stall and even reversing in the post-stall region, it would be difficult and sometimes unproductive to correct for roll before un-stalling the aircraft first. Pilots who do so in the simulation would probably be shown that it is a relatively futile effort.

4.2.3 C_{l_p} Roll Damping

Roll damping becomes unstable past stall in a similar manner to how the ailerons become reversed as shown in Figure 4.11. As the aircraft rolls from wings-level flight, the wing that drops will experience an increase in angle of attack. This would stall the wing if it is nearly stalled and would stall it further if it is already so, hence decreasing lift on the wing and would tend to roll the aircraft further in that direction. $C_{l,p} > 0$ depicts that condition, where a positive roll rate p (rolling to the right) would cause a positive (right) rolling moment, further increasing the roll rate.

Coupled with the loss in aileron effectiveness, and sometimes even reversal, the plane is roll unstable at high angles of attack with the inability to arrest the roll. Although the pilot may still be able to maintain roll attitude at high α in calm conditions, any slight disturbance that imparts a roll rate p to the aircraft, such as a stochastic roll-off or wind gust, would be extremely difficult to stop until the angle of attack is decreased.

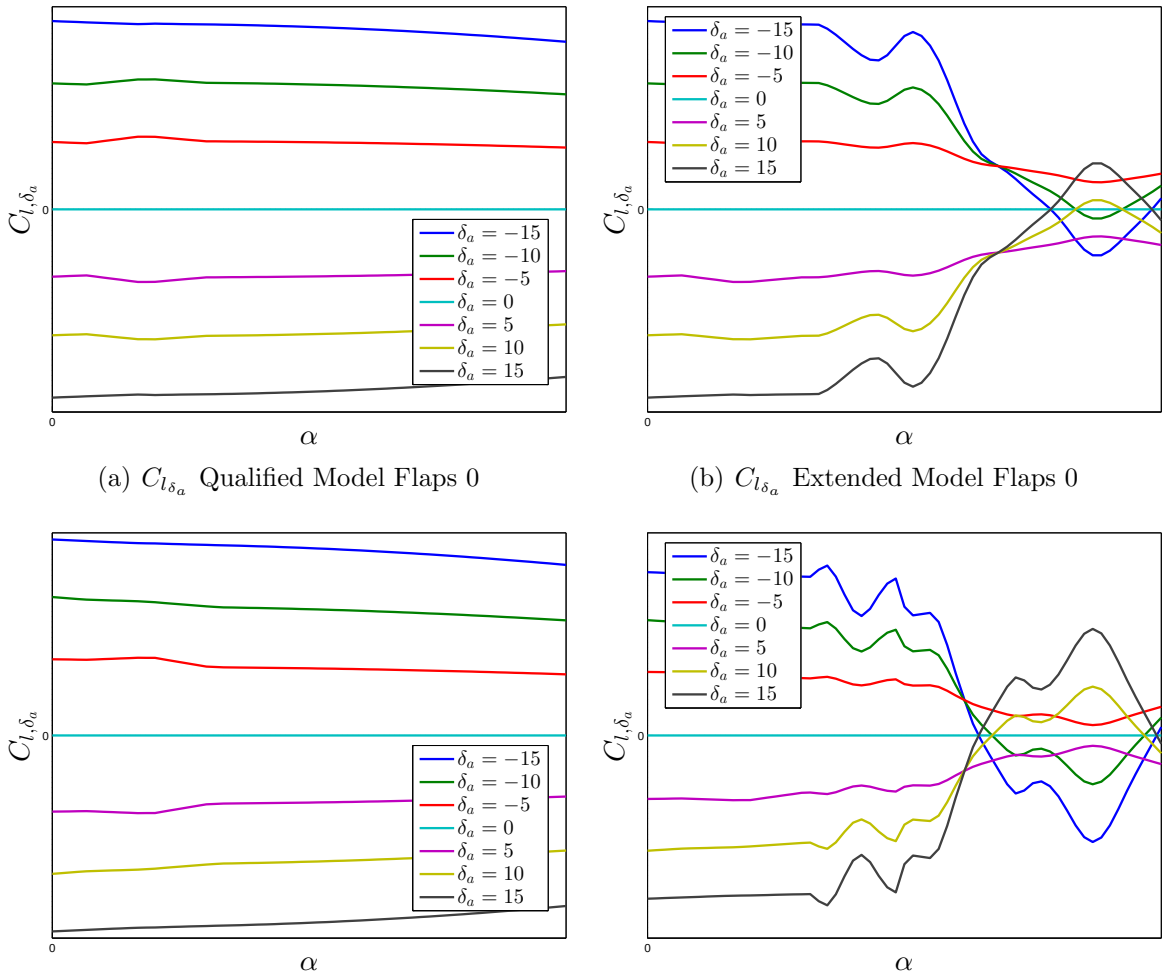

(a) $C_{l_{\delta_a}}$ Qualified Model Flaps 0

(b) $C_{l_{\delta_a}}$ Extended Model Flaps 0

(c) $C_{l_{\delta_a}}$ Qualified Model Flaps 10

(d) $C_{l_{\delta_a}}$ Extended Model Flaps 10

Figure 4.10: $C_{l_{\delta_a}}$ Aileron effectiveness before and after stall extension

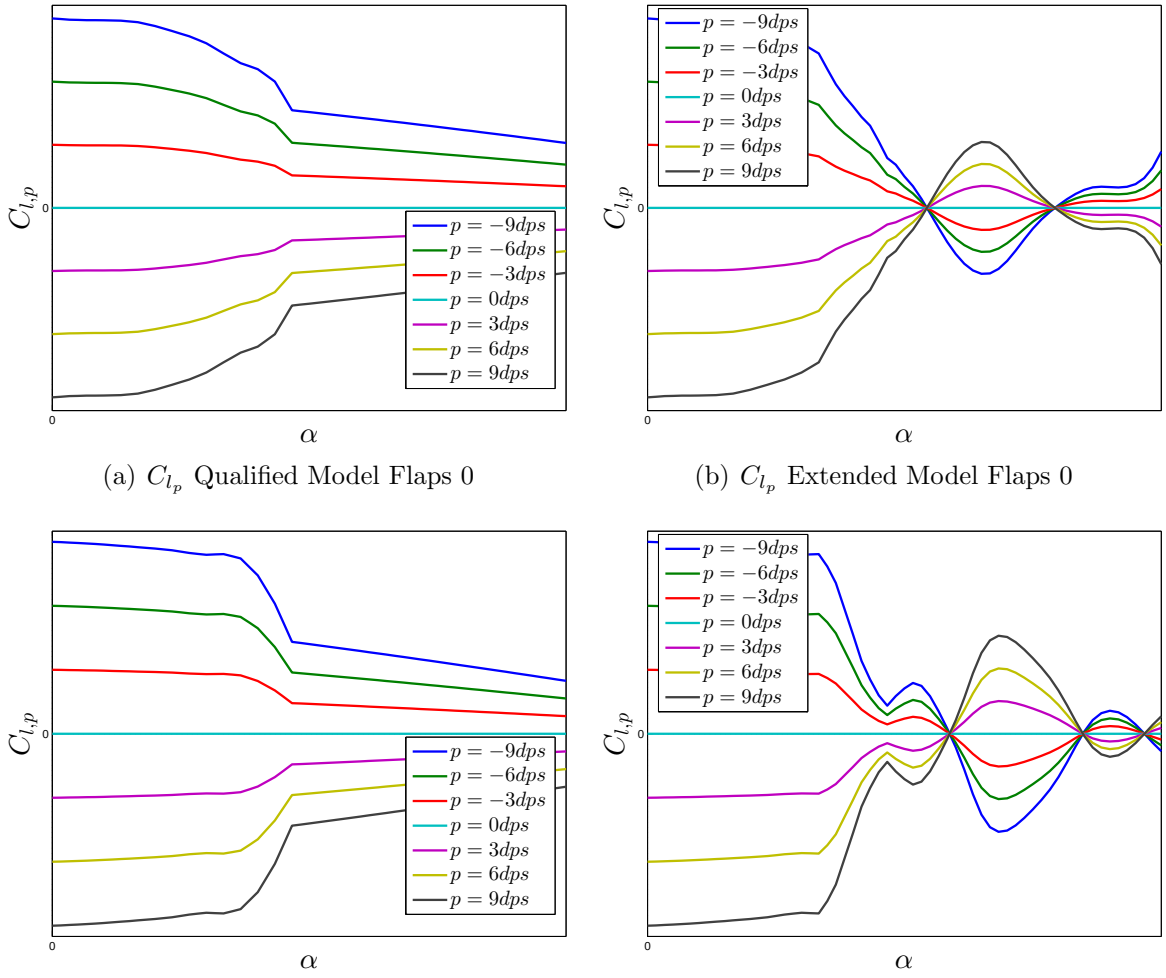

(a) C_{l_p} Qualified Model Flaps 0

(b) C_{l_p} Extended Model Flaps 0

(c) C_{l_p} Qualified Model Flaps 10

(d) C_{l_p} Extended Model Flaps 10

Figure 4.11: C_{l_p} Roll damping before and after stall extension

Shown later in the chapter, integration with the longitudinal stall model shows that the plane near stall cannot maintain lift as it banks, and would pitch down subsequently, decreasing the angle of attack.

4.2.4 C_{n_β} Yaw Stability

When an airplane is at an angle of sideslip β relative to its flight path, the yawing moment produced should be such as to tend to restore it to symmetric flight. With the convention of β being positive for flow approaching from the right of the airplane, $C_{n_\beta} > 0$ would provide that stability. Figure 4.12 shows the yawing moment experienced by the aircraft at various sideslip angles for flaps 0 and flaps 10.

C_{n_β} is mainly provided by the vertical tail of the aircraft [12]. It can be seen that yaw stability reduces significantly near stall, and for the flap 0 case it even reaches 0. As α gets progressively higher past stall, the aircraft becomes yaw stable again. Using engineering judgment, it is hypothesized this is due to the vertical tail becoming unblanketed from the wake of the stalled wing. Dynamic pressure restores over the vertical tail and hence it generates larger forces leading to the stable C_{n_β}. This would also agree with C_{l_β}, where it becomes more roll stable past stall as the tail becomes unblanketed.

4.2.5 $C_{n_{\delta_r}}$ Rudder Effectiveness

Figure 4.13 show that the rudder generates significantly less yawing moment at high α. The reason is twofold; the first is due to the vertical tail being positioned in the turbulent wake of the stalled wing, therefore losing dynamic pressure. The second reason is that the rudder becomes blanketed by the fuselage at higher angles of attack. These two combined effects would make the rudder progressively less effective in generating yaw.

4.3 Integration into full 6-DOF Simulator

The extended aerodynamic model is integrated with the qualified model into a 6-DOF simulator. The longitudinal stall aerodynamic model is co-developed with the lateral stall model and is included as well. For validation of the aerodynamic model, input time history of the elevator from a flight test is fed into the simulation along with the initial conditions of the flight test. The purpose is to verify if the aircraft behaves qualitatively similar to the flight test from an integration of states point of view, and not just comparing the forces and moments at a specific point in time. Aileron and rudder input is

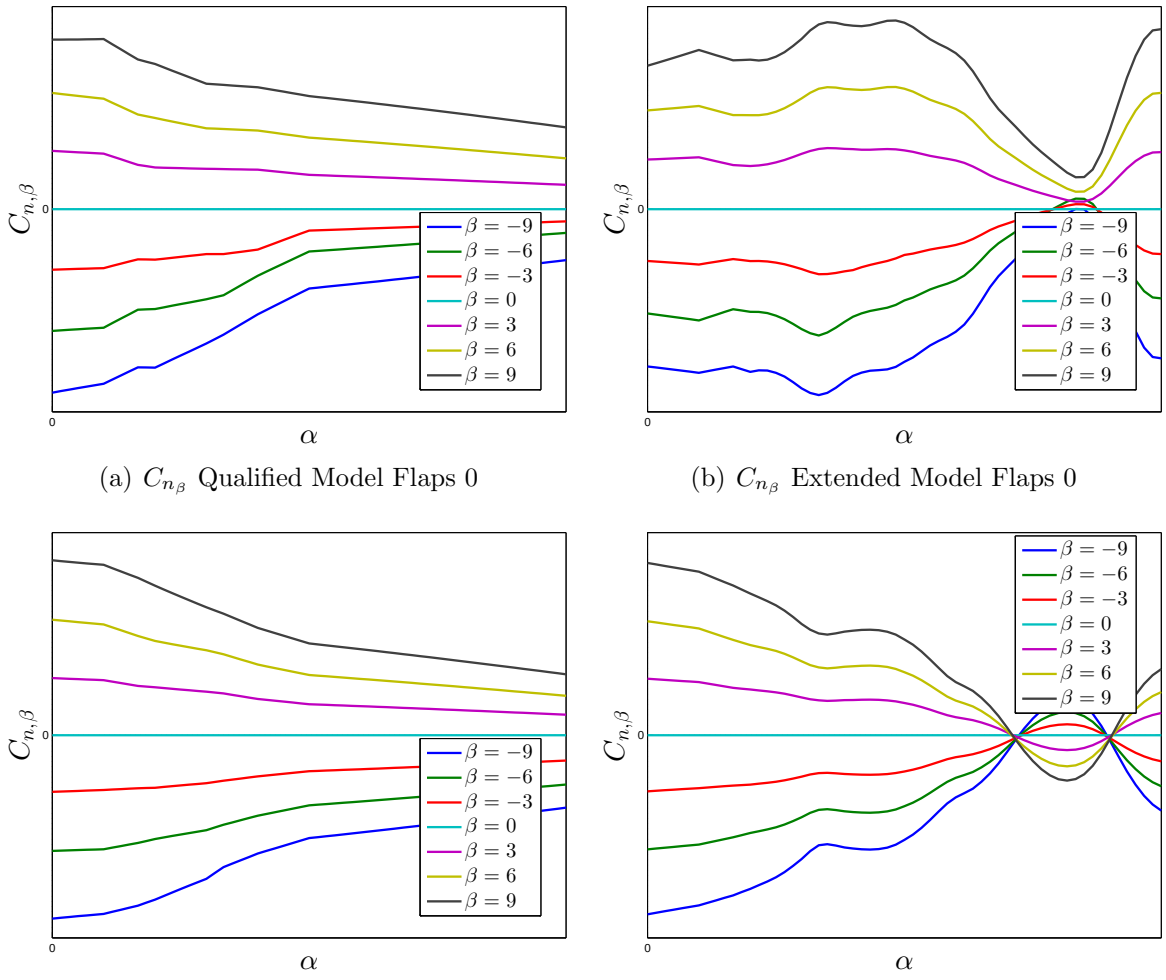

(a) C_{n_β} Qualified Model Flaps 0

(b) C_{n_β} Extended Model Flaps 0

(c) C_{n_β} Qualified Model Flaps 10

(d) C_{n_β} Extended Model Flaps 10

Figure 4.12: C_{n_β} before and after stall extension

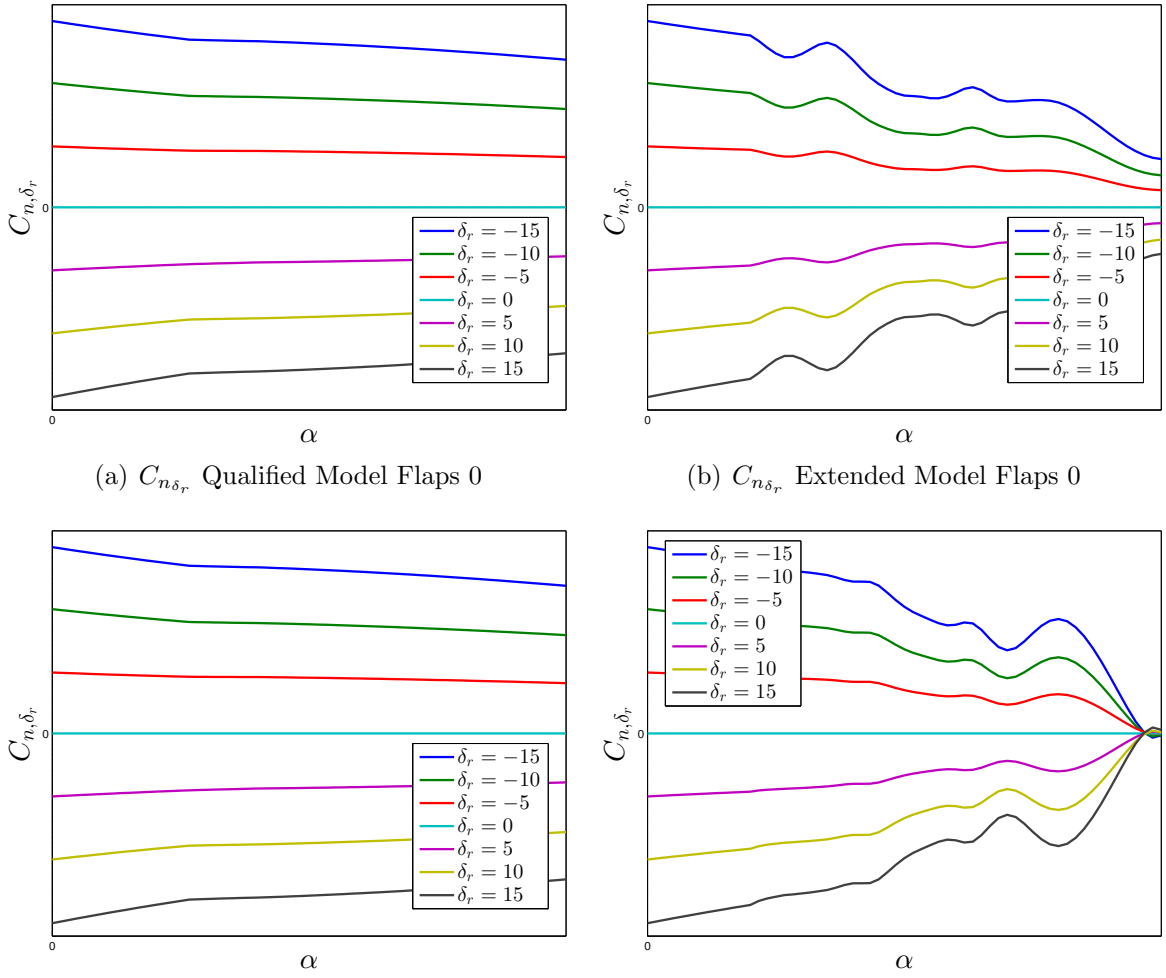

(a) $C_{n_{\delta_r}}$ Qualified Model Flaps 0

(b) $C_{n_{\delta_r}}$ Extended Model Flaps 0

(c) $C_{n_{\delta_r}}$ Qualified Model Flaps 10

(d) $C_{n_{\delta_r}}$ Extended Model Flaps 10

Figure 4.13: $C_{n_{\delta_r}}$ Rudder effectiveness before and after stall extension

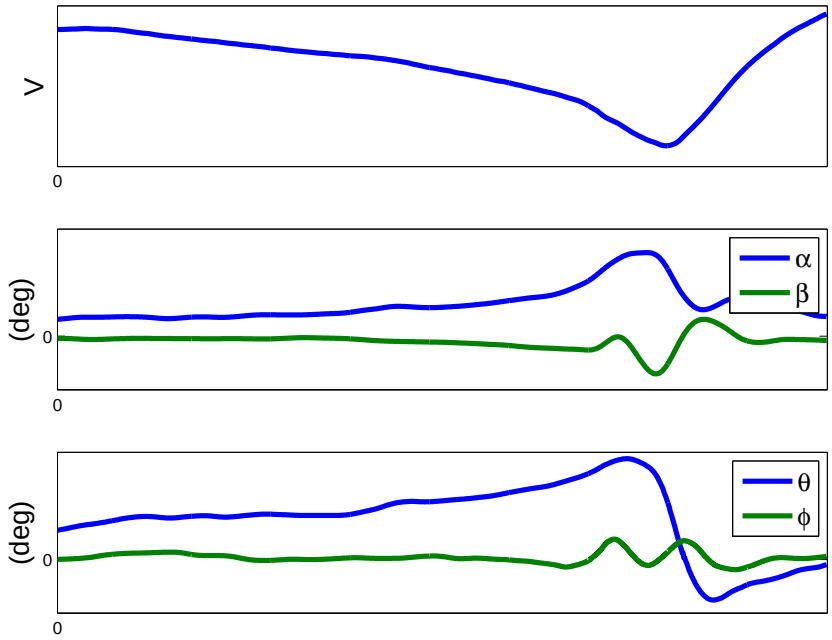

Figure 4.14: Flight test states for validation case 1

zero for the simulation. Figure 4.14 shows the true airspeed V, angle of attack α, sideslip β, pitch θ, and roll ϕ against time of a non-pusher flight. Figure 4.15 is the simulation of that same flight, with the initial conditions set the same as the actual flight data. The measured elevator input is fed into the model to pilot the simulation into a stall and achieve similar angles of attack as the flight test. It can be seen that the simulation qualitatively behaves very similar to the flight test. The aircraft continually slows down over a duration of time, increasing pitch and angle of attack at the same time. The roll is maintained even though there is no aileron input in the simulation, which is expected because the aircraft does not have any sudden changes in rolling moment in the low angle of attack region and it has roll stability. As α continues to increase, roll-off appears in the flight test quite a bit earlier than the maximum angle of attack. The pilots use aileron and rudder to try to maintain roll attitude, as the plane continues to increase α, stalls and pitches downward significantly. The rudder input by the pilot caused some additional sideslip during the recovery part of the flight. The simulation also started the flight very similarly, decreasing airspeed while increasing α and θ. Roll-off also happens quite a bit earlier than the maximum angle of attack; however, due to low roll-damping at high α and no control input to arrest the roll-off, the aircraft continues to roll until C_{l_p} becomes more stable again at even higher α. This flight was done with flaps 0, and that effect can be seen in Figure 4.12(b).

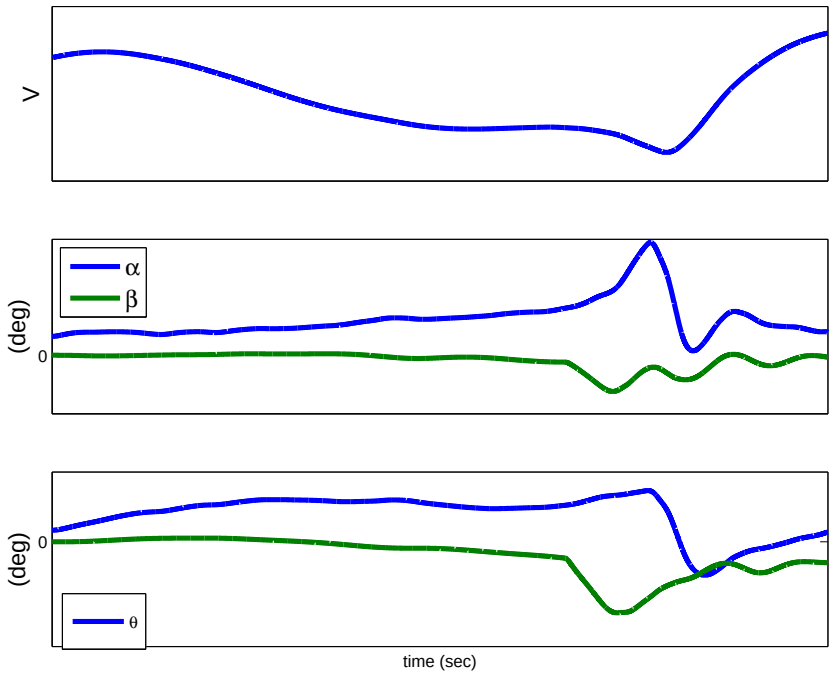

Figure 4.15: Simulation states for validation case 2

Figure 4.16 is another flight case that was selected for comparison with the simulation. Figure 4.17 shows the simulation of the same flight, again with elevator input history fed into the model so the simulation goes into a stall. Again, all the qualitative behaviors are very similar. However, the simulation rolled significantly due to the lack of lateral control input. It finally stopped rolling on its own after the angle of attack lowered after the pitch down, and that the large negative β induced by the left roll caused restoring moment. Overall, the behavior of the lateral stall model is satisfactory. The simulation remained stable throughout and none of the states blew up. It definitely rolls off near stall, and once started, requires significant input from the pilot to keep the roll angle small. According to the FAA Federal Aviation Regulations Part 25, aircraft must demonstrate the following stall characteristics for airworthiness: "For level wing stalls, the roll occurring between the stall and the completion of the recovery may not exceed approximately 20 degrees" [14]. The simulation suggest that the aircraft would not meet this requirement unless the pilot takes proper action to limit the bank angle. For the simulation shown here, the best course of action once a stall is encountered would be to reduce the angle of attack by applying nose down moment to prevent α from climbing. Once it is un-stalled quickly through proper action, then apply ailerons to control the rolling of the aircraft with the now regained effectiveness associated with low angles of attack. This recovery procedure is one of the training outcomes that the new proposed

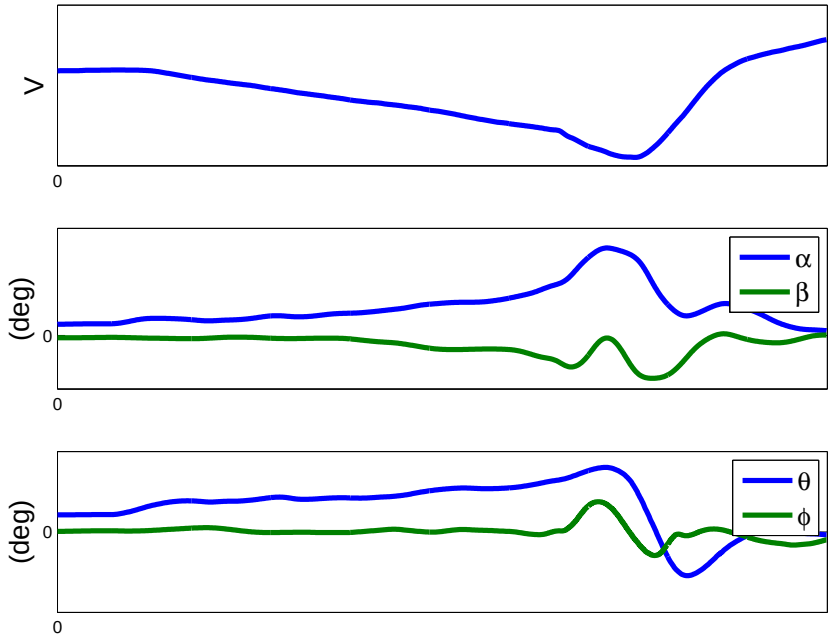

Figure 4.16: Flight test states for validation case 2

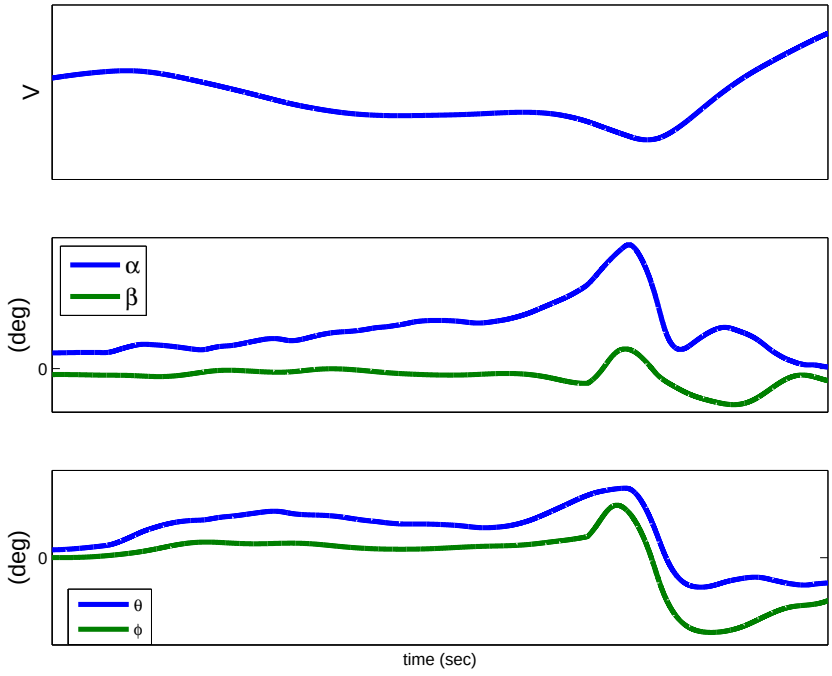

Figure 4.17: Simulation states for validation case 2

rule from the FAA tries to achieve, hence the extended model may be adequate for type-representative stall training as of now. However, that is to be investigated further as experiments are conducted with airline pilots.

Chapter 5

Conclusion and Future Work

5.1 Summary of Work

Loss-of-control resulting from airplane upset is a leading cause of worldwide commercial aircraft accidents [26]. On November 5th 2013, the United States Federal Aviation Administration issued final rule changes to 14 CFR Part 121 regarding the training of pilots in extended envelopes [15] in an effort to reduce Loss-of-control related accidents. The changes demanded that pilots "receive ground training and flight training in recognizing and avoiding stalls, recovering from stalls, and recognizing and avoiding upset of an aircraft, as well as the proper techniques to recover from upset." The industry has to comply to this rule by 2020.

Ground-based flight simulators need to have an aerodynamic model that captures the complicated dynamics at stall in order to provide meaningful training to pilots. However, the flight models in most training simulators are unlikely to be adequate for this purpose and their aerodynamic database must be updated to cover the stall regime.

A method for generating representative stall models adequate for training purposes from certification flight test data is proposed in this thesis. The novelty of the method is that it could be applied with only certification flight test data and a qualified pre-stall model. These prerequisites are easily met for most aircraft in service today since the resources could be obtained from the aircraft manufacturer. The method was applied to extend the lateral aerodynamic database of a Bombardier Aerospace turboprop commuter aircraft to cover the high angle of attack regime, using 198 recorded stall maneuvers for the development. Note that the work documented in this report was done with some non-certification data, which improved the final models.

Time-history comparisons of force and moment coefficients of the model to that of measured values from flight test show satisfactory matches. Close matches were observed even for flight data that was set aside for validation and was not included in the development process. Some of the important effects related to lateral aerodynamics were inspected closely after the model correction. Significant corrections were applied to these effects compared to the qualified model at high angles of attack, including reduced aileron effectiveness, reduced rudder effectiveness, reduced and unstable roll damping, and reduced yaw stability. Roll-off at stall was observed and also added to the model. The corrected aerodynamic database is integrated with the qualified model with the full set of 6-DOF nonlinear equations of motion. Measured elevator states from flight tests were fed into the model to pilot it into a stall. The simulation behaved qualitatively similar to the flight tests and was significantly less stable at stall compared to the qualified model. The rolloff model implementation also meant that significant aileron input is needed to keep the aircraft wings-level at stall.

5.2 Future Work

There are several aspects of the current research that are worth pursuing in future studies. First, the current stall modeling efforts uses data that are assumed to be free of significant sensor bias and systematic errors. These sources of error in the data would affect the accuracy of the parameters being estimated for the stall model. Using data that is corrected by flight path reconstruction to repeat the modeling procedure is one area that should be explored. The process removes systematic errors due to sensor bias and errors so that in theory a higher fidelity stall model could be developed. In addition, some non-linearities in the states are not included in the current model due to not having data information for capturing such effects. For example, at high angles of attack, it was found that the aircraft is roll unstable at low roll rates; however, as $\hat{p}$ becomes excessively large in either direction, it should impart a stabilizing C_l on the aircraft instead of a destabilizing one. A wind-tunnel study by Brandon, Foster, and Shah showed this phenomenon [5]. Unfortunately, wind-tunnel data of such effects for a high-wing turboprop configuration is not available and therefore not included. As part of a similar effort for the FAA, Birhle Applied Research is conducting wind-tunnel tests of a turboprop configuration aircraft at their Large-Amplitude-Multi-Purpose (LAMP) Wind Tunnel [21]. The fidelity of the lateral stall model could be improved further by using extra sources of data for model development.

The objective of this project is to develop a method for generating type-representative stall models, which are supposed to be adequate for upset recovery training for aircraft of one geometry type. This particular project developed a model for a high-wing T-tailed commuter turboprop. Although validation efforts have shown the model to be adequate, the human aspect of upset recovery training has not been validated. Experiments involving experienced pilots testing the model should be conducted to conclude whether the model behaves like the real aircraft and whether it is adequate for training. Such experiments have been planned and UTIAS is currently in the process of contacting prospective pilots to participate in the study.

Bibliography

[1] Nikolay Abramov, M Goman, Alexander N Khrabrov, EN Kolesnikov, Maria E Sidoryuk, B Soemarwoto, and H Smaili. Aerodynamic model of transport airplane in extended envelope for simulation of upset recovery. 2012.

[2] Ralph E Bach Jr. State estimation applications in aircraft flight-data analysis: A user's manual for smack. 1991.

[3] James G Batterson. Estimation of airplane stability and control derivatives from large amplitude longitudinal maneuvers. 1981.

[4] James G Batterson and Vladislav Klein. Partitioning of flight data for aerodynamic modeling of aircraft at high angles of attack. *Journal of Aircraft*, 26(4):334–339, 1989.

[5] Jay M Brandon, John V Foster, Gautam H Shah, William Gato, and James E Wilborn. Comparison of rolling moment characteristics during roll oscillations for a low and a high aspect ratio configuration. In *AIAA Atmospheric Flight Mechanics Conference and Exhibit*, page 5273, 2004.

[6] Judith Bürki-Cohen and Andrea L Sparko. Airplane upset prevention research needs. In *AIAA Modeling and Simulation Technologies Conference and Exhibit*, number AIAA 2008-6871, 2008.

[7] J Chambers and R Hall. 'historical review of uncommanded lateral-directional motions at transonic conditions,' aiaa paper 2003-0590, jan. 2003.

[8] Girish Chowdhary and Ravindra Jategaonkar. Aerodynamic parameter estimation from flight data applying extended and unscented kalman filter. *Aerospace science and technology*, 14(2):106–117, 2010.

[9] Carl De Boor, Carl De Boor, Etats-Unis Mathématicien, Carl De Boor, and Carl De Boor. *A practical guide to splines*, volume 27. Springer-Verlag New York, 1978.

[10] Bureau dEnquêtes et dAnalyses et al. Final report on the accident on 1st june 2009 to the airbus a330-203 registered f-gzcp operated by air france flight af 447 rio de janeiro–paris. *Paris: BEA*, 2012.

[11] Bernard Etkin. *Dynamics of atmospheric flight*. Courier Corporation, 2012.

[12] Bernard Etkin and Lloyd Duff Reid. *Dynamics of flight: stability and control*, volume 3. Wiley New York, 1996.

[13] Bernard J Eulrich and Norman C Weingarten. Identification and correlation of the f-4e stall/post-stall aerodynamic stability and control characteristics from existing test data. Technical report, DTIC Document, 1973.

[14] FAA FAR. 14 cfr part 25 section 203. *Stall Characteristics, Airworthiness standards: Transport category airplanes*, 1995.

[15] Federal Register Federal Aviation Administration. Qualification, service, and use of crewmembers and aircraft dispatchers; final rule, 14 cfr part 121. 78(218).

[16] John V Foster, Kevin Cunningham, Charles M Fremaux, Gautam H Shah, Eric C Stewart, Robert A Rivers, James E Wilborn, and William Gato. Dynamics modeling and simulation of large transport airplanes in upset conditions. *AIAA Paper*, 5933, 2005.

[17] David Gingras, John N Ralston, Ryan Oltman, Chris Wilkening, Robert Watts, and P Desrochers. Flight simulator augmentation for stall and upset training. In *AIAA Modeling and Simulation Technologies Conference*, page 1003, 2014.

[18] Jared A Grauer and Eugene A Morelli. Generic global aerodynamic model for aircraft. *Journal of Aircraft*, 52(1):13–20, 2014.

[19] W Earl Hall and Narendra K Gupta. System identification for nonlinear aerodynamic flight regimes. *Journal of Spacecraft and Rockets*, 14(2):73–80, 1977.

[20] WE Hall Jr, NK Gupta, and RG Smith. Identification of aircraft stability and control coefficients for the high angle-of-attack regime. Technical report, DTIC Document, 1974.

[21] Bihrle Applied Research Inc. Corporate research facility: Large-amplitude-multipurpose (lamp) wind tunnel. `http://www.bihrle.com/company/lamp.dna`, 2016. [Online; accessed 15-September-2016].

[22] Bombardier Aerospace Jay Loftus, Personal Information, December 2014.

[23] Vladislav Klein and James G Batterson. Determination of airplane model structure from flight data using splines and stepwise regression. 1983.

[24] Vladislav Klein, James G Batterson, and Patrick C Murphy. Determination of airplane model structure from flight data by using modified stepwise regression. 1981.

[25] Vladislav Klein and Eugene A Morelli. *Aircraft system identification: theory and practice*. American Institute of Aeronautics and Astronautics Reston, Va, USA, 2006.

[26] AA Lambregts, Gregg Nesemeier, JE Wilborn, and RL Newman. Airplane upsets: Old problem, new issues. In *AIAA Modeling and Simulation Technologies Conference and Exhibit*, page 6867, 2008.

[27] Stacey Fangfei Liu. *Ground-Based Simulation of Airplane Upset Using an Enhanced Flight Model*. PhD thesis, University of Toronto, 2011.

[28] Richard E Maine and Kenneth W Iliff. Formulation and implementation of a practical algorithm for parameter estimation with process and measurement noise. *SIAM journal on applied mathematics*, 41(3):558–579, 1981.

[29] Richard E Maine and Kenneth W Iliff. Application of parameter estimation to aircraft stability and control: The output-error approach. 1986.

[30] Eugene A Morelli. Global nonlinear aerodynamic modeling using multivariate orthogonal functions. *Journal of Aircraft*, 32(2):270–277, 1995.

[31] Eugene A Morelli. System identification programs for aircraft (sidpac). In *AIAA Atmospheric Flight Mechanics Conference*, 2002.

[32] Eugene A Morelli. Efficient global aerodynamic modeling from flight data. In *50th AIAA Aerospace Sciences Meeting*, pages 2012–1050, 2012.

[33] Eugene A Morelli and Vladislav Klein. Optimal input design for aircraft parameter estimation using dynamic programming principles. 1990.

[34] WF Phillips, EA Anderson, and QJ Kelly. Predicting the contribution of running propellers to aircraft stability derivatives. *Journal of aircraft*, 40(6):1107–1114, 2003.

[35] Jeffery A Schroeder, Judith Bürki-Cohen, David A Shikany, David R Gingras, and Paul Desrochers. An evaluation of several stall models for commercial transport training. In *AIAA Modeling and Simulation Technologies Conference*, page 1002, 2014.

[36] Muthuthamby Sri-Jayantha and Robert F Stengel. Determination of nonlinear aerodynamic coefficients using the estimation-before-modeling method. *Journal of Aircraft*, 25(9):796–804, 1988.

[37] Harold L Stalford and S Ramachandran. Application of the estimation-before-modeling (ebm) system identification method to the high angle of attack/sideslip flight of the t-2c jet trainer aircraft. volume 2. simulation study using t-2c wind tunnel model data. Technical report, DTIC Document, 1978.

[38] Transport Canada. *Qualification Test Guide*, 2nd edition, December 2001.

[39] James E Wilborn and John V Foster. Defining commercial transport loss-of-control: A quantitative approach. In *AIAA atmospheric flight mechanics conference and exhibit*, page 4811, 2004.